Adaptive Resource Allocation Algorithms For Data And Energy Integrated Networks Supporting Internet of Things

Yitian Zhang

School of Computer Science and Electronic Engineering

University of Essex

This thesis is submitted for the degree of

***D*octor of Philosophy**

October 2020

Declaration

I hereby declare that except where specific reference is made to the work of others, the contents of this dissertation are original and have not been submitted in whole or in part for consideration for any other degree or qualification in this, or any other University. This dissertation is the result of my work and includes nothing which is the outcome of work done in collaboration, except where explicitly indicated in the text. This dissertation contains less than 80,000 words including appendices, bibliography, footnotes, tables and equations and has less than 150 figures.

Yitian Zhang

October 2020

Acknowledgements

First and foremost, I would like to express my great gratitude to Prof. Kun Yang, who has been my supervisor for 6 years. I am grateful to his unstinting support and great patience to me. I would like to thank my wife, Shuang He, for her support and caring during my studying period. I am grateful to my parents for their consistent and numerous amounts of support and encouragement to me. Finally, I would like to extend my thanks to those who directly and indirectly offered me support throughout my PhD study.

Abstract

According to the forecast, there are around 2.1 billion IoT devices connected to the network by 2022 [1]. The rapidly increased IoT devices bring enormous pressure to the energy management work as most of them are battery-powered gadgets. What's more, in some specific scenarios, the IoT nodes are fitted in some extreme environment. For example, a large-scale IoT pressure sensor system is deployed underneath the floor to detect people moving across the floor [2]. A density-viscosity sensor is deployed inside the fermenting vat to discriminate variations in density and viscosity for monitoring the wine fermentation [3]. A strain distribution wireless sensor for detecting the crack formation of the bridge is deployed underneath the bridge and attached near the welded part of the steel [4]. It is difficult for people to have an access to the extreme environment. Hence, the energy management work, namely, replacing batteries for the rapidly increased IoT sensors in the extreme environment brings more challenges. In order to reduce the frequency of changing batteries, the thesis proposes a self-management Data and Energy Integrated Network (DEIN) system, which designs a stable and controllable ambient RF resource to charge the battery-less IoT wireless devices. It embraces an

adaptive energy management mechanism for automatically maintaining the energy level of the battery-less IoT wireless devices, which always keeps the devices within a workable voltage range that is from 2.9 to 4.0 volts.

Based on the DEIN system, RF energy transmission is achieved by transmitting the designed packets with enhanced transmission power. However, it partly occupies the bandwidth which was only used for wireless information transmission. Hence, a scheduling cycle mechanism is proposed in the thesis for organizing the RF energy and wireless information transmission in separate time slots. In addition, a bandwidth allocation algorithm is proposed to minimize the bandwidth for RF energy transmission in order to maximize the throughput of wireless information.

To harvest the RF energy, the RF-to-DC energy conversion is essential at the receiver side. According to the existing technologies, the hardware design of the RF-to-DC energy converter is normally realized by the voltage rectifier which is structured by multiple Schottky diodes and capacitors [5]. Research [6] proves that a maximum of 84% RF-to-DC conversion efficiency is obtained by comparing a variety of different wireless band for transmitting RF energy. Furthermore, there is energy loss in the air during transmitting the RF energy to the receiver. Moreover, the circuital loss happens when the harvested energy is utilized by electronic components. Hence, how to improve the efficiency of RF energy utilization is considered in the thesis. According to the scenario proposed in the thesis, the harvested energy is mainly consumed for uplink transmission. a resource allocation algorithm is proposed to minimize the system's energy consumption per bit of uplink data.

It works out the optimal transmission power for RF energy as well as the bandwidth allocated for RF energy and wireless information transmission.

Referring to the existing RF energy transmission and harvesting application on the market, the Powecast [7] uses the supercapacitor to preserve the harvested RF energy. Due to the lack of self-control energy management mechanism for the embedded sensor, the harvested energy is consumed quickly, and the system has to keep transmitting RF energy. Existing jobs have proposed energy-saving methods for IoT wireless devices such as how to put them in sleep mode and how to reduce transmission power. However, they are not adaptive, and that would be an issue for a practical application. In the thesis, an energy-saving algorithm is designed to adaptively manage the transmission power of the device for uplink data transmission. The algorithm balances the trade-off between the transmission power and the packet loss rate. It finds the optimal transmission power to minimize the average energy cost for uplink data transmission, which saves the harvested energy to reduce the frequency of RF energy transmission to free more bandwidth for wireless information.

Abbreviations

ACK Acknowledgement

AP Access Point

APS Application Support

BS Base Station

DC Direct Current

DEIN Data and Energy Integrated Network

DEINR Data and Energy Integrated Network Receiver

DEINT Data and Energy Integrated Network Transmitter

DP Data Packet

EP Energy Packet

GPIO General Purpose Input/Output

IC Integrated Circuit

IoT Internet of Things

MAC Media Access Control

MCU Microprogrammed Control Unit

MIMO Multiple Input Multiple Output

MISO Multiple Input Signal Output

OFDM Orthogonal Frequency Division Multiplexing

OFDMA Orthogonal Frequency-Division Multiple Access

PA Power Amplifier

PCB Printed Circuit Board

PnP Plug and Play

PS Power Splitting

QoS Quality of Service

RF Radio Frequency

RF PA Radio Frequency Power Amplifier

RSSI Received Signal Strength Indictor

SDMA Space Division Multiple Address

SDR Software-defined Radio

SINR Signal to Interference plus Noise Ratio

SS Spatial Switching

SWIPT Simultaneous Wireless Information and Power Transfer

TDMA Time Division Multiple Address

TS Time Switching

UART Universal Asynchronous Receiver-Transmitter

USB Universal Serial Bus

WET Wireless Energy Transmitter

WIT Wireless Information Transmitter

WLAN Wireless Local Area Network

WSN Wireless Sensor Network

Contents

List of Figures

Chapter 1

Introduction

1.1 Background

The Internet of Things (IoT) is a definition of a kind of internet connectivity, which links various electronic, physical devices and provides a communication platform to these devices. The IoT is widely involved in enterprise scenarios such as factory, hospital and office building. By 2022, it is estimated that there will be 2.1 billion devices deployed in enterprising IoT applications [1]. As the primary purposes of these enterprising devices are monitoring and control, considering the complex commercial and industrial environment, the devices are generally deployed wirelessly. With the platform of the IoT network, the multiple wireless technologies such as 3G, 4G, Wi-Fi, Bluetooth and ZigBee can co-exist in the same network scenario or even in the same

device [13].

In the enterprise scenario, a wireless technology, the Wireless Sensor Network (WSN), it could be used as a part of the IoT network. It has the advantages of the reliability of data transmission, low power consumption, easy to generate an extensive network system and low-cost [14]. Due to the advantages of WSN, hundreds or thousands of WSN devices can join the same network. In addition, with the help of IoT platform, WSN devices in the different network can be linked together. Based on the enterprise scenario, most of the WSN devices are wireless sensors, switches or digital controller. Their typical application scenarios are manufacturing shop, hospital, office building, etc. In these scenarios, they are normally deployed in a large-scale way and have to work all the time. Furthermore, most of them are battery-powered devices, their energy resource is limited. Moreover, the WSN system could not allow devices' malfunction caused by lack of energy, if the devices' replied message is very critical. Hence, energy is one of the main issues in WSNs. Due to the rapid increment of the WSN devices, it brings challenges to energy management work for WSN devices, namely, the battery replacement work rapidly increases.

According to the traditional methods, the strategy for reducing the workload of battery replacement is saving the battery energy. So far, some approaches have been proposed to minimize the energy usage of WSN devices. The applied mechanisms are how to put the device into sleep mode [15] [16] [17] in time and how to minimise the energy consumption caused by the most energy-intensive peripherals such as Radio Frequency (RF) Power Amplifier

(PA) circuitry [18], relays and LEDs. These approaches extend the lifetime of the battery, and the battery replacement work becomes infrequent. However, manual battery replacement work for WSN devices in a large scale network is still costly. Furthermore, for some specific scenarios, the WSN devices are deployed in some extreme environments such as on the roof, underneath the floor, inside the boiler, etc. The battery replacement work is tough for human beings. To reduce the frequency of battery replacement, the energy harvesting system is proposed by researchers [19]. The system enables energy self-management to the WSN devices.

During the last decade, many research efforts have been made on the energy harvesting technologies. In the aspect of the energy type to harvest and its related harvesting methods, the widely applied instances are piezoelectric energy [20] [21], solar energy [22] [23] [24], electromagnetic energy [25] [26] and RF energy [27]. The piezoelectric energy can only generate while the exogenetic force is applied to the piezoelectric device. Solar energy highly depends on the sunshine. Electromagnetic energy harvesting technology requires close contact for transmitter and receiver. In the thesis's proposed scenario, the energy receiver, namely, the IoT wireless sensors, are statically deployed in the place people feel difficult to access. Normally, they are fitted indoor where requires long charging distance. Hence, RF energy becomes the optimal choice for the enterprise scenario proposed in this thesis. According to the literature, the RF energy charging mechanisms can be summarized into two methods. The first one is utilizing the ambient signal such as Wi-Fi, digital TV, FM, etc [28]. The second one is using the customized RF energy transmitter and frequency [29]. The RF energy transmitter is spe-

cific designed by the researchers themselves. The frequency for sending the RF energy is specially selected, which only depends on the hardware of the transmitter. The frequency does not belong to any existing wireless network system. In addition, some research efforts have been made on migrating the RF energy harvesting technologies to the existing network system, which aims to achieve a Data and Energy Integrated Network (DEIN) [30] [31] [32].

1.2 Motivation and Objectives

So far, according to the market, the Powercast company [7] who is the only organization has developed a RF energy harvesting system in practice. They have designed their RF energy transmitter and receiver from the beginning. On the RF energy receiver, they develop an Integrated Circuit (IC) specific for converting the RF energy to Direct Current (DC) energy with as high as 75% RF-to-DC conversion efficiency. They use supercapacitor as the DC energy storage, which reduces the charging time within one minute from 0 to 3.3 volts. They have customized the RF energy receiving antenna with a gain of 6 dBi for greater sensitivity, which has the maximum charging distance of 14 meters. Their RF energy receiver is designed as an energy source for electronic gadgets such as the WSN devices. However, RF energy transmission is independent of the WSN devices' network. The charging process can't be controlled via any network devices. Besides, it is difficult to apply their RF energy harvesting solution to the existing WSN system as their RF energy transmitter is independent. It cannot be set as a controllable

part in the existing WSN system. Also, the existing WSN devices have to be redesigned for embedding their ICs. According to the literature [11], if utilizing the ambient RF signal as the RF energy, renovation work is only needed on the WSN devices. For instance, RF-to-DC and energy management circuitry could be equipped to the WSN devices for harvesting the RF energy from the ambient signal. Then, the harvested energy could supply the WSN devices. However, the ambient RF signal, such as the digital TV signal, the microwave signal and the base station's signal, is not ubiquitous and controllable. It cannot supply stable and constant RF energy to the WSN devices. As a result, on the hardware side, there is no ready-made RF energy transmission/harvesting solution for automatically managing the energy of WSN devices without human intervention.

Approaches [33] [34] [35] have been proposed by researchers to integrate RF energy transmission and data communication in an existing network scenario. [33] propose a DEIN system with a power splitting device equipped on the receiver, which can receive both information and energy from the base station continuously at the same time. [34] utilizes multi-sine waveforms for energy transfer and their distinct peak-to-average-power-ratios for information transmission. [35] uses joint transmit power and time-switching control scheme for transmitting both RF energy and data. However, most of the ideal is proposed based on theory. Hence, there is no existing standard for managing the RF energy and data transmission for a practical a DEIN system. Hence, the blank area of the hardware and the software for a DEIN system motivates the thesis to investigate the approach for building a practical DEIN system and study the protocol and algorithm based on it. The

objectives of the thesis are summarized as follows:

- Develop a practical DEIN system platform which integrates the RF energy transmission/harvesting and data communication. Different from the existing works, the thesis aims to practically design a controllable ambient RF energy resource, which can be controlled by the thesis's designed algorithms running in the DEIN system. The experiment platform is used for evaluating the thesis's designed algorithms.

- Implement a adaptive energy management mechanism to linked WSN devices. Develop relevant software based on the practical IoT system platform. Design protocols for the DEIN system and the WSN devices to exchange energy-related information. Design protocols for controlling the RF energy resource. With the help of these specially designed protocols, the Data and Energy Integrated Network Transmitter (DEINT) will dynamically adjust its RF energy transmission according to the periodic report of the energy-hungry degree from the DEINR.

- Implement the algorithm for better throughput of wireless information. Furthermore, to achieve an energy-efficient DEIN system, the thesis aims to maximize the efficiency of RF energy utilization. As most of the harvested energy is utilized for uplink data transmission, the thesis aims to minimize the system's energy consumption per bit of uplink data. Moreover, implement the energy-saving algorithm for harvested energy.

1.3 Problem Statement

On the hardware side, the essential problem for building the DEIN system is how to provide stable and controllable RF energy to WSN devices. Powercast [7] uses customized RF energy transmitter and frequency. They use supercapacitor to store the harvested energy. However, they haven't realized a self-management mechanism to maintain the supercapacitor's voltage level. They have to charge the receiver all the time as their RF energy transmitter is manually controlled. [36] uses rechargeable batteries to store the harvested RF energy. The charging time could be an issue as the time to charge to the battery to full is not clarified in their system evaluation. Hence, how to store and manage the harvested RF energy deserves to be considered. On the software side, [37] uses a dedicated power beacon transmitter. Time slots for RF energy transmission are scheduled by software. However, he hasn't realized a closed-loop to adaptively adjust the schedule according to the receiver's energy level. Other existing jobs only propose theoretical methods. Hence, how to practically achieve a self-control (adaptive)) energy management mechanism for the WSN devices deserves to be considered. For instance, how to achieve the feedback of the WSN devices' energy level. How to adaptively adjust the RF energy transmission if the DEIN system has received the feedback. A feedback-based synchronization scheme is proposed in [38] to correct the sleep clock of the WSN system. The scheme is realized based on their designed protocol achieved by their customized communication packets. Since there is no related protocol work for the DEIN system, the protocol is required to adaptively control the RF energy transmission according to the

feedback of the WSN devices' energy level. Consequently, how to design the packet format for the protocol deserves to be considered. Also, to achieve a high-efficiency protocol, the packet size needs to be designed as short as possible but contains sufficient information.

Migrating the RF energy transmission to the existing network may affect the existing data communication. The RF energy transmission may share the system resource with the data communication. On the transmitter side, if RF energy and wireless data are transmitted through a device with a single RF source, they have to share the transmission channel and cannot be transmitted at the same time. The time resource must be allocated for separating them, and the original bandwidth for data communication is partly occupied by the RF energy transmission. Related works have been proposed in [39] [35] [40]. But they are based on a cellular network scenario, which cannot be applied to the practical WSN based DEIN system. If the RF energy transmitter is independent of the data function devices, their behaviours still need to be scheduled as the RF energy may bring interference to the data communication. On the receiver side, if the RF energy harvesting system and the data transmission/receiving circuitry are combined, the time must be allocated for activating them by turns [41]. Improper allocation method will affect the balance between RF energy harvesting and data transmission. For instance, the harvested energy can't afford the energy usage for data transmission or the speed of data transmission must be slow down due to the energy harvesting is not timely. As a summary, the problem of how to migrate the RF energy transmission to the existing network without affecting its current performance is raised.

Furthermore, the energy consumption will be increased as the energy conversion efficiency for RF-to-DC is quite low. It isn't avoidable as the hardware determines the energy conversion efficiency, and the fading loss in the air can't be avoided. Related works are proposed in [42] [43] [44]. They consider how to minimize the transmission power to minimize the energy consumption of RF energy transmission. However, they didn't consider the efficiency to utilize the transmitted RF energy. In addition, the harvested DC energy in the WSN devices is worth treasuring. All the behaviours of the WSN devices will depend on it. Energy-saving works such as putting WSN devices into sleep mode [45] [46] and reducing transmission power [47] [48] are designed for battery-powered WSN devices. Besides, they are not designed for a practical adaptively system. Hence, how to save the harvested RF energy for the DEIN system deserves to be considered.

1.4 Contributions

1.4.1 A Self-management DEIN System

A self-management DEIN system is designed in the thesis, which is also an instance of IoT system. The DEIN system consists of a Wi-Fi-based Wireless Local Area Network (WLAN) and a ZigBee-based WSN. In hardware, the DEINT is designed through applying hardware modification to the traditional ZigBee router device. A high-gain RF PA is equipped to the RF terminal of the ZigBee router. The Data and Energy Integrated Network

Receiver (DEINR) is designed to replace the batteries of the ZigBee end-device with an RF energy harvesting adaptor. All the involved devices are designed from Printed Circuit Board (PCB). In software, a central control system is designed for managing the DEIN system. All connected devices can share information via the central control system. Also, it enables system users to access information about connected devices.

The RF energy transmission is achieved by transmitting customized ZigBee packets via the DEINT's RF PA circuitry. The energy enhanced ZigBee packet is treated as the Energy Packet (EP), which are specifically designed for the RF energy harvesting adaptor of the DEINR. The typical wireless packets with normal energy are recognized as the Data Packet (DP). The DEINR can only harvest the RF energy from the EPs and convert them into DC energy stored in a supercapacitor. Furthermore, the thesis proposes an adaptive energy management mechanism for the battery-less DEINR. With the help of the mechanism, the voltage level of the supercapacitor on the DEINR is maintained within a range from 2.9 to 4.0 volts, which prevents the DEINR from power off. With a specially designed energy management protocol, the DEINT will dynamically adjust its RF energy transmission according to the periodic report of the energy-hungry degree from the DEINR. Different from the existing related works who utilizes the ambient RF energy resource or uses customized RF energy transmitter and frequency, the thesis proposed self-management DEIN system designs a stable and controllable ambient RF energy resource. It enables fully automatic energy management to the battery-less DEINR.

1.4.2 Bandwidth Allocation Algorithm to Maximize the Throughput of Wireless Information

Based on the self-management DEIN system, a scheduling cycle model is designed to organize EPs and DPs transmission. During a scheduling cycle, an EP is transmitted at the beginning. After that, the remaining time in the scheduling cycle is left for DPs transmission. The DEIN system will cautiously repeat the scheduling cycle, which allocates time slots for the RF energy transmission and data communication. Due to the scheduling cycle mechanism, the bandwidth was for data transmission is partly occupied by the EPs transmission. Hence, an idea is proposed in this thesis that is always transmitting the minimum required RF energy to charge the DEINR.

The amount of transmitted RF energy during each scheduling cycle is based on the packet size of the EP, and the length of the scheduling cycle. To estimate the relationship between the initial transmitted RF energy and the final increased DC energy in the DEINR, a training process involving four sets of RF energy charging experiments are carried out. Based on the collected experimental data, the mathematical expression is concluded to quantify the relationship between the increased amount of DC energy in the DEINR's supercapacitor and the parameters of the scheduling cycle. Then, a bandwidth allocation algorithm is designed with the help of the energy conversion equation. In the practical DEIN system, the DEINR reports its rated power to the system periodically. The report is recognized as an input to the algorithm, which indicates the minimum energy requirement of the

DEINR. Then, the algorithm can calculate the optimal bandwidth allocation factors to configure the scheduling cycle. The allocated bandwidth for RF energy transmission, namely transmitting EPs, just meets the minimum energy requirement of the DEINR. Consequently, the bandwidth for DPs transmission, namely, the throughput of wireless information, is maximized. As a summary, according to the experimental results, the bandwidth for transmitting DPs with the bandwidth allocation algorithm is 61.77% higher than the cases without, and the throughput of wireless information is significantly improved.

1.4.3 Resource Allocation Algorithm for Energy-Efficient DEIN

According to the so far proposed DEIN system, the energy conversion efficiency from the DEINT to the DEINR is quite low. It is inevitable that the RF energy loss in the air. Also, RF-to-DC efficiency is determined by the hardware characters. To the DEINR, the only energy source is the RF energy. Hence, to achieve an energy-efficient DEIN system, the thesis aims to maximize the efficiency of RF energy utilization. As most of the harvested DC energy is utilized for uplink data transmission, the thesis aims to minimize the system's energy consumption per bit of uplink data.

Based on the thesis's proposed topology involving multiple DEINRs, a new RF energy transmission method is designed. Related works [49] [37] who have built a practical RF energy transmission use a static directional

antenna to face the receiver directly. Normally, their system only consists of a single RF energy receiver. To transmit RF energy to multiple DEINRs, the DEINT's transmission (directional) antenna is designed with a rotation function. The DEINT can rotate its transmission antenna opposite to every DEINR to charge them in different time slots. Besides, a time allocation model is designed to organize the RF energy transmission and uplink data transmission in different time slots for all devices in the DEIN system. During the RF energy transmission process, a series of EPs are transmitted to a target DEINR. After harvesting the RF energy from the EPs, the DEINR will immediately utilize the just-harvested energy for uplink data transmission. Also, the process of uplink data transmission will run out the just-harvested energy for transmitting as much uplink data as possible.

Based on the time allocation model, a resource allocation algorithm is proposed and evaluated. It is designed to allocate the optimal time for RF energy transmission and the uplink data transmission for each DEINR. Also, it works out the optimal transmission power of the DEINT. With the algorithm, the numeric results show that the system's energy consumption per bit of uplink data is minimized, which maximizes the DEIN system's efficiency of RF energy utilization.

1.4.4 Adaptive Energy-Saving Algorithm to Minimize the DEINR's Energy Usage

The harvested energy will be stored in a supercapacitor. To save the harvested energy, an energy-saving algorithm is proposed by the thesis. It aims to reduce the DEINR's energy consumption to lengthen the lifetime of the battery-free WSN device. Different from the related works, the thesis's proposed energy-saving algorithm is adaptive for the practical DEIN system. As the most energy of the WSN device is consumed by radio function, reducing its transmission power will therefore reduce the energy consumption of the WSN device. However, the transmitted packet could be lost due to the low transmission power. If the packet transmission is failed, the WSN device will take a maximum waiting time to wait for a non-existent Acknowledgement (ACK) packet. The waiting time is much longer than the ACK waiting time after a successful packet transmission. Since the DEINR has to switch on the radio function for receiving the expected ACK packet during the waiting time, the longer waiting time caused by the failed packet transmission results in more energy consumption on radio function. Hence, the thesis proposes a mathematical model to represent the DEINR's average energy consumption by considering the transmission power and the packet loss rate. Based on the model, an energy-saving algorithm is designed to adaptively adjust the DEINR's transmission power (configured by setting the transmission current of the hardware), which minimizes the DEINR's average energy consumption. According to the hardware characters, radio function for transmission consumes more energy than receiving. Although extra energy is consumed

for waiting ACK due to the failed packet transmission, the algorithm will save more energy by reducing DEINR's transmission power. As a result, the algorithm balances the trade-off between the DEINR's transmission power and the packet loss rate. It reduces the transmission power to slightly sacrifice the packet receive rate, which obtains the minimum average energy consumption for the battery-less WSN device.

1.5 Structure of the Thesis

The rest of the thesis is organized as follows.

In Chapter 2, a detailed survey is presented. Firstly, it introduces off-the-shift energy harvesting technologies. Then, the RF energy charging methods are introduced and summarised. Thereafter, the approaches to combine RF energy transmission/harvesting and wireless information communication are summarised. Then, the resource allocation mechanisms and algorithms for throughput maximization and energy consumption minimization are reviewed. Finally, the energy-saving mechanisms for minimizing the energy consumption on the energy harvester side are summarised.

In Chapter 3, the architecture of the self-management DEIN system is introduced involving the role of each connected device. Then, the hardware structure of each designed device is described in details. Thereafter , a designed software framework for the proposed DEIN system is introduced as well as the control protocol for the adaptive energy management mechanism.

Finally, the experiments for transmitting both RF energy and wireless data are carried out, and the performance of the DEIN system is analysed.

In Chapter 4, firstly, the scheduling cycle model and the RF energy transmission and harvesting model are introduced. Then, it describes the details of the derivation process of the energy conversion equation as well as the utilized experimental methods. Thereafter, the designed bandwidth allocation algorithm is described. Finally, it shows the experimental results to prove the energy conversion equation and the benefit of the bandwidth allocation algorithm.

In Chapter 5, firstly, a multiple DEINRs based DEIN topology is proposed. Then, based on the topology, system models which are energy estimation model and time allocation model are proposed. In addition, the problem of how to minimize the system's energy consumption per bit of uplink data is proposed. Thereafter, the method and related algorithm to solve the proposed problem is described. Finally, it evaluates the performance of the algorithm, and the numeric results prove its validity.

In Chapter 6, firstly, the energy consumption model is proposed for estimating the energy cost for both successful and failed packet transmission. Based on the model, the average energy consumption for packet transmission is estimated. Then, an energy-saving algorithm is proposed to minimize the average energy consumption. Finally, the experimental results evaluate the performance of the algorithm.

In Chapter 7, the achievements of the thesis are summarised, and some

future research directions are identified.

Chapter 2

Literature Review

2.1 Energy Harvesting Technologies

The development of the DEIN system designed for IoT scenario is structured by utilizing existing energy harvesting technologies. In this section, several most commonly used energy harvesting technologies are introduced as well as their applications. Finally, the comparison is made among these energy harvesting technologies, and the advantages and disadvantages are discussed.

2.1.1 Piezoelectric Energy Harvesting

The piezoelectric material is specially made by using two parallel metal plates filled with the Lead Zirconate Titanate (PZT) in between [50]. The electricity

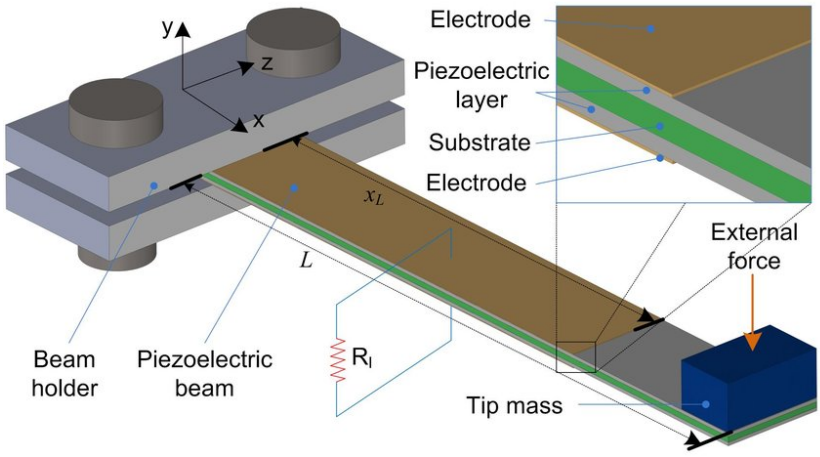

Figure 2.1: Piezoelectric harvester with a substrate and two electrodes [8]

is generated due to the piezoelectric effect by pressing the metal plates, which converts mechanical energy to electric energy. A cantilevered piezoelectric energy harvester described in [51] is designed to trigger the resonance by the external vibration at a specific frequency. The resonance repeatedly bends the cantilevered piezoelectric material to generate the electricity, which can be harvested by a power management circuit. The resonant frequency can be adjusted by putting different tip mass on the edge of the cantilever. Eventually, three piezoelectric energy harvesters are respectively designed with 115, 120 and 125 Hz resonant frequency to match the broadband characteristics of the WSN in their application scenario, and the results show there is unremitting voltage output from the set of harvesters in the frequency band of their WSN system. The piezoelectric energy harvester is also commonly used in the vibrative environment. The cantilevered piezoelectric energy harvester is utilized in [52] to power the wireless sensors in the running vehicle. According to the vibration frequency tested when the vehicle is running

Figure 2.2: The dynamic offset parabolic mirrored reflector dish aided solar energy harvester [9]

at a speed of 90 km/h, its resonant frequency is adjusted to 15 Hz, which outputs an average power of 3 µW eventually. Another application of the piezoelectric energy harvester is proposed in [53], which is used for powering the sensor nodes to monitor the aircraft structural health. The Macro-Fibre Composite material is used for making the harvester. Therefore, it can be integrated with the wing structure and bear the most potent strain. Hence, the vibration from the wing causes the vibration to the harvester.

2.1.2 Solar Energy Harvesting

The silicon-based solar cell is the critical material for converting solar energy into electric energy [54]. Most of solar energy harvesting systems focus on the traffic sign and signal system [55], outdoor lighting [56] [57], spacecraft [58],

and personal power station [59]. However, there are still some attempts to utilize the solar energy harvesting technology for charging the network gadgets [60]. The solar photovoltaic cell employed in [61] is to harvest solar energy for WSN node. A sun position tracking technique is proposed by calculating the solar angle and position to adjust a gear and spring driver, which keeps the solar panel always facing the sun directly. As a result, according to the simulation result, the solar energy harvesting system can output average power of 37.5 µW to the WSN node. Compared to the traditional static solar panel, a dynamic offset parabolic mirrored reflector dish is introduced in [9] to increase the harvesting efficiency. In order to enhance the stability for continually generating the electric power, the solar tracking system is designed for rotating the solar dish to face the sun based on the local solar time. Eventually, the proposed system can generate an average output voltage of 7.822 volts and a current of 6.144 milliamperes to the connected power regulator, which is 81 per cent more efficient than the static solar panel system.

2.1.3 Electromagnetic Energy Harvesting

The electromagnetic energy harvesting technology introduced in this section is based on the inductive charging technology [62] [63], which is widely used in the smartphone and smartwatch nowadays. It is typically implemented by the coupling circuit, which mainly consists of two coils. The electromagnetic field is generated on one coil by applying a high-frequency current, and the energy is transferred to the other coil by electromagnetic induction [64]. A typical application is embedding this technology into near-field

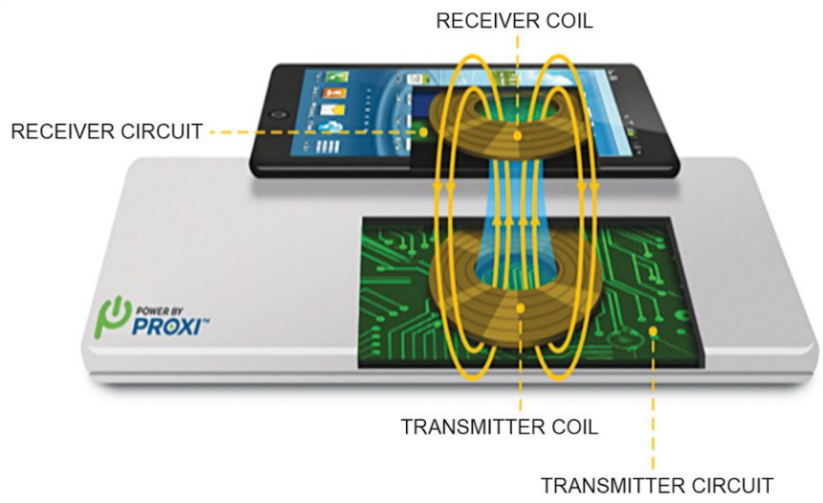

Figure 2.3: The coupling circuit based electromagnetic charging system [10]

communication (NFC) system [65]. The two induction coils are designed as flat spiral and fitted in pads, and the charging frequency is set to 130 kHz. Considering the charging efficiency affected by the placement and alignment variation between the two coil pads, the energy transmission pad is designed as a cognitive wireless charger, which can control the operation frequency adaptively based on the implicit feed to optimize the energy transmission performance [66] [67]. Not only limited to the small devices, a high power inductive charging system is designed in [68] for electric taxi vehicles. The energy transmission coil, namely, the primary coil, is embedded in the street, which is designed as a charging station. The secondary coil is placed underneath the vehicle for harvesting the electromagnetic energy when it is in the station. The charging frequency is set to 20 kHz, and the transferred power is up to 200 kW, which eventually provide an overall efficiency of nearly 69%.

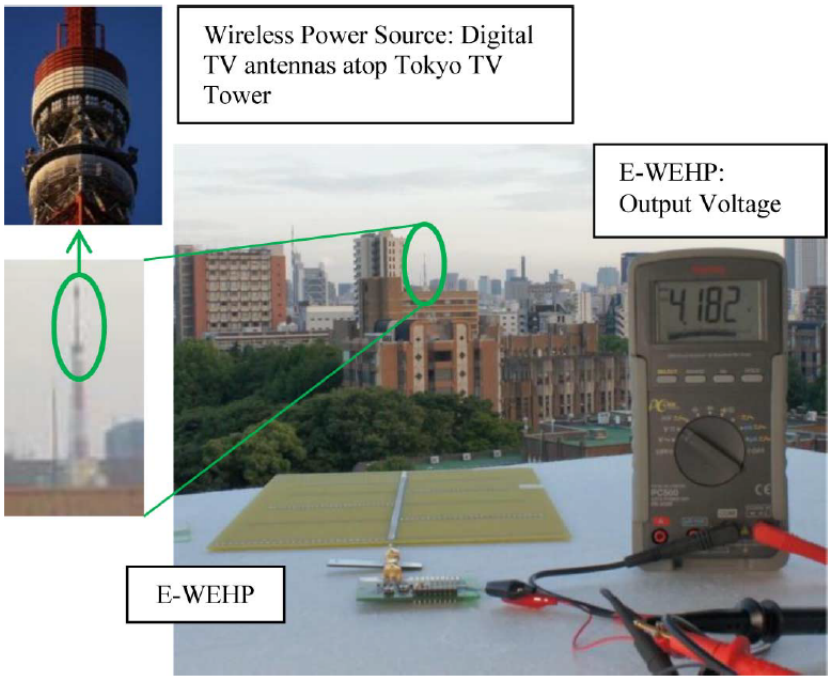

Figure 2.4: The RF energy harvester to harvest wireless energy from multi-carrier wireless digital TV signals broadcasted from the Tokyo TV tower [11]

2.1.4 RF Energy Harvesting

The RF energy harvesting technology refers to harvest energy from RF waves, which is usually applied for far-field charging scenario. The energy source can be the existing RF signals in the air, such as digital TV, GSM, FM, Wi-Fi, etc. In order to harvest the energy from a standard signal source, the harvester is designed to match its specific frequency. For instance, a harvester for collecting energy form 2.4 GHz Wi-Fi signal is designed in [69], which consists of a 2.4 GHz antenna, a matching network circuit, a rectifier, a power converter and a rechargeable battery. The load of the harvester is

the microcontroller and the sensors, which derives energy from the rechargeable battery. In order to maximize the harvested RF energy, some attempts are made at the harvester side to increase the energy conversion efficiency. A rectenna designed by using 2×2 circuit waveguide array antenna is proposed in [29], which is for harvesting RF energy from 1.8 GHz GSM signal. Furthermore, the pump-charge circuit is designed for capturing more RF energy, which is sensitive to minimum -10 dBm. Not only the standard RF signal,but the manmade RF waves with customized radiation frequency can be used as RF energy source [70]. A customized RF power transmitter is developed by Powercast company, which can broadcast meaningless RF waves at 915 MHz with 3 W transmission power. Also, the harvester is designed for receiving energy from the RF waves around that frequency, and the charging distance can be several meters.

2.1.5 Comparison of Energy Harvesting Technologies

The piezoelectric and solar energy harvesting technologies have sufficient energy conversion efficiency to supply wireless sensors. However, they highly depend on the external environment. The piezoelectric material generates electricity based on the vibration, and the solar cell needs sunlight to activate. Hence, they are not suitable for charging the wireless sensors in our IoT scenario as our sensors are motionlessly deployed indoor or in a concealed place. The electromagnetic energy harvesting technology has the best energy conversion efficiency, but the nearest charging distance requirement. The RF energy harvesting technology can meet the far-field charging requirement.

Furthermore, both the ubiquitous ambient RF signal and the manmade signal can be the energy source. Moreover, many optimization designs have been made at the harvester side to enhance the energy harvesting efficiency, which is able to meet the energy demand of our IoT sensors. As a result, the RF energy harvesting technology is our optimal choice for structuring our DEIN system.

2.2 RF Energy Charging Methods

An RF energy harvesting system at least consists of an RF energy transmitter and a harvester. Designing the harvester relies on the transmitter as the matching circuit on the receiver is designed based on the centre frequency of the RF waves from the transmitter. By investigating various RF energy transmitters in state of the art, the approaches of the transmitters can be classified into two aspects, utilizing the ambient RF signal from the environmental wireless signal transmitter and using customized RF energy transmitter and frequency.

2.2.1 Utilize The Ambient RF Signal

Some instances to harvest the ambient TV, AM and FM signal are described in [28] [71]. In [11], an instance is described to harvest the ambient digital TV signal in urban area. The harvested energy is able to power a designed battery-less embedded sensor-platform. The digital-TV broadcasts are de-

signed to beam out long-duration TV programs with broader coverage in the most urban areas. The receiving antenna is specially designed to fit the maximum gain in the 500 MHz to 600 MHz bandwidth range, which is to match the wireless spectrum of the chosen digital-TV signal. Behind the antenna interface, an RF to DC charge-pump is designed by employing five-stage half-wave rectifier circuits, which contains ten Schottky diodes in total. As a result, the RF energy receiver, the antenna together with the RF to DC charge-pump, is tested with the sensitivity of -14.6 dBm (4.67 µW) carrier wave. The sensing peripherals on the microcontroller can be successfully powered under the peak carrier power level of -7 dBm (199.5 µW) within the 6.3 Km charging distance from the TV tower.

Some research efforts are made to harvest ambient microwave signals [72] [73] [74] [75]. For instance, a system to harvest energy from the ubiquitous Wi-Fi signal is described in [76]. In order to harvest the only 100 µW RF signal from the Wi-Fi router, an integrated antenna array is designed. Each antenna is designed as a planar patch, which has the same size as a coin. On the back of each planar patch antenna, the signal-stage full-wave Greinacher circuit [77], namely, the rectifier is deployed for rectifying the sinusoidal signal from each antenna. To combine the DC energy from each rectifier, a power management module is designed to regulate all the DC inputs, and output a stable voltage of 1.8 V to power on the sensors. The module consists of a charge pump IC and a step-up regulator, which are S882Z from Seiko Instruments and AS1310 from AMS respectively. As a summary, the RF energy harvester has a minimum -40 dBm RF power sensitivity and outputs a typical 10 µA current.

Since the ambient RF signal is used as the energy source, the core of the charging system is the RF energy harvester as there is no way to interfere the ambient RF signal, and the design of the harvester needs to cater the characters of the energy source. Therefore, this RF energy harvesting system relies on the external RF resource, and the signal strength of the RF resource must fulfil the minimum receiving sensitivity of the harvester. In order to overcome the dependence on the external RF resource, some approaches are introduced in the following section to develop dedicated RF resources.

2.2.2 Using Customized RF Energy Transmitter And Frequency

Some approaches have been made on developing dedicated circuits for getting specific frequency as RF energy source [29] [78] [79] [80]. A dedicated RF resource based on ultra-wideband retro-reflective beamforming is proposed in [49]. This charging system module has multiple antenna elements distributed in space evenly. The harvester sends short impulses regularly to the distributed antennas. According to the received impulse at each antenna, a radar tracking system is employed to locate the position of the harvester. Thereafter, the antenna elements jointly construct beamforming to the target harvester according to the detected location. This dedicated RF source, the beamforming, can efficiently combat some space energy losses due to wireless channel attenuation, which increase the charging efficiency. Another dedicated RF source, the power beacon, is proposed in [37]. The charging system uses a dedicated power beacon transmitter, which consists of a signal

generator(Tektronix TSG-4104A), an RF amplifier(RFMD RF2173), a Yagi antenna(Laird PC904N) and an FPGA module. The 920 MHz RF signal is from the signal generator, and its transmission power is substantially enhanced while the RF signal is passed through the RF amplifier. After that, the enhance RF signal is moved to the antenna. The FPGA module generates a PWM signal to the enable pin of the RF amplifier, which produces the on-and-off RF signal, namely, the power beacon, to the antenna. At the harvester side, the harvester module, the P1110 from Powercast, is employed to draw the energy from the power beacons. The supercapacitor is used to store the converted DC energy from the harvester module, which powers a connected sensor module. A ready-made RF energy transmitter, the TX91501 from Powercast company, is used for a WSN based RF energy harvesting system [81]. The P2110 energy harvester is equipped for each WSN node, which is also a ready-made device from Powercast company. A testbed that consists of multiple RF energy harvester aided WSN nodes, an energy transmitter, a synchronizer is implemented. The energy transmitter generates RF waves at 915Mhz, and the RF energy harvester embedded in the WSN nodes is sensitive to the same frequency. A sink-synchronized polling approach is proposed to optimize the usage of the harvested energy for each sensor node. The synchronizer operates as a coordinator, which broadcasts the synchronizer frame to control the duration of activating each WSN node according to their estimated harvested energy.

2.2.3 Summary of Comparison

The RF energy charging method, utilizing the ambient RF signal, requires the harvesting system to be more sensitive to the signal strength of the external RF energy resource. Due to the uncertainty of the external RF energy resource, the second charging method, using customized RF energy transmitter and frequency, provides a more stable RF energy resource to the harvesting system. However, the customized transmitter brings more cost for upgrading the existing system. Furthermore, the customized RF frequency may interfere with the traditional wireless communication in or around the current system as the transmitter generally uses high transmission power. Moreover, it's difficult to merge the propagated RF waves to the communication protocol of the current system as the customized RF wave does not contain any meaningful information. Hence, controlling the RF energy resource is only through the on-off management to the RF energy transmitter. The thesis's designed RF energy harvesting system embraces the advantages of both charging methods, which utilizes a controllable ambient RF signal. The system is designed according to the ZigBee based WSN system. With merely upgrading the hardware of the ZigBee router by way of embedding an RF amplifier to its baseboard, the router can work as an RF energy transmitter. At the ZigBee end-device side, an RF energy harvester designed as an adapter is equipped on the device, which replaces the batteries to power the primary circuit. To the harvester, the available RF resource to harvest is the controllable ambient ZigBee signal from the ZigBee router. The RF energy resource, the RF waves sent through the RF PA, is generated by

modulating thesis's designed application data packets, which complies with the standard ZigBee protocol. Hence, the RF waves sent from the energy transmitter belongs to the ZigBee packets but with enhanced signal strength, and they do not interfere with the existing wireless communication as they are organized by the ZigBee protocol. Furthermore, the RF energy resource can be controlled by managing the duration and the frequency of sending the thesis's designed application data packets. Moreover, the designed application data packets also contain the information of the current charging state, and they contribute to the thesis's designed RF charging protocol, which is friendly merged to the existing ZigBee protocol to achieve the adaptive charging management.

2.3 Simultaneous Wireless Information and Power Transfer

To achieve architecture of the DEIN, the technology of Simultaneous Wireless Information and Power Transfer (SWIPT) is critical. In order to deal with the integrated information and power based on the SWIPT, three splitter based receiver architectures are illustrated in which the signal is split into spatial, power and time domains, respectively. Apart from different signal splitting approaches, these three receiver architectures share the other components in common. After being received by the receiver, the RF signal is split into two parallel flows. One is for energy reception, where the rectifier plays an essential role in converting the RF signal to DC before it can be stored in the

receiver's battery. The other is for conventional information reception, where the RF signal is transformed from the passband to the baseband for further demodulation and decoding operations before it arrives at the information destination. Due to the signal splitting operation, the tradeoff between the energy reception and the information reception clearly exists. An optimal signal splitting approach in order to serve different purposes is crucial for the design of a splitter based receiver architecture. Next, the implementation of three typical splitting approaches will be studied, namely the Spatial Switching (SS), the Power Splitting (PS) and the Time Switching (TS). Without loss of generality, the splitting factor is denoted as $\rho(0 \leq \rho \leq 1)$, which indicates that a portion ρ of the RF signal will be invoked for delivering the energy and the rest $(1-\rho)$ of the RF signal will be invoked for delivering the information.

2.3.1 Splitting Data and Energy Based on Spatial Splitting Model

In the SS based receiver, as shown in Fig.2.5, the signal is split by allocating the different number of antennas at the receiver for the energy and information receptions, respectively. For the implementation of the SS based receiver, the antenna selection on the receiver side has to be jointly optimised as well as the transmit power allocation on the transmitter side so as to achieve the maximum information rate subject to the requirement of the energy reception. For example, in [82], by invoking an antenna selection scheme and the interference alignment technique, the authors partitioned the

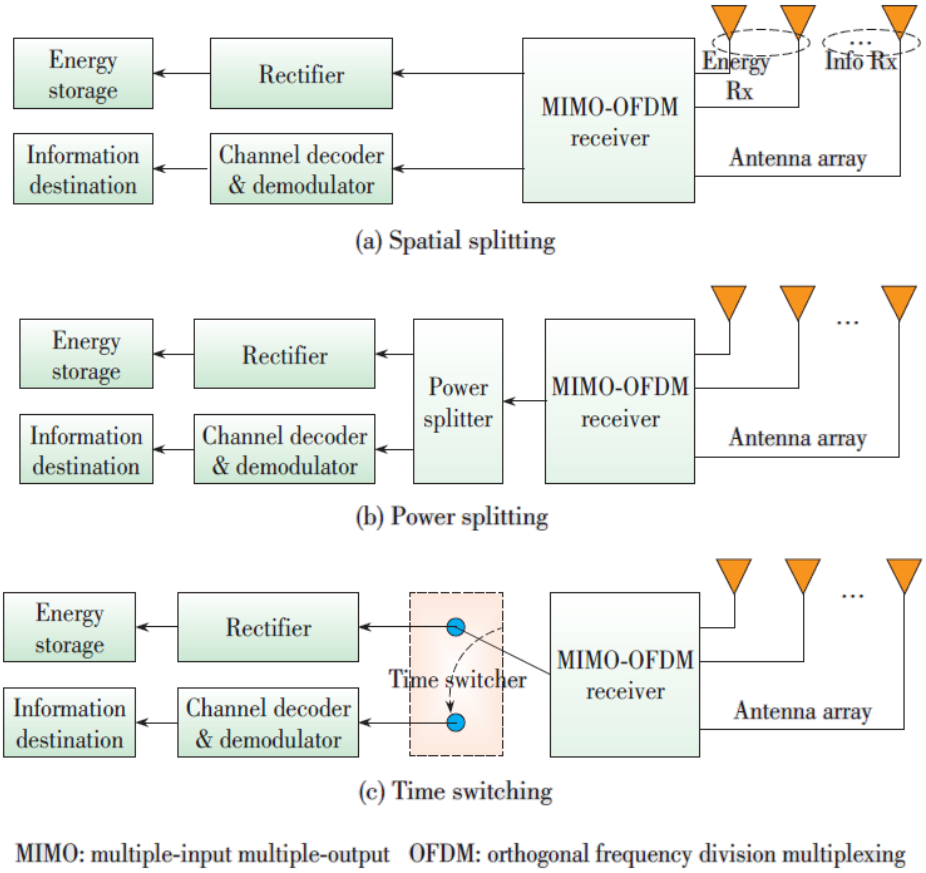

Figure 2.5: Three signal splitting based receiver architecture for devices in DEINs: (a) Spatial splitting based receiver architecture;(b) Power splitting based receiver architecture; and (c) Time switching based receiver architecture.

received signal into two orthogonal spaces in order to achieve simultaneous information and energy transfer. In [83], the problem was formulated as a joint optimisation of both the antenna selection and the transmit covariance matrix design in order to achieve the maximum information rate subject to

the energy harvesting constraint.

2.3.2 Splitting Data and Energy Based on Power Splitting Model

In the PS based receiver, the signal is split by the power splitters for realising the independent energy and information receptions, as illustrated in Fig.2.5 With the aid of the Multiple Input Multiple Output (MIMO) system, the transmission of several independent information flows can be realised and hence substantially increase the information throughput. In order to extract energy from these independent information flows, each receive antenna should be equipped with a power splitter. These power splitters are capable of adaptively tuning themselves to conceive specific splitting factors. As a result, for the implementation of the PS based receiver, it has to jointly optimise the splitting factors for each antenna on the receiver side as well as the transmit power allocation on the transmitter side so as to achieve the balance between the information rate and the energy reception. For example, the authors of [84] focused their attention on the impact of channel estimation on the performance of integrated data and energy transfer by jointly designing the PS factor as well as the duration of both the training phase and the transmission phase. Furthermore, the authors of [85] extended the point-to-point scenario to a multi-relay cooperative network. They proposed a harvest-use-store PS relaying strategy with distributed beam-forming for wireless-powered multi-relay cooperative networks. Wang et al. [86] propose a joint power allocation and splitting for data and energy integrated system

over such channels with the objective of maximizing the achievable data rate with constraints on the delivered energy. It helps the data and energy integrated system in vehicular networks to extend the lifetime of sensors installed on vehicles and roadside units.

Furthermore, several existing works focus on the circuit design for a practical power splitter of high performance. For example, the authors of [87] proposed a 1-V wideband CMOS phase and power splitter with an RLC network load and frequency compensation capacitor. This power splitter could only produce a 7 degree error for phase and 1.4 dB power imbalance. The authors of [88] presented a V-band active one-to-four power splitter in 90 nm LP CMOS process for phased-array transmitter. In their power splitter, 0.75 dB power imbalance and 4.3 degree phase error were achieved.

2.3.3 Splitting Data and Energy Based on Time Splitting Model

In the TS based receiver, the signal is split in the time domain by a time switcher for the independent energy and information receptions, as illustrated in Fig.2.5c. For its practical implementation, it is only needed to partition a typical transmission frame into two parts, namely the energy transfer sub-frame and the information transfer sub-frame dedicated for the energy and information receptions respectively. However, having diverse TS factors for each antenna is not quite realistic since this operation may result in the mismatch of the RF signals received by the independent channels, which may

significantly complicate the subsequent signal and energy processing. As a result, all the antennas on the receiver side are assumed to have identical TS factors. Therefore, for the implementation of the TS based receiver, it has to jointly optimise both the power allocation on the transmitter side and the TS factors on the receiver side in order to achieve the balance between the information rate and the energy reception. For example, the authors of [89] studied the trade-off between energy consumption and the transmission delay by proposing a dynamic algorithm for optimally allocating the transmit power and deciding the TS factor. In [90], the authors maximised the end-to-end achievable information rate in the decode-and-forward relay network by jointly optimising both the transmit power and the TS factor. Al-habob et al. [91] propose a modified time-switching relaying protocol for dual-hop relay networks with data and energy integrated technique. They consider a dual-hop multi-destination relay network where the DF relay node has no embedded power source, and thus needs to harvest energy from the source signal. In such system, the transmission power of the relay depends on the source-relay channel and it is less compared to that of the source. They propose a modified time-switching relaying protocol that reduces the outage threshold of the second hop and consequently enhances the overall system performance. Khan et al. [92] propose a time switching based D2D link energy efficiency maximization approach for devices enabled with data and energy integrated system.They have divided the time frame into three sub-slots for optimum trade-off between EH and ID.

2.4 Resource allocation for DEIN

At present, the DEIN receiver of the achieved DEIN system is always designed as the battery-free mode. The kind of architecture used for the DEIN receiver does not affect the result. As the DEIN receiver powered by the harvested energy is only for a short period; Consequently, the harvested energy only gives the limited lifetime to the receiver. The higher network output requires the DEIN receiver to deal with more data during a unit time. When the DEIN receiver needs to upload and download more data, it consumes more harvested energy as well as reducing the lifetime of the receiver. If it takes more time to transmit energy at the DEIN transmitter side, the lifetime of the DEIN receiver can be lengthened. However, it can lead to more energy consumption. Excessive energy transmission causes unnecessary energy consumption if the DEIN receiver needs less energy than the energy actually received. Some RF energy is weakened before energy reaching to the receiver side. In addition, the transmitter's data throughput can be affected by allocating more communication resource such as transmission power, frequency band to energy transmission, and so on. Thus accordingly, there are tradeoffs among the harvested energy, transmitter's energy consumption and network data throughput. When considering these tradeoffs to improve network performance, research and studies have been made on communication resource allocation. In the following section, three aspects are discussed based on the aim of the resource allocation schemes. The three aspects are throughput maximisation, fairness and energy consumption minimization.

2.4.1 Throughput Maximization

Both Zhou et al. [93] and Yin & Qu [94] have investigated the maximisation of the total throughput of multiple DEIN receivers subject to a minimum requirement on the energy harvested, and subject to a peak and/or total transmission power constraint in the downlink of a multi-UE Orthogonal Frequency Division Multiplexing (OFDM) system. Notably, the weighted sum-rate of all DEIN receivers has been maximised in [93], and it is used for guaranteeing the fairness among all the DEIN receivers; Meanwhile, the maximising the conventional sum-rate has been the objective in [94]. By contrast, the DEIN receivers at conventional Wireless Information Transmitter (WIT) networks only receive data information from BSs. It is assumed by Zhou et al. [93] and Yin & Qu [94] that the DEIN receivers may extract both data and energy from their received RF signals synchronously. Zhou et al. [93] have considered both Time Division Multiple Address (TDMA) and Orthogonal Frequency-Division Multiple Access (OFDMA) in terms of having access to multiple DEIN receivers. In the TDMA protocol scenario, the DEIN receivers use time switching based receiver architectures to receive the requested data simultaneously and charge the batteries. The optimal power allocation and the optimal splitting factors of time switching based receivers are determined dependent on Lagrange duality [93]. In the OFDMA protocol scenario, the DEIN receivers use power splitting based receiver architectures. The authors have put forward an iterative algorithm in order to optimise both the power and the sub-carrier allocation. The optimal splitting factors of power splitting based receivers are obtained when the algorithm converges. Fur-

thermore, Yin & Qu [94] have proposed a sub-carrier separation scheme the information and energy are transferred separately on different sub-carriers. The sum-rate optimisation has been formulated as a mixed-integer programming problem. When both optimal and suboptimal solutions have been got, they are compared to the time switching based scheme of [93]. In summary of the aforementioned studies, the sub-carrier separation scheme performs better than the time switching based scheme, especially when the DEIN receivers require higher energy.

Another study has been carried out by Wang and Brown [95], who has studied the sum-throughput maximisation problem by optimally allocating the time duration for the downlink Wireless Energy Transmitter (WET) and for the uplink WIT. The "harvest-then-transmit protocol" is advocated for the batteryless DEIN receivers. In this protocol, the DEIN receivers first harvest energy emitted by a Base Station (BS) during its downlink transmission and then upload their data information to the BS in a TDMA manner during their uplink transmission by exploiting the energy harvested from the BS. Though Wang and Brown [95] have firstly solved the sum-throughput maximisation problem, the doubly near-far phenomenon exists in the "harvest-then-transmit protocol" aided system. In this system, a DEIN receiver far from the BS receives less energy than a DEIN receiver close to the BS, but this DEIN receiver has to transmit at a higher power during its uplink transmission in order to achieve the same information rate because that its peer close to the BS. As a result, more resources have to be allocated to the DEIN receivers closer to the BS than to those far away from the BS, so that it can achieve the maximum sum-throughput. Obviously, this allocation

scheme ignores the fairness among DEIN receivers, since the DEIN receivers far away from the BS obtain limited resources to accomplish their uplink transmissions.

2.4.2 Fairness

Besides the sum-throughput, fairness is another important metric that needs to be considered in resource allocation for the integrated WET and WIT. In [96] and [95], the minimum uplink throughput among all the DEIN receivers has been maximised for fairness achieving. In contrast with the aforementioned cite, the weighted sum-throughput has been maximised for fairness achieving, and the weights of DEIN receivers represent their specific needs in resource allocation in [97]. When the "harvest-then-transmit" protocol is adopted for the downlink WET and the uplink WIT , Wang and Brown [95] has studied the doubly near-far phenomenon, which leads to low uplink rates among DEIN receivers.

With the aim to surmount the adverse effects of this phenomenon, Wang and Brown [95] have maximised the common-throughput to reduce the differences among the DEIN receivers' uplink transmission rates. The results have shown that the common-throughput maximisation is capable of overcoming the doubly-near-far phenomenon, despite at a cost of some sum-throughput degradation.There are other researchers who studied the doubly-near-far phenomenon. Liu et al. [96] and Ju and Zhang [97] have maximised the minimum uplink throughput among all DEIN receivers, which is similar to [95], but

the DEIN receivers upload their data to the BS in a TDMA manner in [95]. In comparison with [95], all the DEIN receivers simultaneously upload their data to the BS using Space Division Multiple Address (SDMA) in [96].

Liu et al. [96] have also considered a BS having multiple antennas by extending the results of [95]. They have studied the throughput fairness for the multiple DEIN receivers supported by the SDMA protocol, which has higher spectrum efficiency than its TDMA counterpart. The minimum uplink throughput among all the DEIN receivers has been maximised by jointly optimising the time allocation for downlink and uplink transmissions with the aid of downlink energy beamforming and by beneficial power allocation for the DEIN receivers' uplink transmissions. A two-stage algorithm has been developed to solve this optimisation problem. Additionally, a pair of low-complexity suboptimal solutions has also be developed. It is used to compared to the optimal counterpart. To achieve more balanced uplink transmission throughputs, Ju and Zhang [97] have maximised the weighted sum-rate of all DEIN receivers by jointly optimising the time and power allocation.

Kim et al. [98] proposes an adaptive proportional fairness scheduling algorithm in SWIPT-enabled multi-cell downlink networks. they define an adjustable weighted sum of achievable rate and harvested energy as the utility function of each user and investigate fairness among utilities of users. Through extensive simulations, they evaluate the proposed scheduling algorithm in terms of rate-energy trade-off, the fairness of achievable rate and harvested energy. Al-Wani et al. [99] investigate beam design and user clus-

tering from the throughput-fairness trade-off perspective. they present an optimal power allocation that can achieve a high data rate for the overall system without sacrificing the sum-rate of weak users under full and partial channel state information.

2.4.3 Energy Consumption Minimization

In order to create an environment-friendly DEIN system, another important objective is to minimise the energy dissipation of the DEIN system itself, while maintaining the Quality of Service (QoS) of the DEIN receivers' WET and WIT services. The minimisation of the total transmit power of the BSs in DEIN systems, subject to the specific Signal to Interference plus Noise Ratio (SINR) requirements and received energy requirements have been studied in [100] and [44] [42] [43] [101] for a Multiple Input Signal Output (MISO) aided DEIN system supporting multiple DEIN receivers, where the transmitter is equipped with multiple antennas, while the DEIN receivers are equipped with a single antenna. The power splitting based receiver architecture has been conceived for integrated data and energy reception.

Shi et al. [100] have formulated the energy consumption minimisation as a non-convex problem. Then, the problem has been solved by exploiting the Software-defined Radio (SDR) technique, and they have proved that their solution is optimal for the sake of minimising the total energy consumption. Furthermore, a pair of suboptimal algorithms, namely the zero-forcing based algorithm and the beam-forming algorithm for optimising the SINR has been

developed in order to reduce the computational complexity. Their numerical results have demonstrated that the performance of the proposed suboptimal solutions is close to the optimal one. Moreover, Liao et al. [44] have proposed an SDR aided randomisation approach for finding the upper-bound of their energy consumption minimisation problem. Compared to the solution of [100], the algorithm advocated in [44]significantly reduces the computational complexity, while achieves near-optimality in terms of the energy consumption minimisation.

In order to consider the practical implementation of resource allocation schemes, imperfect channel state information has been considered in [42] and [43]. Specifically, Wang et al. [42] have developed a pair of robust joint beam-forming and power splitting schemes for minimising the energy consumption of the transmitter. In the first scheme, both the worst-case SINR and energy harvesting constraints have been taken into account. They have demonstrated that the worst-case of the joint beam-forming and power splitting optimisation problem can be relaxed to a semi-definite programming problem by equivalently transforming the linear matrix inequality based constraints to the robust quadratic matrix inequality based constraints. In their second scheme, the chance constraints8 for both the SINR and energy harvesting requirements have been considered. Hence, the chance-constrained joint beam-forming and power splitting problem has been transformed into another convex semi-definite programming problem by exploiting both the semi-definite relaxation and Bernstein-type inequality restriction. Furthermore, in [43], the effects of the imperfect channel estimation have been further considered. In the first case, the channel estimation error has been modelled

by a Gaussian random variable, when the transmitter estimates the channel based on the DEIN receivers' uplink transmissions and the channel states are correlated. In the second case, all the estimated results of the channel covariance matrix have been modelled by independent Gaussian distributed random variables, which is justified by the fact that the estimation errors of the covariance matrix are generated by multiple independent "error sources". Timotheou et al. [101] have explored the exploitation of constructive interference in MISO downlink channels for improving the performance of both the information decoding and energy harvesting. They have also demonstrated that the constructive interference with the aid of beam-forming can be exploited for improving the power level of the received RF signals, which may thus increase the amount of energy harvested.

2.5 Energy-Saving Mechanisms

Referring to literatures, most mechanisms which are used to reduce energy consumption can be summarized as two aspects, namely, how to put IoT devices in sleep mode and how to reduce transmission power of IoT devices. To be a conclusion, the two mechanisms can all be recognised as how to utilise the RF functions. Because, almost energy for IoT based wireless devices are consumed while the RF function is on.

2.5.1 Transmission Power Reduction

A non-decreasing and a non-increasing order maps proposed like a breathing pattern is proposed by Vijeth [47]. The map is fitted by using an increasing or decreasing values of transmission power, which looks like a digital sequence of values of transmission power. Also, the numerical order indicates the order of resource blocks which is allocated to IoT based LTE devices by base station. By calculating the practical resource blocks required by IoT devices and the SINR detected by IoT devices, the critical required transmission power over each resource block assigned to each IoT device will be calculated. Then, the calculating results will be recognized as inputs to do mapping guided by using the designed breathing map. The results show that the energy consumed by base station is reduced by selecting the optimum transmission power over resource block to IoT devices. Also, the SINR of IoT devices is enhanced.

C Carmona [48] proposes a transmission power management algorithm, which is used to adjust transmission power in order to control energy consumption. The decision to adjust transmission power level is based on the link quality parameter. This algorithm is evaluated by two nodes and suitable for energy management in ZigBee end-devices side. Certainly, there are also other methods to reduce energy consumption for ZigBee based WSN. Y Li [102] presents a novel Media Access Control (MAC) protocol, which improves the energy efficiency and enhance latency and jitter. Y Peng [103] proposed an energy-aware routing mechanism, which can prolong a lifetime of ZigBee network. S Hu [104] proposes a transmission power control strategy

for cluster heads based on multi-packet reception in clustering WSNs. According to the strategy, a cluster heads selection algorithm is designed. The transmission power levels of each cluster head are determined according to the number of cluster heads in monitoring area. With restrictions of successive interference cancellation algorithm in sink, transmission power control strategy for cluster heads are determined by distance from cluster heads to sink and residual energy of cluster heads. The power control strategy can reduce the energy consumption of sensor nodes as well as increasing network throughput.

2.5.2 Sleep Scheduling

At the first point, M Lopez [45] proposed a duty cycle algorithm to determine the short time-period cycle to active WSN nodes. At the rest of time-period, WSN nodes are in sleep mode. It introduces an expression to determine the duty cycle window size. In addition, the characteristics of a noise channel have been considered in this expression. The algorithm is designed for reducing active-mode energy consumption in terms of minimizing the duty cycle time. J Azevedo [46] implements a sleeping technology for all ZigBee nodes and also includes full function nodes. In the practical ZigBee based WSN, it typically consists of a ZigBee coordinator, router and end-device. The ZigBee coordinator and router are called full function devices because they are always in active mode. A time synchronization mechanism is developed to deal with the clock drift of nodes. This kind of mechanism sets up a certain sleep period and synchronizes this period to each node. Moreover, the

mechanism also enables the recovery of lost messages. P Guo [105] proposes a sleep scheduling method to reduce the delay of alarm broadcasting from any sensor node in WSNs. Two determined traffic paths is designed. One is for the transmitting alarm messages, and the other is for level-by-level offset based wake-up pattern according to the paths. When a critical event occurs, an alarm is quickly transmitted along one of the traffic paths to a center node, and then it is immediately broadcast by the center node along another path without collision. W Liu [106] proposes a logical correlation-based sleep scheduling mechanism to implement energy-efficient WSNs in ambient-assisted homes. The sleep scheduling mechanism analyses sensory data generated by different human behaviours to detect the logical correlations between sensor nodes in an ambient-assisted homes. By utilizing the particular logical correlations of an ambient-assisted homes to predict its usage status, the sleep scheduling mechanism deactivates sensor nodes accordingly to save energy when they are not expected to sense any valuable event. M Collotta [107] proposes the simultaneous use of two fuzzy logic controllers to dynamically adjust the sleeping time and the transmission power of the nodes in order to optimize energy consumption. It aims to the proper trade-off between the power saving and the WSN performance.

Chapter 3

A Self-management DEIN System

3.1 Introduction

In order to overcome the weakness of the two commonly used RF energy charging methods illustrated in the literature review 2.2, this chapter proposes a self-management DEIN system, which is an instance of IoT system. The DEIN system consists of a Wi-Fi-based WLAN and a ZigBee-based WSN. In hardware, the DEIN system is structured by a smart gateway, a ZigBee dongle, a DEINT and a DEINR, which are all designed from PCB. The smart gateway is embedded with an open-source Linux system (OpenWrt). The designed algorithms can be compiled in the system. The smart

gateway integrating a Wi-Fi module works as an Access Point (AP). The ZigBee dongle is programmed as a ZigBee coordinator. By plugging the ZigBee dongle into the Universal Serial Bus (USB) port of the smart gateway, the smart gateway's embedded Linux system bridges the Wi-Fi-based WLAN organized by the smart gateway and the ZigBee based WSN structured by the ZigBee dongle.

The DEINT is designed through applying hardware modification to the traditional ZigBee router device. By equipping a high-gain RF PA to the RF terminal of the ZigBee router, the thesis's customized ZigBee packets, namely, the EP, are amplified when they are sent through the Radio Frequency Power Amplifier (RF PA). The energy-enhanced carrier wave is treated as RF energy, which is the controllable RF energy resource for the DEINR. The DEINR is designed to replace the ZigBee end-device's traditional batteries with an RF energy harvesting adaptor. The ZigBee end-device works as a wireless temperature sensor node in the experiment platform. It can be any type of sensors or controllers according to the practical application scenario. The RF energy harvesting adaptor supply energy to the ZigBee end-device. The adaptor converts the harvested RF energy to DC energy and stores the energy in a supercapacitor via a power management circuit. When the supercapacitor is charged to a threshold voltage, the ZigBee end-device is activated (switched on). The first step for the ZigBee end-device is networking. The stored energy in the supercapacitor must meet the energy requirement of the networking process. Hence, the selection of the supercapacitor depends on the characters of the practical ZigBee device.

In the aspect of the software, the novelty is that the energy management mechanism to maintain the energy level of the ZigBee end-device is adaptive. According to the energy feedback of the ZigBee end-device, the control system can adaptively adjust the RF energy charging intensity. With the help of the mechanism, the voltage level of the supercapacitor on the ZigBee end-device can be kept in a range of 2.9 to 4.0 volts. It makes the ZigBee end-device be always on. Accompany with the mechanism, an energy management protocol is designed. It works for energy information exchange between the DEIN system and the ZigBee end-device. Also, it helps the DEINT to dynamically adjust the RF energy charging intensity based on the periodic report of the energy-hungry degree from the ZigBee end-device.

The remainder of this chapter is organized as follows. In Section 3.2, the DEIN architecture is introduced involving the role of each relevant device. In Section 3.3, the hardware structure of each designed device is described in details. In Section 3.4 , the thesis's designed software framework for the proposed DEIN system is introduced as well as the control protocol for the adaptive energy management mechanism. In Section 3.5, the experiments for transmitting both RF energy and wireless data are carried out, and the performance of the DEIN system is analysed.

3.2 The DEIN Topology

The thesis's designed DEIN system is depicted in Fig.3.1, which consists of the smart gateway configured as an AP, the Wi-Fi devices, the ZigBee don-

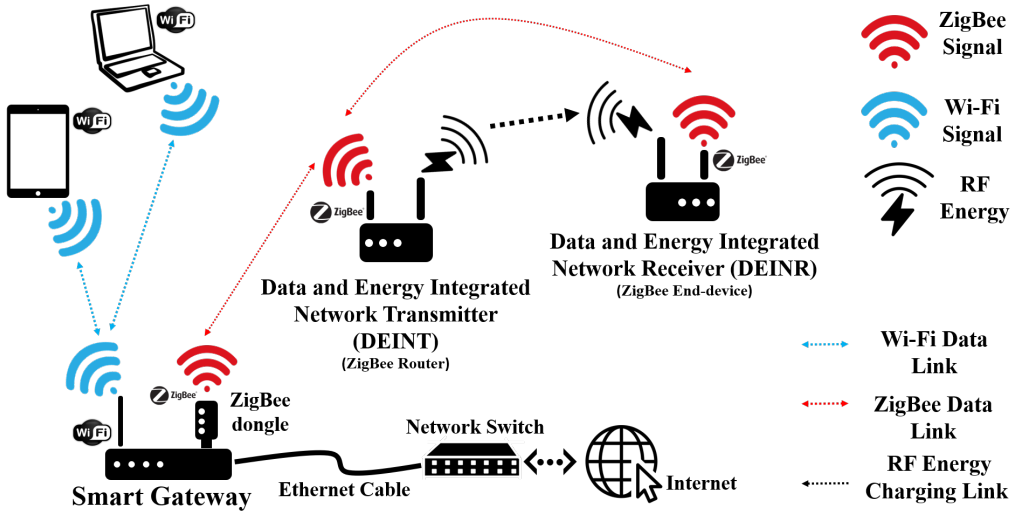

Figure 3.1: Network topology of thesis's designed DEIN

gle programmed as a ZigBee coordinator, the DEINT and the DEINR. The smart gateway, together with the ZigBee dongle, organizes two wireless networks, which are Wi-Fi standard WLAN and ZigBee based WSN. The smart gateway is connected to the network switch via ethernet cable, which connects the DEIN to the world. Wi-Fi devices such as the iPad and laptop are able to access the internet by connecting to the smart gateway. In the aspect of network behaviour, the DEINT works as a ZigBee router and the DEINR works as a ZigBee end-device. They are all managed by the ZigBee dongle. As ZigBee dongle is plugged into the USB port on the smart gateway, the Linux system running inside the smart gateway allows data communication between them. Hence, data exchange among all the devices in the DEIN can happen in the smart gateway. Therefore, ZigBee based devices in the DEIN can be remotely controlled and monitored by the network users who are in

charge of the DEIN. The standards used for Wi-Fi and ZigBee are IEEE 802.11n [108] and IEEE 802.15.4 [109], respectively.

Both the DEINT and the DEINR have two antennas. The Omni antenna serves for ZigBee based data communication, and the directional antenna is used for RF energy transmission or receiving. During the RF energy charging mode, the Omni antenna on the DEINT for data communication is disabled, and the RF energy, the power enhances carrier wave, is sent through the other directional antenna. When the power enhances carrier wave reaches to the DEINR side, the directional antenna on the DEINR's RF energy harvesting adapter only receives the energy from the carrier wave because the carrier wave will be passed to the RF-to-DC circuitry directly. The Omni antenna on the DEINR is used for receiving the data contained in the carrier wave as the Omni antenna will pass the carrier wave to the demodulator. In the typical data communication mode, the directional antenna on the DEINT for RF energy transmission is disabled. The communication happens only between the Omni antennas of the DEINT and the DEINR.

3.3 Hardware Design of DEIN Devices

3.3.1 The Smart Gateway

As the hardware structure described in Fig.3.2, the smart gateway is mainly structured by three parts, which are Wi-Fi module, USB circuitry and the

peripheral circuitry. The principal part is the Wi-Fi module with a high-speed Microprogrammed Control Unit (MCU) which is the AR9331 [110] from Atheros Communications, Inc. A fit Linux system, namely, the OpenWrt, is embedded in the Wi-Fi module, which embraces the Wi-Fi protocol stack. The PCB antenna on the module is responsible for Wi-Fi communication. The second part is the USB circuitry, which consists of a USB hub circuitry and four extended USB ports. The primary IC utilized for the USB hub circuitry is the USB2514B [111], a USB hub controller, which supports both USB 2.0 [112] and 1.1 [113] standard to compromise the low-speed ZigBee dongle. Furthermore, helped by the driver subjects to the USB 1.1 standard installed in the OpenWrt system, the USB circuitry provides a Plug and Play (PnP) manner to the ZigBee dongle. The peripheral circuity includes the Ethernet and General Purpose Input/Output (GPIO) ports. The smart gateway is connected to a network switch through the Ethernet port and cable, and the GPIO ports are left for future extension application.

3.3.2 The ZigBee Dongle

The hardware structure of ZigBee dongle depicted in Fig.3.3 is more straightforward than the smart gateway. Two main parts, the ZigBee circuity and the USB-to-serial converter, structures the ZigBee dongle. In the ZigBee circuity, the primary IC is the CC2530F256 [114], a MCU with the ZigBee protocol stack installed, which is programmed as a ZigBee coordinator. The chosen USB-to-serial converter is PL-2303HX [115], which converts the data from the CC2530F256's Universal Asynchronous Receiver-Transmitter

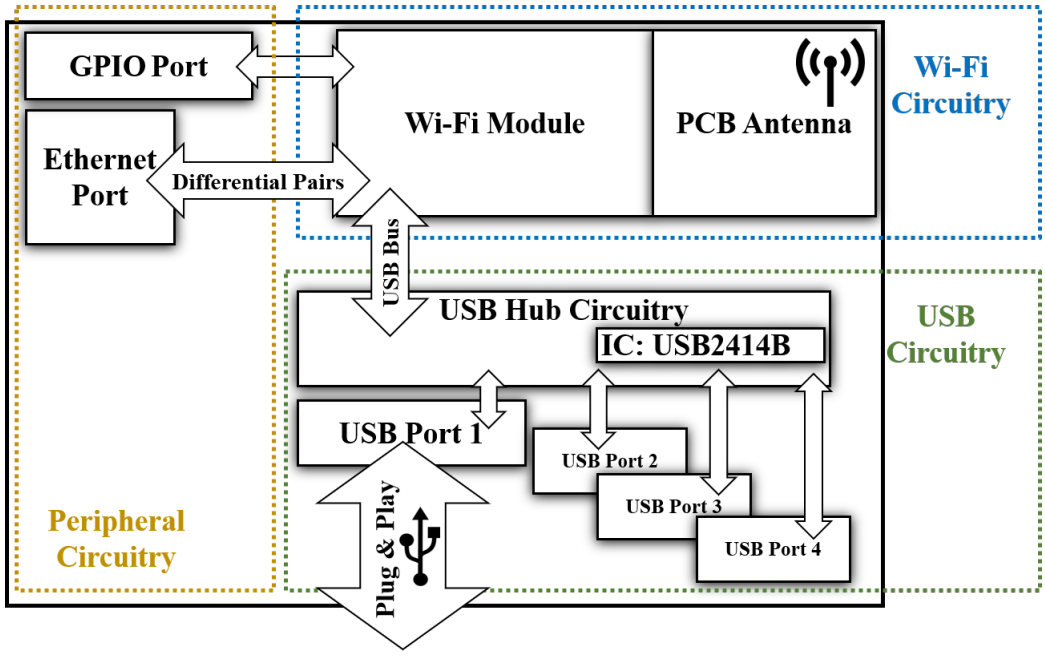

(a)

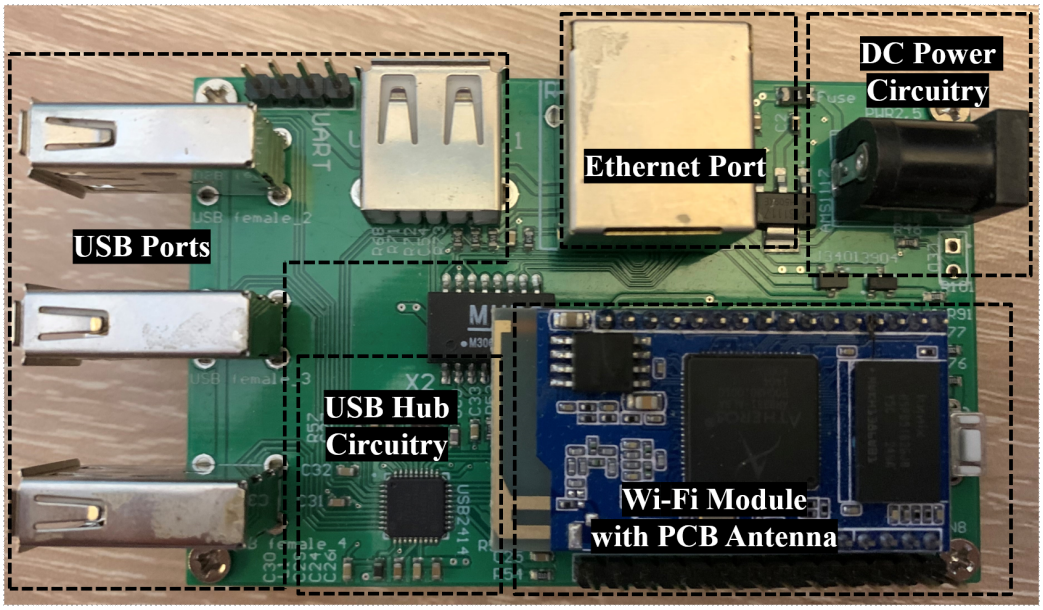

(b)

Figure 3.2: The hardware structure of the smart gateway: the block diagram (a) and the real product (b)

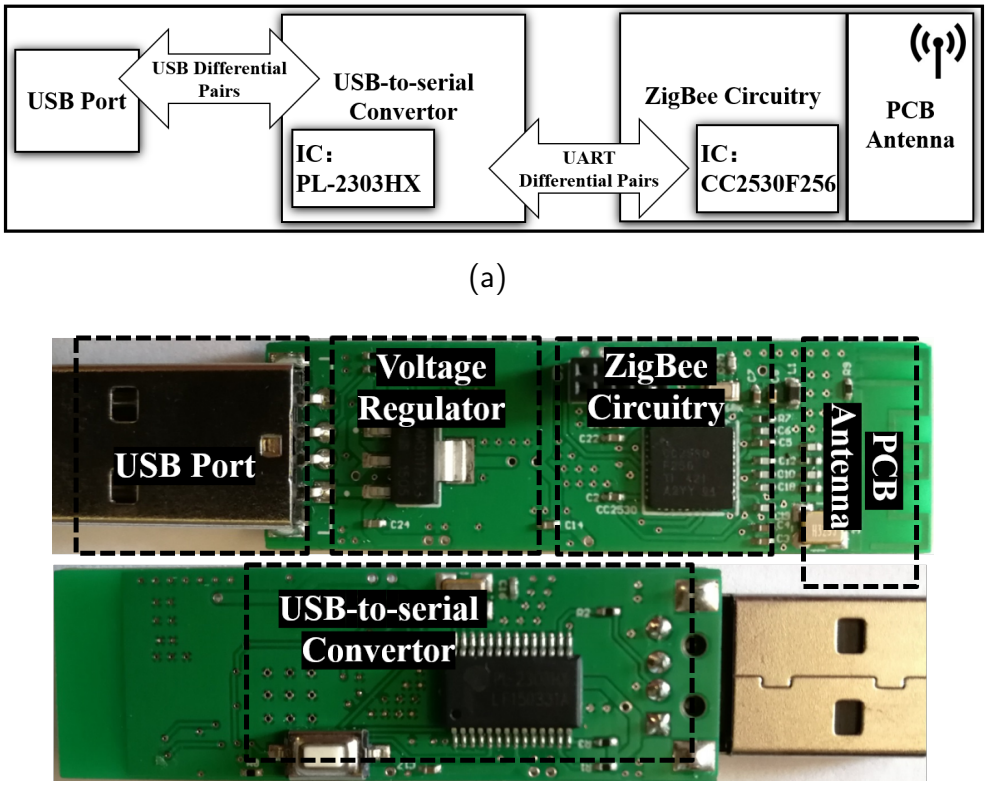

Figure 3.3: The hardware structure of the ZigBee dongle: the block diagram(a) and the real product(b)

(UART) pins to the differential pairs of the USB port and vice versa. The USB data speed is limited by the UART speed, which only complies with the USB 1.1 standard.

3.3.3 The Data and Energy Integrated Transmitter

The thesis's designed DEINT is described on the left side of the block diagram Fig.3.4a. The DEINT is structured with the DC supplier , ZigBee module, RF path selector, RF PA and two antennas. For the DC supplier, The chosen IC is the MP1584 [116], a step-down switching regulator to generate 5 V and up to 3 A constant DC power, which is a specific choice for the RF PA. The rest of the IC requiring 3.3 V power is supplied by another step-down DC-DC converter, the MCP16311/2 [117]. The ZigBee module integrates the CC2530F256 [114], a radio function IC with ZigBee standard protocol stack installed, which is configured as a ZigBee router by software. The AS179-92LF [118] is chosen as the RF path selector, which is a single-pole, double-throw switch. The single input pin of the RF path selector is connected to the unique RF interface of the ZigBee module, and its switching is controlled by the GPIO port of the ZigBee module. The SZM-2066Z [119] is utilized as the RF PA to increase the transmission power up to 33.5 dBm for sending the EPs.

Base on the ZigBee standard protocol stack running in the CC2530F256, the additional procedure is added to control the RF path selector and the RF PA for transmitting the RF energy. During the RF energy transmission mode, the RF PA is enabled, and the DEINT itself starts to create EPs. Then, the RF path selector is switched to move the created EPs to the RF PA with 2 W transmission power. Thereafter, the EPs are transmitted through the 14 dBi directional antenna. While in the communication mode,

the path to RF PA is blocked, and the conventional ZigBee data packets are sent through the Omni antenna directly.

3.3.4 The Data and Energy Integrated Receiver

The battery-less DEINR is described on the right-hand side of the block diagram Fig.3.4a. It is also designed with two antennas. The Omni antenna on the ZigBee module is used for fetching data from both DPs and EPs, while the directional antenna is only used for extracting the energy from the EPs. The impedance match circuit is deployed to maximize the RF energy from the antenna to the PCB trace. The Schottky diode, the HSMS-2862 [120], is utilized for building the rectifier. The rectifier is designed as a four-stage voltage doubler [121], which converts the RF waveform to high enough DC voltage to active the BQ25504 [122], the chosen IC for the power management circuitry. When the BQ25504 is activated by the DC voltage coming from the rectifier, it starts to boost the input voltage to charge the connected supercapacitor. Meanwhile, the BQ25504 draws the energy from the supercapacitor to the VSTOR pin, namely the output pin to drive the load. In other words, the voltage at the VSTOR pin represents the voltage of the supercapacitor. The VBAT_OK pin, the digital logic output, outputs logic 1 when the voltage of the supercapacitor is in the range from 3.9 to 2.5 V. The voltage range is hardware-programmed by deploying the registers with different values in the power management circuitry.

The TPS73101 [123] is deployed to regulate the voltage from the power

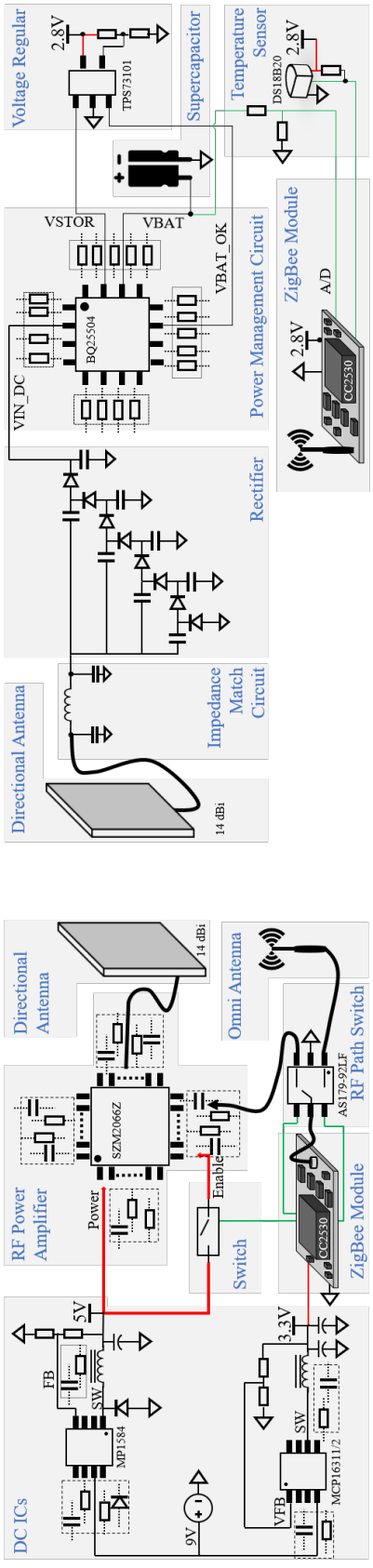

(a)

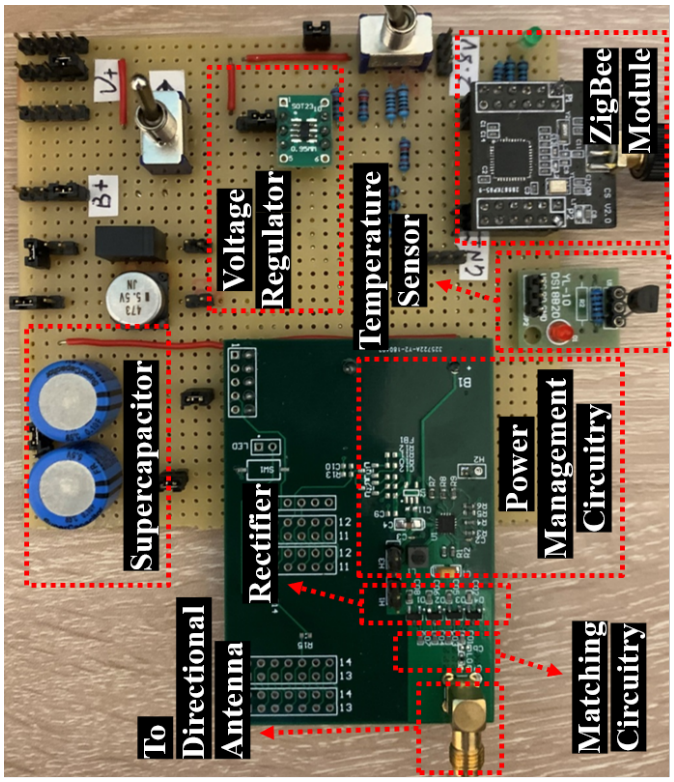

(c)

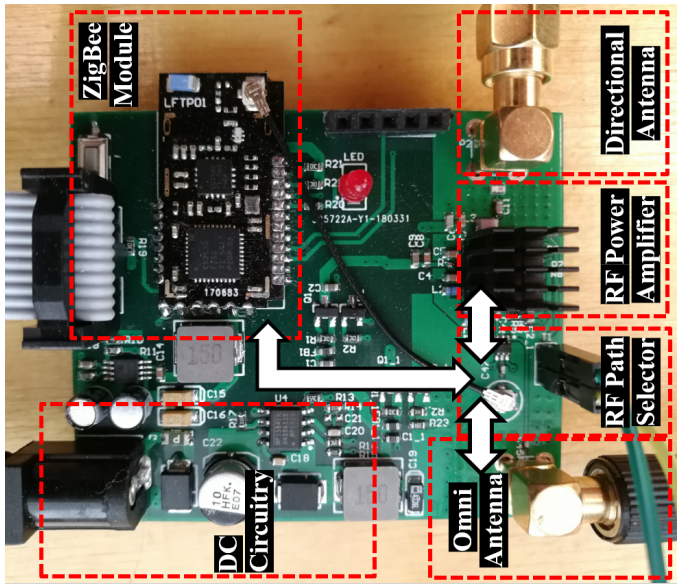

(b)

Figure 3.4: The hardware structure of the DEINT and DEINR: the block diagram (a), the real made DEINT(b) and the real made DEINR(c)

management circuitry to supply constant voltage for the ZigBee module and the temperature sensor. Its voltage-input pin is connected to the VSTOR pin, and the enable pin is connected to the VBAT_OK pin. After the voltage of the supercapacitor rises to 3.9 volts, the logic 1 is output from the VBAT_OK pin to enable the voltage regulator until the supercapacitor drops to 2.5 volts, and the TPS73101 is configured by the external registers to produce a stable 2.8 volts. The ZigBee module is programmed as a ZigBee end-device to collect the temperature sensor data then send the data to the ZigBee coordinator(ZigBee dongle) periodically. Meanwhile, it also monitors and sends the voltage of the supercapacitor regularly to the ZigBee coordinator.

3.4 Software Design for DEIN System

3.4.1 System Software Framework

The designed software framework for the DEIN system is depicted in Fig.3.5, which is constituted by the smart gateway system (OpenWrt system) and the ZigBee system organized by the ZigBee coordinator(dongle). The smart gateway has a higher authority than the ZigBee system, and it controls the ZigBee system by the method of writing character strings to the USB port where the ZigBee dongle is plugged in. In order to build the communication channel between the two systems, the protocol, namely, the AT command, is designed for exchanging data or sending instructions between the two systems. Furthermore, the AT command provides an instruction list, which

allows the smart gateway to control the ZigBee system such as creating or deleting a system event, adjusting the scheduling time for a specific system event, changing the network behaviour or transmission power for an individual ZigBee device, etc. Moreover, the reports from the ZigBee system, such as the temperature data, supercapacitor's voltage level of the DEINR, are uploaded to the smart gateway system via the AT command.

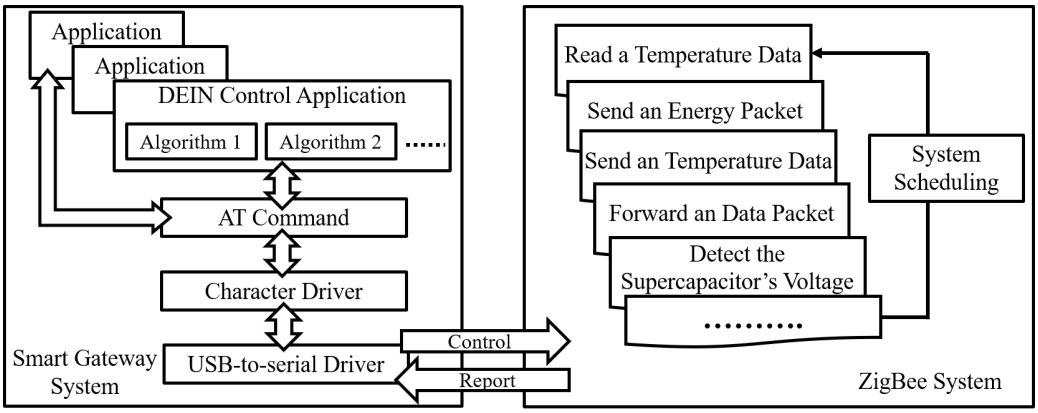

Figure 3.5: The software framework for the DEIN system

In the smart gateway system, the decisions for adjusting the DEINT or DEINR is made in the DEIN control application. According to the decision, the subsequent operations to the ZigBee system are translated as instructions in the form of a character string by the AT command protocol. Thereafter, the character string instructions are sent to the target USB port and finally to the ZigBee dongle through the character driver and USB-to-serial driver. Meanwhile, the character strings received from the ZigBee dongle are translated by AT command protocol. Then, the protocol passes the received data to the relevant application.

3.4.2 Utilize the Unoccupied Bandwidth for RF Energy Transmission

In the ZigBee based WSN system, normally, the ZigBee sensor data is uploaded at intervals of several seconds or minutes. There is unoccupied bandwidth left when the ZigBee sensor is not in data transmission or receiving mode. If the practical ZigBee based WSN is small-scale such as the WSN involved in the thesis's proposed DEIN, there will be more unoccupied bandwidth in the ZigBee based WSN. Therefore, the unoccupied bandwidth is utilized for sending the EPs created in the DEINT periodically, which is depicted in Fig.3.6a. At the beginning of time slot t_{EP}, the DEINT shifts to RF energy transmission mode, and an EP is created in the ZigBee module and then moved to the RF PA to transmit through the directional antenna. The value of the t_{EP} is determined by the duration of sending the EP, which relies on the EP's packet size. At the end of t_{EP}, the DEINT shifts back to conventional communication mode. The EPs are sent in every 10 ms, which is configured in a count down timer of the ZigBee system. The rest time is left for transmitting the conventional ZigBee DPs.

The packet format designed for the EP is described in Fig.3.6b, which complies with the framework of the Application Support (APS) sub-layer. The EP is broadcasted to all the network device without encrypted, and they can recognise the EP because of a 2-bytes field in the APS header, namely, the cluster identifier. In the APS payload field, the first byte indicates the charging status, which is filled with the boosting or the maintaining state.

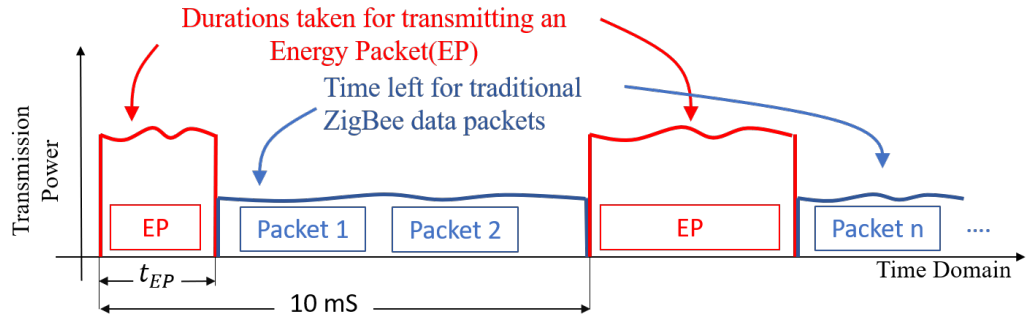

(a)

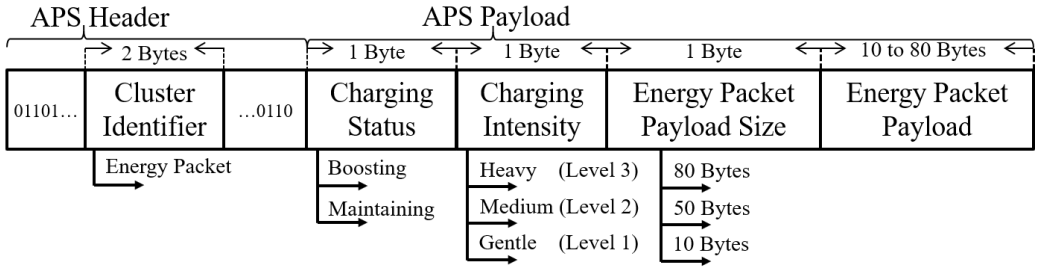

(b)

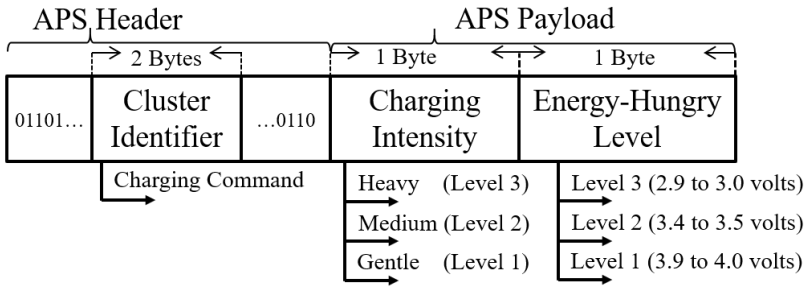

(c)

Figure 3.6: (a) The unoccupied bandwidth utilized for transmitting EPs; (b) Packet format designed for the EP; (c) Packet format designed for the charging command for controlling the DEINT

In the beginning, the supercapacitor on the battery-free DEINR has a nearly zero-volts initial voltage. When the system starts to charge and activate the DEINR, the charging status field in the EP is filled with the boosting state. After the DEINR is activated (powered on) and successfully joins the ZigBee network, the charging status field in the EP will be updated with the maintaining state. The boosting state tells other network devices not to communicate with the DEINR as it is still in off mode, while the maintaining state indicates that the DEINR is alive and the voltage of its supercapacitor will be maintained in a suitable range. The second byte in the APS payload field indicates the current charging intensity, and the third byte counts the number of bytes filled in the last packet field, namely, the energy packet payload field. The charging intensity is classified into three degrees, and its degree value determines how many bytes are required in the packet payload field. As a result, the EP has three different packet size, and the EP with bigger size requires a longer time to transmit, which represents the stronger charging intensity.

The packet format designed for the charging command is described in Fig.3.6c, which is also structured according to the ZigBee APS framework. Unlike the EP, the charging command packet is not transparent to all the network devices. If the charging command packet is transmitted from the ZigBee coordinator (ZigBee dongle) to the DEINT, it is used for controlling the charging intensity. However, if the charging command packet is sent from the RF energy harvester embedded ZigBee end-device to the ZigBee coordinator, it is for feedback. In the charging command packet, the APS payload field is designed only with two bytes, which represent the charging intensity

degree and the energy-hungry level of the battery-less DEINR, respectively.

The first byte indicates the degree of charging intensity. It is determined in the smart gateway, and the value of the first byte is assigned in the ZigBee coordinator. Before triggering the RF charging, the DEINT will not send any EP to the DEINR until the DEINT receives the charging command packet from the ZigBee coordinator. Furthermore, which size of EP should be created and sent by the DEINT is determined by that one-byte field. Moreover, the value of the charging intensity degree will be assigned to the field with the same name in the EP which is going to be created. The second byte in the APS payload field, the energy-hungry level, is only assigned by the battery-less DEINR. After the DEINR is powered on, it detects the voltage of the supercapacitor at regular intervals and grades its energy-hungry level according to the acquired sample values. As a result, the charging command packet used as feedback contains the latest DEINR's energy-hungry level, and the value of the charging intensity degree field is copied from the field with the same name in the last received EP.

3.4.3 An Adaptive Energy Management Mechanism

A designed adaptive energy management mechanism to maintain the energy level of the DEINR is described in the Fig.3.7, which describes the charging process from the voltage boosting stage to the voltage maintaining stage. The voltage feedback mechanism is applied in the voltage maintaining stage to achieve the adaptive charging control to manage the voltage level of the

supercapacitor on the battery-less DEINR and keep the DEINR always alive. At the beginning of the voltage boosting stage, the DEINR is in power-off mode, and the charging command is sent from the ZigBee coordinator to instruct the DEINT to broadcast the EPs with the highest charging intensity at constant intervals. Once the voltage of the supercapacitor on the DEINR reaches to 3.9 V, then the voltage regulator on the DEINR is enabled, which powers on the ZigBee module and its peripherals to activate the ZigBee function. Thereafter, the voltage maintaining stage starts.

In the voltage maintaining stage, the ZigBee module on the DEINR detects the supercapacitor's voltage in every 5 seconds and grades its energy-hungry level. The energy-hungry level is classified into three levels according to the acquired voltage, and the corresponding grading standard is indicated in Fig.3.6c. The lower the voltage is detected, the higher the energy-hungry level is classified. For instance, if the detected voltage is 3.9 volts, the current energy-hungry level is classified as level 1. After a while, if the voltage level is dropped to 3.8 volts, the current energy-hungry level is still level 1 until the voltage decreases to 3.5 volts. Then, the energy-hungry level will be updated to level 2. Once the energy-hungry level is confirmed, the value of the charging intensity degree will be fetched from the latest received EP, which is used for comparing with recent detected energy-hungry level. If they are equal, the voltage detection process will be executed again in the next 5 seconds. Otherwise, their values will be assigned to a charging command packet, which will be sent from the DEINR to the ZigBee coordinator as feedback. Thereafter, the feedback will be handed over to the smart gateway, and then the coordinator will prepare the charging command packet according to the

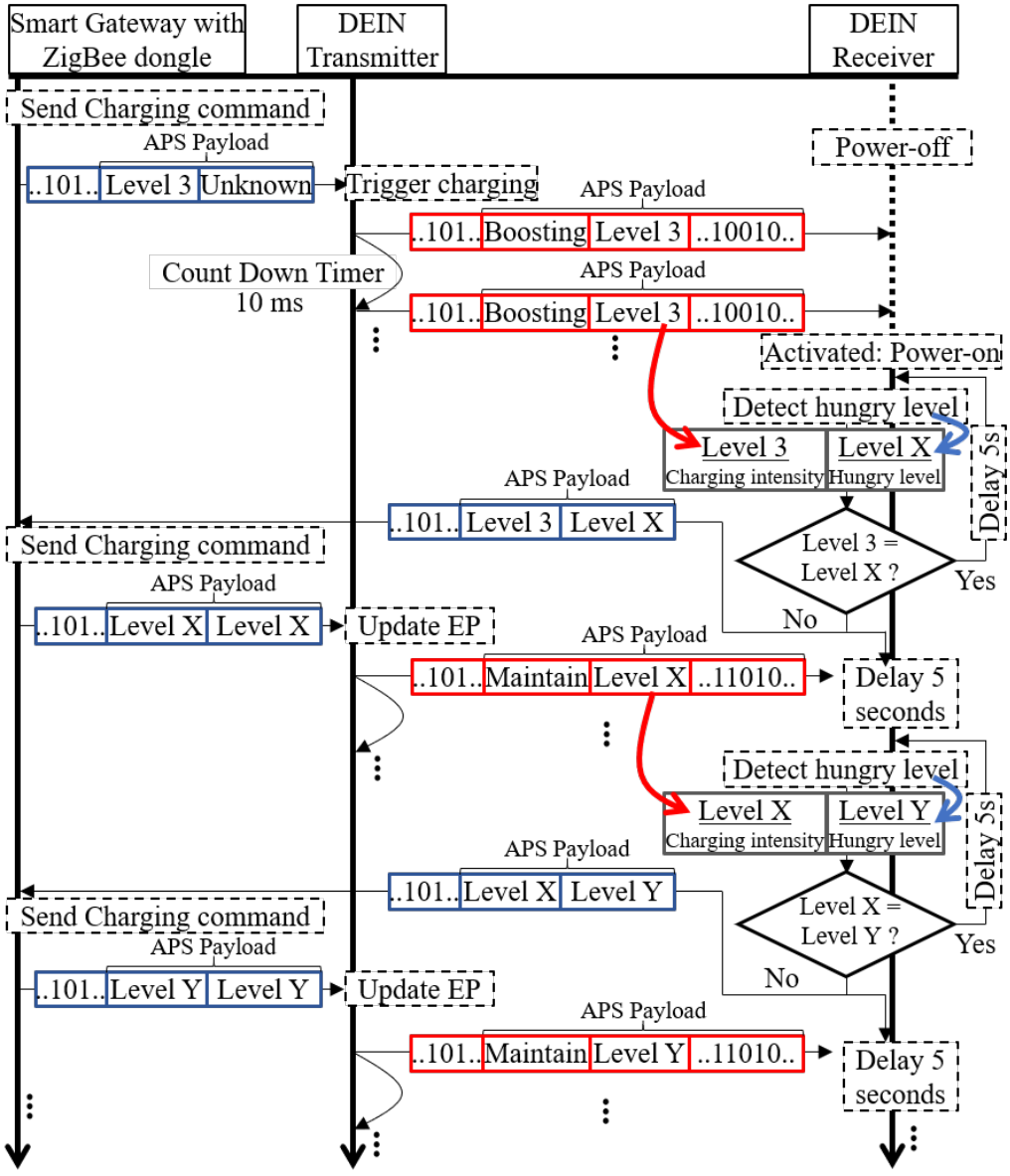

Figure 3.7: The adaptive energy management mechanism designed to maintain the energy level of the DEINR

decision made by the smart gateway and sent to the DEINT to update the charging intensity.

3.5 System Evaluation

3.5.1 The Experiment Platform

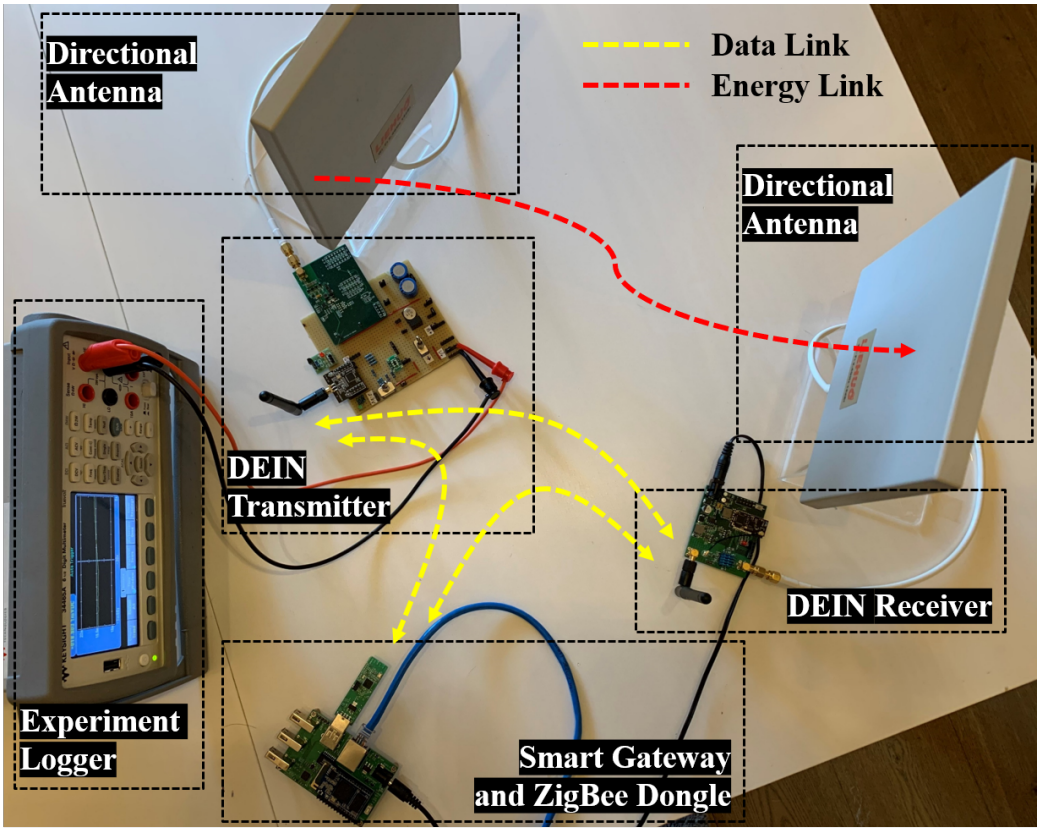

Figure 3.8: Experimental platform of DEIN

The experiment platform for the thesis's designed DEIN system is de-

picted in Fig.3.8, which consists of a pair of ZigBee based DEINT and DEINR, a smart gateway with ZigBee dongle plugged in and an experiment logger. The DEINT and DEINR are programmed as ZigBee router and end-device, respectively. The DS18B20, the temperature sensor, is equipped on the DEINR. The capacitance of the supercapacitor embedded on the DEINR is 0.2 F, which is obtained by connecting two 0.1 F supercapacitors in parallel. Two 14 dBi panel shape antennas are deployed only for RF energy transmission and receiving. One is connected to the DEINT's RF PA, and the other is connected to the DEINR's RF energy harvesting adapter. The small Omni antennas on the DEINT and DEINR are only used for sending or receiving the DPs. The instructions to control the DEINT are come from the ZigBee dongle programmed as the ZigBee coordinator. A digital multimeter is invoked as an experiment logger for monitoring and recording the variation of the supercapacitor's voltage level during each experiment.

3.5.2 RF Energy Charging Experiment

The experiments carried out in this section are designed for evaluating the RF energy charging performance of the thesis's designed DEIN system. The experiments aim to study the impacts of the different experimental parameter on the RF energy charging speed, such as different RF energy transmission distance between the two directional antennas and the EPs with different APS payload size. Therefore, two sets of experiments are designed. The first set uses the same EP but different RF energy transmission distances. The second set uses the same RF energy transmission distance but EPs

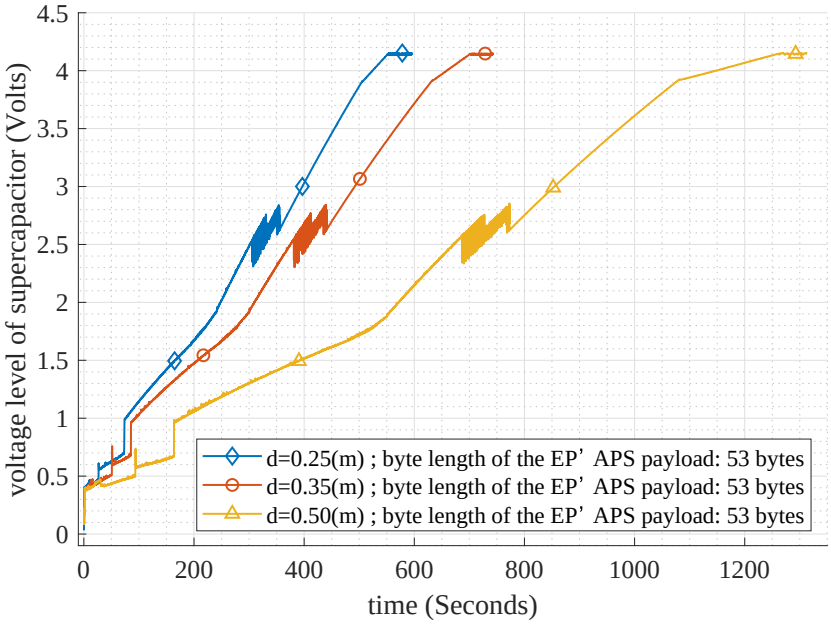

(a)

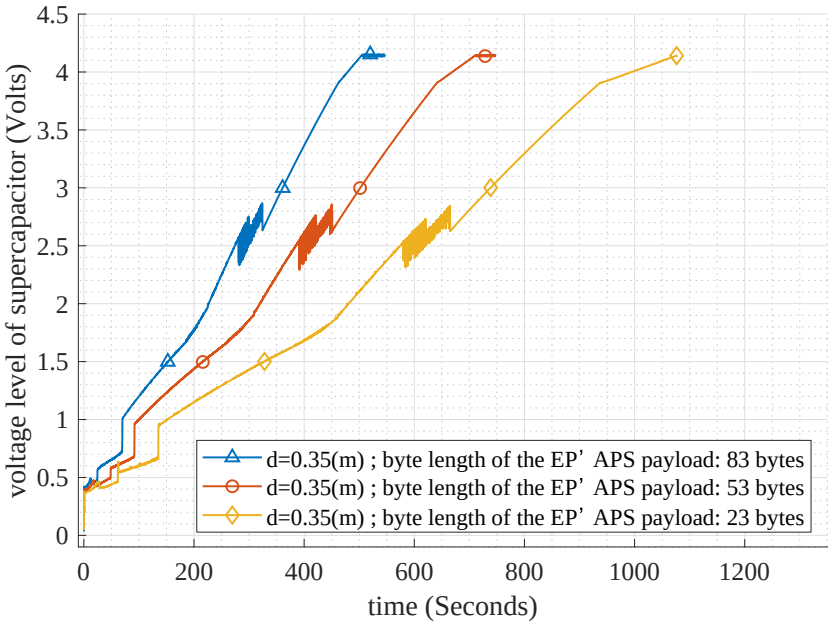

(b)

Figure 3.9: The voltage level of the DEINR's supercapacitor; (a)when different RF energy transmission distance $d = \{0.20, 0.35, 0.50\}$ m is considered with using the same byte length (53 bytes) to fill in the EP's APS payload field; (b) when different APS payload sizes, 23, 53 and 83 bytes, are used for creating EPs with a fixed RF energy transmission distance $d = 0.35\,\text{m}$.

with different APS payload sizes. At the beginning of each experiment, the supercapacitor's voltage is reset to 0 V. During each experiment, the DEINT transmit an EP to charge the DEINR in every 10 ms, and a voltage logger is used for tracing the supercapacitor's voltage. To prevent the energy usage of the ZigBee circuitry and the sensor on the DEINR from affecting the supercapacitor's voltage, the voltage regulator which supplies constant DC voltage to the ZigBee related circuitry is switched off. Therefore, in each experiment, the target voltage level of the supercapacitor is 4.15 V, which is restricted by the power management circuitry. As a result, the captured traces of the supercapacitor's voltage along the timeline and plotted in Fig.3.9.

Observe from the first set of experiments in Fig.3.9a, the rising speed of supercapacitor's voltage reflects the RF energy charging speed. In this set of experiments, the impact of different RF energy transmission distance d on the rising speed of supercapacitor's voltage is studied. Observe from Fig.3.9a that increasing the transmission distance d can substantially increase the charging time to achieve the targeted 4.15 V. For example, when the transmission distance is $d = 0.25$ m, the voltage of the DEINR's supercapacitor reaches to 4.15 V after 550 seconds around. By contrast, when the transmission distance is increased to $d = 0.50$ m, the voltage of the supercapacitor reaches to 4.15 V after 1200 seconds. This is because a longer transmission distance imposes a higher path loss on the RF signal, which may induce more energy loss. Therefore, the charging time can be substantially increased.

The impact of different byte length utilized to fill in the EP's APS pay-

load field on the RF energy charging speed is also studied, where the RF energy transmission distance is fixed to 0.35 m. Observe from Fig.3.9b that using bigger size APS payload to create EPs for RF energy transmission can speed up the charging. During each experiment, if the created EP uses 83 bytes to fill in its APS payload field, it takes 500 seconds around to charge the supercapacitor from 0 V to 4.15 V. By contrast, when the EP's APS payload only contains 23 bytes, it takes more than 1000 seconds to charge the supercapacitor to the desired voltage.

3.5.3 The Adaptive Energy Management Experiment for DEINR

The experiment for evaluating the adaptive energy management mechanism is carried out in this section. Two directional antennas are placed face to face with the distance of 0.45 m. The voltage logger is used for monitoring the voltage level of the supercapacitor on the DEINR, and its voltage trace along the timeline is plotted in Fig.3.10a. At the beginning of the experiment, the supercapacitor is discharged to 0 V, and the DEINR is in power-off mode. The highest charging intensity level is used for the initial charging state, namely, the boosting state. The periodically created EP for charging the DEINR is filled with 80 bytes dummy data in its energy packet payload field, and the 10 ms interval between sending adjacent EPs is configured in the system count down timer. During the boosting state, the voltage of the DEINR's supercapacitor rapidly grows by harvesting the energy contained in the EPs from the DEINT.

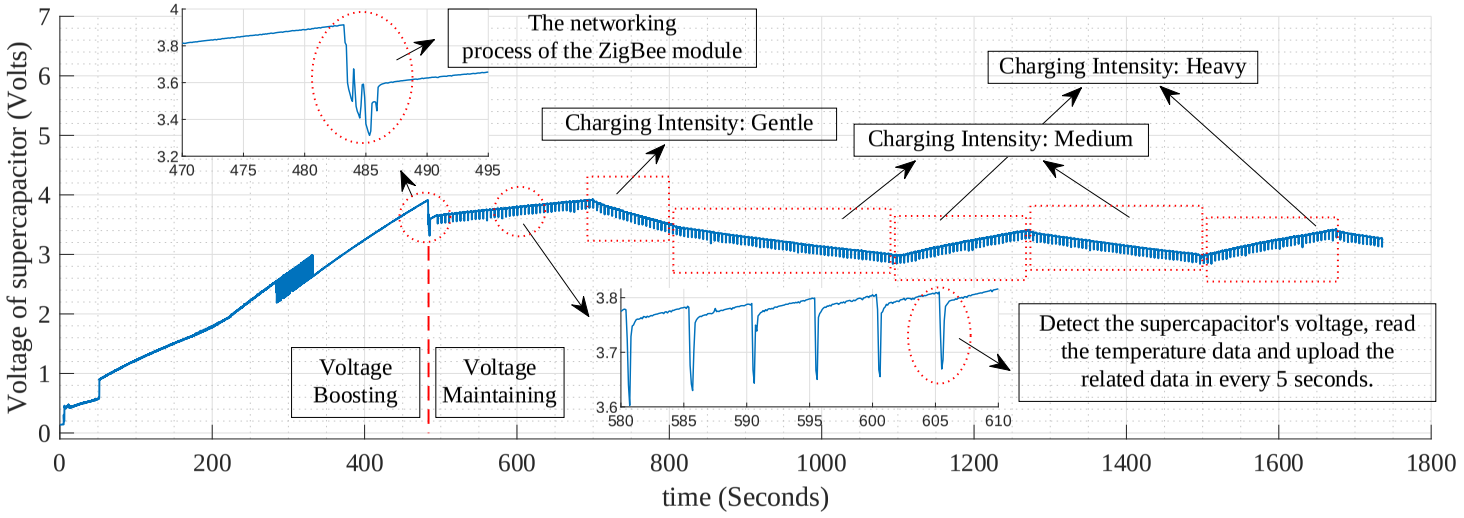

(a)

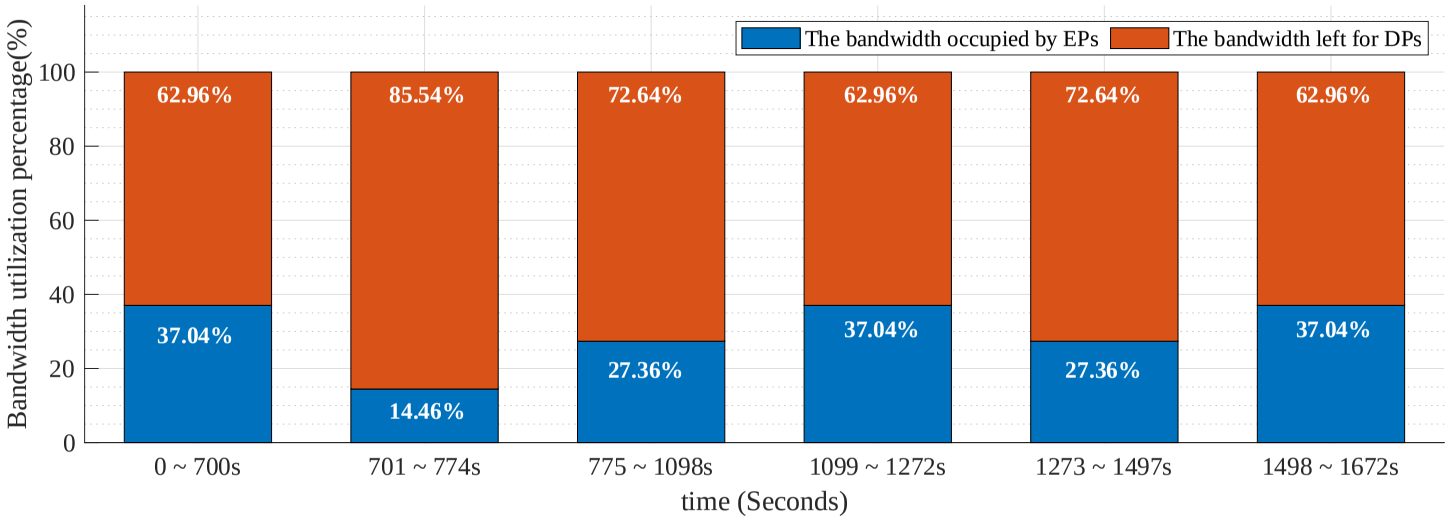

(b)

Figure 3.10: The voltage level of the DEINT's supercapacitor(a) and the bandwidth utilization percentage for EPs and the remaining bandwidth for the conventional ZigBee data communication(b) when applying the adaptive energy management mechanism

At the 483 seconds of the experimental timeline, the supercapacitor's voltage rises to 3.9 V, which is the threshold voltage to enable the DEINR's voltage regulator. Thereafter, the voltage regulator converts the supercapacitor's voltage to 2.8 V and powers on the ZigBee module together with the temperature sensor. Then, the immediate networking process after powering on the ZigBee module is carried out, which takes about 3 seconds and causes a massive voltage drop on the supercapacitor. After joining in the ZigBee network, the ZigBee module is scheduled to detect the supercapacitor's voltage, read the temperature data and upload the acquired data at every 5 seconds interval, which causes the regular sharp voltage drop along the timeline. When the ZigBee dongle(coordinator) recognizes that the DEINR is activated, the voltage maintaining state begins.

Since the first sample value of the supercapacitor's voltage is higher than 3.5 V but lower than 3.9 V, which does not belong to either the energy-hunger level 2 nor 1 classified in Fig.3.6c. Hence, at the beginning of the voltage maintaining state, the charging intensity is still kept with the highest level until the supercapacitor's voltage rises to 3.9 V, the boundary value of the energy-hunger level 1. Thereafter, at the 700 seconds of the experimental timeline, the charging intensity is changed to the lowest level, and the supercapacitor's voltage starts to decrease. Around the 800 seconds of the experimental timeline, the supercapacitor's voltage drops into the range of the energy-hunger level 2, and the medium charging intensity is applied to the DEINR, which slows down the voltage decrease. After a while, the supercapacitor's voltage drops into the range of the energy-hunger level 3, and the highest charging intensity is applied again. Under the medium charging

intensity, the harvested energy cannot afford the energy consumption caused by the behaviours of the DEINR. However, under the highest charging intensity, the harvested energy is higher than the energy demand, and the unused energy accumulated in the supercapacitor rises its voltage level. Hence, at the tailer of the experimental timeline, the supercapacitor's voltage alternatively decreases and recovers.

According to the functionality of the RF PA employed in the DEINT, its power detector pin can output a reference voltage to indicate the real-time transmission power when amplifying and transmitting the RF waves. Since the RF PA is only used for transmitting EPs, it shows periodic pulses when using the oscilloscope to trace the output voltage from the power detector pin during the experiment. Hence, the time taken for sending the EP is obtained by measuring the pulse width from the oscilloscope. Thereafter, the bandwidth utilization percentage of EP can be worked out by calculating the ratio between the measured duration for sending the EP and the constant interval between adjacent EPs. Fig.3.10b shows the percentage of bandwidth utilized for transmitting EPs and the bandwidth left for the conventional data communication along the experimental timeline. The higher the charging intensity is applied, the more bandwidth is occupied for transmitting EPs. As a conclusion, a maximum 37.04% bandwidth is utilized for surviving the DEINR when the highest charging intensity is applied. In average, the 69.95% bandwidth is still available for conventional ZigBee data communication.

3.6 Chapter Summary

In this chapter, an author's proposed DEIN system is introduced. Also, the hardware design of all included devices is described in details. Besides, the developed software framework for controlling the system is described. Based on the DEIN system platform, an adaptive energy management mechanism is proposed to automatically maintain the voltage level of the supercapacitor on the DEINR. To realize the mechanism, an energy management protocol is designed to exchange the energy information between the DEIN system and the DEINR. Also, the protocol is responsible for adjusting the RF energy charging intensity based on the energy feedback from the DEINR. Relevant packet formats are designed for the protocol such as the packet format of the EP, the command to adjust the RF energy charging intensity and the energy feedback packet to indicate the energy-hungry level of the DEINR. The experiments have shown that the supercapacitor's voltage increase to 3.9 volts from 0 volts as time goes on. Then, the DEINR is switched on to join in the network. It proves that the RF energy contained in the EPs from the DEINT is successfully harvested by the DEINR and converted to the DC energy in the DEINR's supercapacitor. What's more, the adaptive energy management mechanism is successfully applied to boost and then maintain the supercapacitor's voltage to power the DEINR and keep it always on. Meanwhile, the ZigBee module of the DEINR behaves as ZigBee end-device to periodically upload the temperature data, which proves the data communication and the RF energy transmission/harvesting can coexist in the author's designed DEIN system. In the end, the bandwidth utilization

percentage for EPs and the remaining bandwidth for the traditional ZigBee data communication is analysed.

Chapter 4

Bandwidth Allocation Algorithm to Maximize the Throughput of Wireless Information

4.1 Introduction

As discussed in Chapter 3, the adaptive energy management mechanism relies on the periodic feedback of the supercapacitor's voltage level from the DEINR. According to the acquired voltage level, the DEIN system decides which charging intensity (EP's packet size) should be used for RF energy

transmission. However, according to the results plotted in Fig.3.10a, the highest charging intensity supplies more RF energy to the DEINR than the energy required by the DEINR to stay alive, and the lowest charging intensity supplies insufficient RF energy. Furthermore, the higher charging intensity means sending bigger size EPs , which squeezes more bandwidth which was used for wireless information transmission, namely, the conventional ZigBee data communication in the thesis's designed DEIN. Hence, a solution, transmitting the minimum required RF energy to the DEINR, is proposed in this chapter, which optimizes the bandwidth for sending EPs to free more bandwidth for the conventional ZigBee data communication, namely, maximize the throughput of wireless information in the DEIN. The minimum required RF energy keeps the voltage of the DEINR's supercapacitor on a stable level after it successfully joins the ZigBee network, which compensates the energy consumed due to the DEINR's behaviours such as reading temperature data, sending/receiving wireless data, turning on an LED light, etc.

In section 3.4.3, the constant interval (10 ms) is used for transmitting adjacent EPs. It is realized by resetting a count down timer before sending each EP. As the DEINT is designed based on the ZigBee router, the computing power of the DEINT is less than the smart gateway as the microcontroller of the ZigBee router is less powerful. Use constant interval makes less calculation burden, which makes the DEINT more stable. However, the adaptive energy management mechanism didn't consider the impact on the throughput of wireless information. It prioritises RF energy transmission. In this chapter, a scheduling cycle model is proposed to organize EPs' transmission, which offers an adjustable interval to send EPs. Furthermore, the energy

conversion model is proposed to model the relationship between the transmitted RF energy from the DEINT and the final stored DC energy in the DEINR's supercapacitor. If the DEINR's minimum required energy is known to the DEIN system, based on the model, the system can precisely control how much RF energy should be transmitted. Moreover, based on the energy conversion model, the mathematical equation to represent the conversion of energy from the DEINT to the DEINR is worked out by the experimental methods. Finally, with the help of the mathematical equation, a bandwidth allocation algorithm is designed to maximize the bandwidth allocated for normal ZigBee data communication to maximize the throughput of wireless information in the DEIN. It optimizes the arguments in the mathematical expression such as the EP's packet size and the interval to send adjacent EPs to minimize the bandwidth for sending EPs in the condition of meeting the DEINR's minimum energy requirement.

The remainder of this chapter is organized as follows. The scheduling cycle model and the RF energy transmission and harvesting model are introduced in Section 4.2. Section 4.3 introduces the derivation of the energy conversion equation as well as the utilized experimental methods. In Section 4.4, the designed bandwidth allocation algorithm is described. The last Section 4.5 shows the experimental results to prove the energy conversion equation and the benefit of the bandwidth allocation algorithm.

4.2 System Modelling

4.2.1 A Scheduling Cycle Model

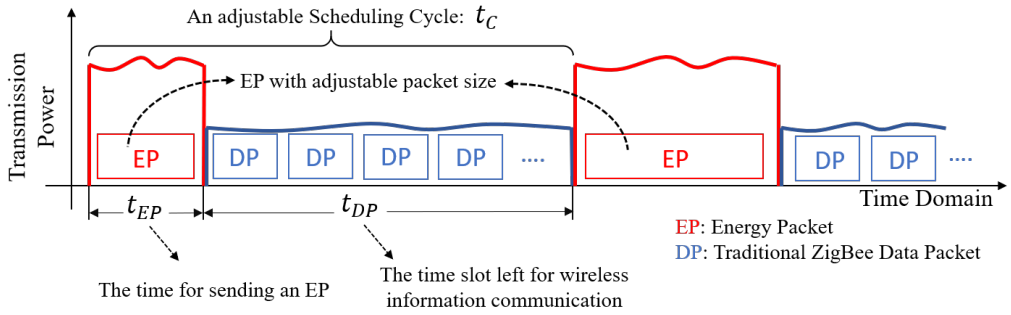

Figure 4.1: The scheduling cycle model to organize the EPs and DPs in different time slot.

To reduce the interference to conventional ZigBee data communication caused by sending EPs, different time slots are allocated for sending EPs and the conventional ZigBee data packets. Based on this time-division concept, a scheduling cycle model is proposed and described in Fig.4.1. It is a new scheduling method, which is specifically designed for allocating EPs and DPs. According to the model, t_C represents the adjustable interval between sending two adjacent EPs. The t_{EP} is the time taken to send an EP in the DEINT, which depends on the packet size of the EP. The rest of the time slot, t_{DP} is allocated for the conventional ZigBee data communication, and packets involved in the data communication are simply named as DP. Since the EPs and DPs are organized by the scheduling cycle in the different time slot, only a unique EP or DP is transmitted at a specific time. Hence, the scheduling

cycle integrates the RF energy and wireless information transmission by the time-division method.

Due to the energy loss in the air, the RF energy transmission distance is less than 1 m in the practical DEIN system. If the longer distance is applied, the DC energy produced from the RF-to-DC circuit cannot active the energy management circuit. The latter is used for boosting the DC energy to charge the supercapacitor. Compared to the duration of t_{EP}, the EP's propagation time from the DEINT to the DEINR is extremely short and can be ignored. Hence, it is recognized that EP's transmission in the DEINT and harvesting by the DEINR happen simultaneously. In a single scheduling cycle (t_C), the harvested DC energy during time t_{EP} shall afford the energy usage of the DEINR during the whole cycle time.

4.2.2 RF Energy Transmission and Harvesting Model

The model depicted in Fig.4.2 describes the process of energy conversion through transmitting a EP from the DEINT to the DEINR. In the beginning, the EP is created in the sending buffer of the DEINT and moved to the RF PA. Then, it is transmitted to the DEINR in the form of RF energy. Thereafter, the RF energy is converted as inductive energy by the receiving antenna. With the help of the energy conversion circuitry, the inductive energy is finally converted to DC energy stored in the supercapacitor. Also, the energy loss in the energy conversion circuitry is introduced. By referring Friis transmission equation [124], the relationship between the transmitted

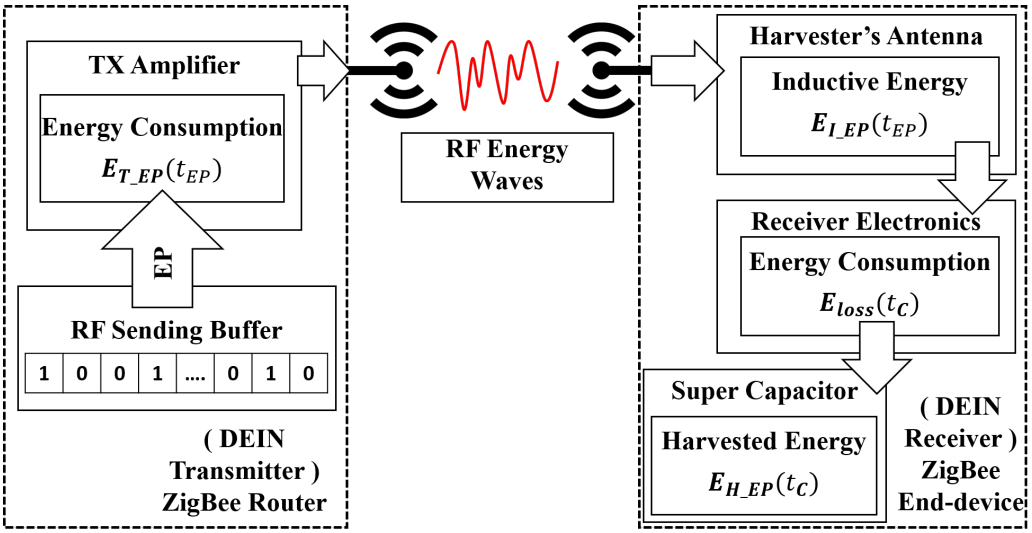

Figure 4.2: Energy conversion model for transmitting and harvesting an EP

energy from the DEINT and the inductive energy by the receiving antenna is modelled as,

$$\begin{aligned} E_{I\_EP}(t_{EP}) &= E_{T\_EP}(t_{EP}) \times \frac{P_r \times t_{EP}}{P_t \times t_{EP}} \\ &= E_{T\_EP}(t_{EP}) \times G_r G_t (\frac{\lambda}{4\pi d})^2 \end{aligned} \tag{4.1}$$

As the propagation time of the RF waves is not taken into account, t_{EP} is the time of sending the EP by the DEINT as well as the time of harvesting its RF energy by the DEINR. $E_{T\_EP}(t_{EP})$ represents the transmitted RF energy contained by an EP, and $E_{R\_EP}(t_{EP})$ represents the inductive energy through receiving the EP via the receiving antenna. P_r and P_t are power fed into the transmitting and power delivered at the receiving antennas, respectively. G_t and G_r are antenna gain of the transmitting and receiving antennas, respectively. λ is the wavelength of the RF wave, and d is the RF energy transmission distance between transmitter and harvester.

According to the scheduling cycle model, the time taken for transmitting and receiving is t_{EP} in a single scheduling cycle. However, the possible energy loss happens in the circuitry of the DEINR may last from the beginning to the end of the single scheduling cycle. Hence, considering a single scheduling cycle, the harvested DC energy in the supercapacitor, the $E_{H\_EP}(t_C)$, is expressed as,

$$E_{H\_EP}(t_C) = E_{I\_EP}(t_{EP}) - E_{loss}(t_C) \tag{4.2}$$

Where $E_{loss}(t_C)$ is introduced to represent all possible energy loss in the DEINR circuitry during a scheduling cycle t_C. Thereafter, if the event, the $E_{I\_EP}(t\_EP)$, is replaced by equation(4.2), the relational expression between the $E_{H\_EP}(t_C)$ and the $E_{T\_EP}(t_{EP})$ is expressed as,

$$E_{H\_EP}(t_C) = E_{T\_EP}(t_{EP}) \times G_r G_t (\frac{\lambda}{4\pi d})^2 - E_{loss}(t_C) \tag{4.3}$$

4.3 Energy Conversion Equation

In order to keep the voltage level of the DEINR's supercapacitor stable, the whole harvested DC energy must meet the sum of energy consumption in the DEINR. By considering a single scheduling cycle, the harvested DC energy stored in the supercapacitor during this period shall be sufficient for the energy usage of the DEINR. Based on this concept, with the help of Equ.4.3, the supercapacitor's increased DC energy during a single scheduling cycle t_C

is expressed as,

$$\begin{aligned} E_{inc}(t_C) &= E_{H\_EP}(t_C) - E_{usage}(P_R, t_C) \\ &= (E_{T\_EP}(t_{EP}) \times G_r G_t (\frac{\lambda}{4\pi d})^2 - E_{loss}(t_C)) \\ &\quad - E_{usage}(P_{DEINR}, t_C) \end{aligned} \tag{4.4}$$

Where

$$E_{T\_EP}(t_{EP}) = P_{DEINT} \times t_{EP}$$
$$E_{usage}(P_{DEINR}, t_C) = P_{DEINR} \times t_C$$

The $E_{usage}(P_{DEINR}, t_C)$ defines the sum of energy usage of the DEINR in a scheduling cycle t_C. The $E_{H\_EP}(t_C)$ is the harvested and free-to-use DC energy in supercapacitor in t_C. The P_{DEINT} is the transmission power of the RF PA on the DEINT to transmit the EP, and the P_{DEINR} is the equivalent power depends on the activities of the DEINR such as reading data from sensors, uplink communications, flashing the LED, etc. Hence, the transmitted RF energy in time t_{EP}, namely, the $E_{T\_EP}(t_{EP})$, is expressed as $P_{DEINT} \times t_{EP}$, and the $E_{usage}(P_{DEINR}, t_C)$ is represented by $P_{DEINR} \times t_C$.

Basing on the practical DEIN scenario, the RF energy transmission distance d between the DEINT and DEINR is known to the system. Besides, the P_{DEINT}, the G_r, the G_t and the λ are constant coefficients according to the hardware design. Therefore, the system variables in Equ.4.4 are P_{DEINR}, t_C, t_{EP} and $E_{loss}(t_C)$. With the help of the energy conversion Equ.4.4, the required number N of the scheduling cycles (t_C) to send EPs is modelled as mathematical expression(4.5), which charge the DEINR's supercapacitor

from a certain voltage level to a required voltage level.

$$N = \begin{cases} \dfrac{E_{cap\_gap}}{E_{inc}(t_C)}, & (E_{inc}(t_C) > 0) \\ \infty, & (E_{inc}(t_C) = 0) \\ not\ applicable, & (E_{inc}(t_C) < 0) \end{cases} \tag{4.5}$$

Where

$$E_{cap\_gap} = \tfrac{1}{2}(V_{end}^2 - V_{start}^2) \times C$$

C is the capacitance of the supercapacitor. V_{end} and V_{start} represent the end and the beginning voltage of the supercapacitor respectively in a RF energy charging duration. The V_{start} and the V_{end} can be measured by the voltage logger prior to triggering the charging procedure and after the terminating sending any EPs, respectively. Hence, according to the capacitor's energy definition, E_{cap_gap} defines the supercapacitor's energy gap between its voltage level from V_{start} to V_{end}. By introducing the definition of $E_{inc}(t_C)$, the number(N) of required scheduling cycles to charge the supercapacitor from V_{start} to V_{end} is classified into three situations. When $E_{inc}(t_C)$ is positive, it means the harvested DC energy is higher than the energy usage of the DEINR, and there is energy increment in supercapacitor in each scheduling cycle. When $E_{inc}(t_C)$ is equal to 0, the harvested DC energy is entirely consumed by the DEINR during each scheduling cycle. In this state, the continuous and infinite scheduling cycles holds the supercapacitor's voltage level without any variation. However, if $E_{inc}(t_C)$ is negative, the harvested energy cannot afford the energy usage of the DEINR, and the supercapacitor will continually discharge, which cannot be accepted in the DEIN system.

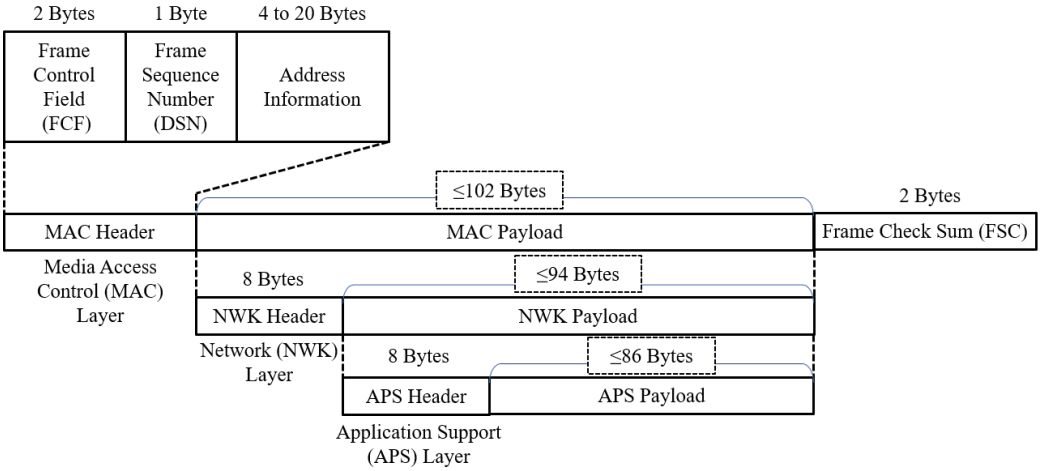

Figure 4.3: The format of ZigBee based MAC layer packet involving a ZigBee standard APS data packet.

4.3.1 The t_{EP}: Time of Transmitting an EP

The EP is created as a ZigBee standard APS data packet and finally packeted as a ZigBee based MAC layer packet to transmit. Fig.4.3 shows the format of the MAC layer packet as well as the format of its contained APS data packet. Since the purpose of the APS data packet is defined in the APS header, the other devices in the DEIN system can tell the EP packet without accessing its payload. Subject to the ZigBee standard [125], the maximum byte length of the APS payload is restricted within 86 bytes as the size of the header in each layer is regulated by the ZigBee standard and the maximum byte length of the MAC layer packet is limited to 127.

As a significant input of (4.4), the t_{EP}, namely, the time of transmitting the EP, needs to be configured precisely in the DEIN system. However,

t_{EP} cannot be directly configured, and the only method is adjusting the byte length used for filling in the EP's APS payload field. Therefore, the mathematical relation between the t_{EP} and the number of bytes filled in the EP's APS payload field is essential. It is used for instructing the DEIN control system that how many bytes are needed to fill in the EP's APS payload field to obtain the desired t_{EP}. In this section, the mathematical relationship is derived by using the experimental methods.

A set of experiments are carried out to send the EPs by constant intervals (40 ms). As the duration of sending the EP is measured via oscilloscope, a relative longer interval could be easier to measure due to the limited sample rate of the oscilloscope. By considering the restriction on the APS payload size, the different byte length is used for filling the APS payload field of the created EPs in each experiment, and all involved byte lengths in the set of experiments are within 86 bytes. the t_{EP} can be measured by an oscilloscope in each experiment, and a set of t_{EP} values are finally collected versus different APS payload sizes. After that, the curve is structured to fit the set of collected t_{EP} values. Finally, the mathematical relation between the t_{EP} and the byte length of the APS payload is obtained based on the structured curve.

The SZM-2066Z [119], the RF PA chip embedded in the DEINT, integrates an RF power detector. According to the datasheet of the SZM-2066Z, the transmission power of the RF PA can be detected by measuring the voltage on the output pin of the RF power detector. Furthermore, the higher transmission power the RF PA uses, the higher voltage can be detected on

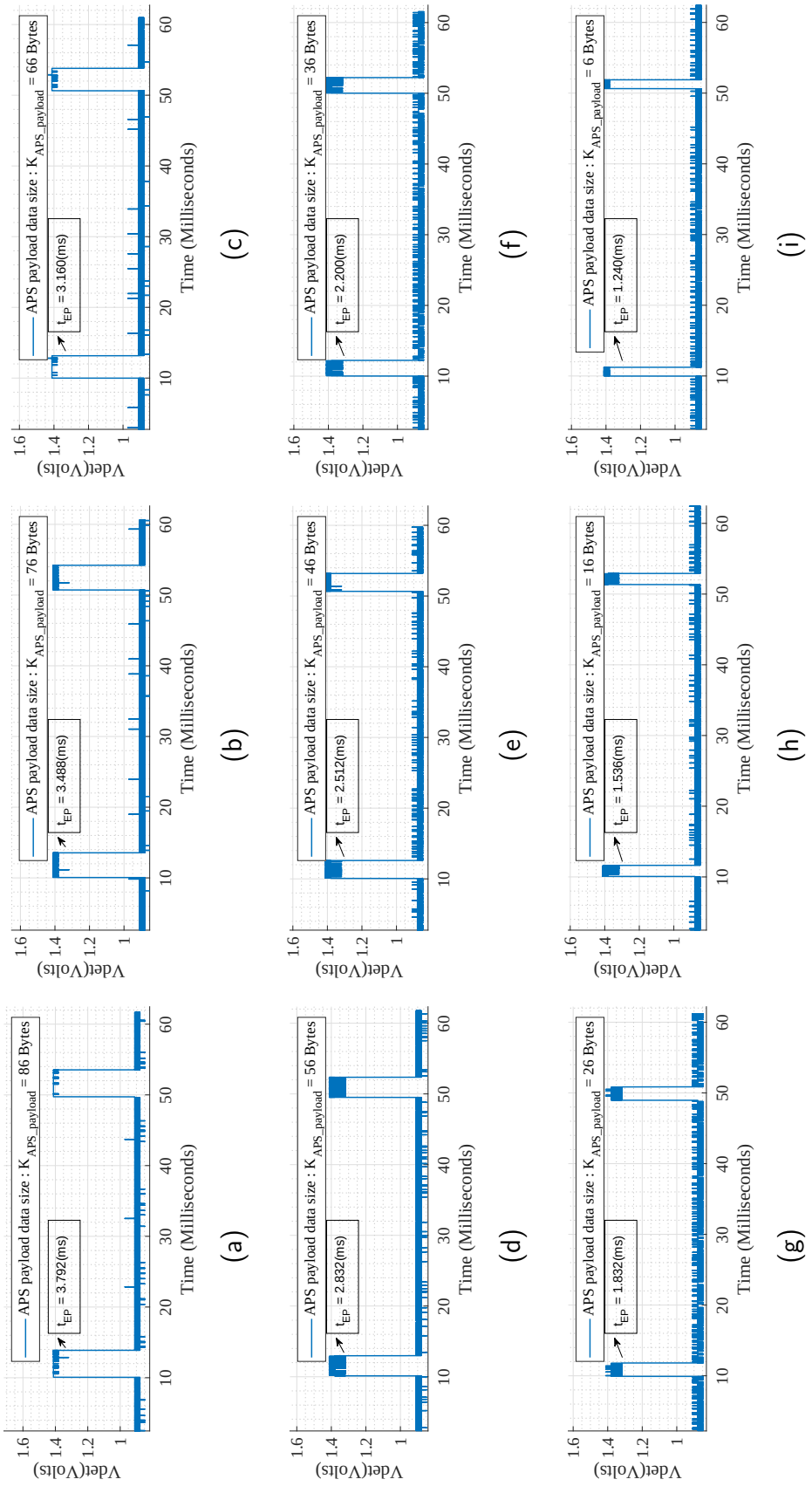

Figure 4.4: The voltage trace (Vdet) on the output pin of the RF power detector when sening EPs with different APS payload size: The EPs are built by padding 86 bytes(a), 76 bytes(b), 66 bytes(c), 56 bytes(d), 46 bytes(e), 36 bytes(f), 26 bytes(g), 16 bytes(h) and 6 bytes(i) in the APS payload field.

the output pin of the RF power detector. As the EPs are sent through the highest RF power (2 W), the output pin of the RF power detector generates a square pulse when sending an EP, and it keeps silent when the RF PA is not in use. Therefore, in the process of transmitting an EP, an oscilloscope is applied to trace the voltage on the output pin of the RF power detector, and the t_{EP} is obtained by measure the square pulse width.

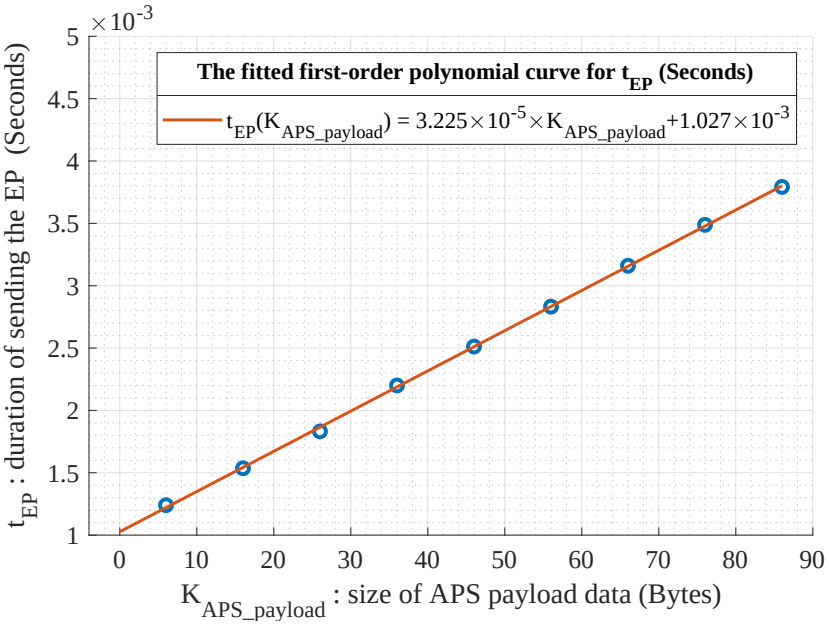

Figure 4.5: The fitted curve to represent the mathematical relation between the time (t_{EP}) of sending the EP and the byte length ($K_{APS\_payload}$) of the its APS payload

In this section, 9 experiments are carried out to send EPs and measure the related t_{EP}. The involved EPs are built with different byte lengths from 6 to 86 bytes in the step of 10 bytes to fill in the APS payload field. The voltage traces captured by the oscilloscope are plotted in Fig.4.4. Obviously,

the square pulse occurs when the RF PA is in the process of sending an EP. Also, the measured square pulse width in each experiment is indicated in each subplot.

The set of t_{EP} values are plotted in Fig.4.5 versus different APS payload size. According to the trend of the plots, the t_{EP} value increases linearly when the APS payload size increases. Therefore, the set of t_{EP} values are used for fitting the first-degree polynomial curve, and the derived mathematical relation between the t_{EP} and the byte length of the APS payload is written as,

$$t_{EP}(K_{APS\_payload}) = a \times K_{APS\_payload} + b, \quad K_{APS\_payload} \in [1, 86] \tag{4.6}$$

Where

$$a = 3.225 \times 10^{-5}$$
$$b = 1.027 \times 10^{-3}$$

the $K_{APS\_payload}$ represents the byte length of the APS payload. Since the $K_{APS\_payload}$ is limited to a value range, the t_{EP} has a maximum value of 3.8005 ms and a minimum value of 1.027 ms.

4.3.2 The $E_{loss}(t_C)$: The Circuital Energy Loss in A Scheduling Cycle

The $E_{loss}(t_C)$ in (4.4), the circuital energy loss during a scheduling cycle, is critical to the DEIN system. The value of the $E_{loss}(t_C)$ can instruct the

DEINT that how much additional RF energy is required in a scheduling cycle, which is for making up the energy loss on the DEINR. The circuital energy loss is primarily caused when the rectifier circuitry converts the energy contained in RF waves to DC energy because of the low efficiency in the RF-to-DC conversion process. Furthermore, the resistance loss and the discharge loss of the supercapacitor also cause energy loss. As a conclusion, the circuital energy loss in the DEINR depends on its hardware condition. By analysing the energy conversion progress, the $E_{loss}(t_C)$ value can be obtained by calculating the energy gap between the inductive energy from the receiving antenna of the DEINR and the increased DC energy stored inside the supercapacitor in a scheduling cycle t_C.

Training progress involving 3 sets of RF energy charging experiments are carried out to work out the mathematical expression to represent $E_{loss}(t_C)$. In the training progress, the ZigBee module and the sensor on the DEINR are switched off, which means there is no energy usage in the DEINR during the RF energy charging experiments, and the $E_{usage}(P_{DEINR}, t_C)$ in (4.4) equals to 0. That is to say, the inductive energy from the receiving antenna of the DEINR is partly consumed due to the circuital energy loss, and the rest is converted to the increased DC energy stored inside the supercapacitor. During each RF charging experiment, a voltage logger is used for tracing the voltage level of the DEINR's supercapacitor, and the beginning and end voltage values are recorded. Therefore, the total increased DC energy in the supercapacitor throughout each experiment can be calculated by referring to the capacitor's energy definition indicated in Equ.4.5. Furthermore, the number of scheduling cycles are counted in the DEIN control software dur-

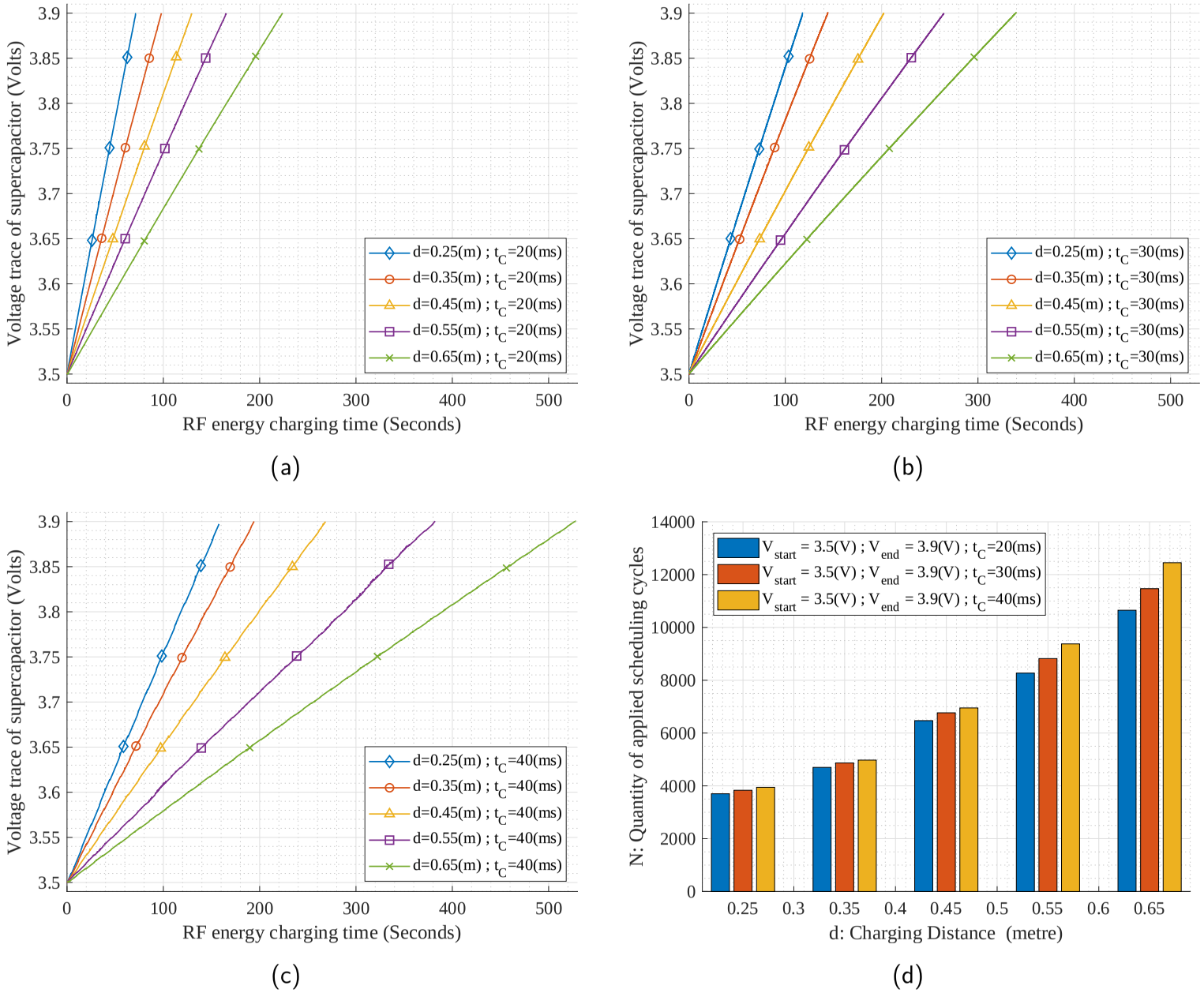

Figure 4.6: The 3 sets of RF energy charging experiments of the training progress: The captured traces of supercapacitor's voltage during each set of experiments by applying 20 ms(a), 30 ms(b) and 40 ms(c) scheduling cycle,respectively. (d) The counted scheduling cycles carried out in each individual experiment for charging the supercapacitor from V_{start} to V_{end}.

ing the process of charging the supercapacitor from the starting to the end voltage. Therefore, by referring to (4.5), the $E_{inc}(t_C)$, the supercapacitor's increased DC energy in a single scheduling cycle is calculated through the supercapacitor's total increased DC energy divided by the counted number of scheduling cycles carried out throughout each experiment. According to Equ.4.4, with the help of the calculated $E_{inc}(t_C)$, the $E_{loss}(t_C)$ is calculable as the remaining parameters and arguments are known to each RF energy charging experiment, which are list in Table 4.1. After the training progress, a series of $E_{loss}(t_C)$ values are obtained. Thereafter, the curve is constructed based on the collected E_{loss} values and fit a characteristic curve to them. Finally, based on the fitted curve, the mathematical expression of $E_{loss}(t_C)$ is derived.

Table 4.1: Constant experimental parameters for the training progress

Description	Notation	Value
APS payload size of EP	$K_{APS\_payload}$	66 Bytes
Time of sending an EP	$t_{EP}(K_{APS\_payload})$	3.16 ms
RF power for sending an EP	P_{DEINT}	2 W
Transmission Antenna Gain	G_t	14 dBi
Receiving Antenna Gain	G_r	14 dBi
2.4 GHz wavelength	λ	$12.49 \times 10^{-}2$ m
Equivalent DEINR's power	P_{DEINR}	0 W
Supercapacitor's starting voltage	V_{start}	3.5 V
Supercapacitor's end voltage	V_{end}	3.9 V

Fig.4.6 shows the traces of the supercapacitor's voltage captured by a

voltage logger and the counted number of the applied scheduling cycles in each experiment. The training progress involves 3 sets of RF energy charging experiments, which use 20, 30 and 40 milliseconds scheduling cycle for transmitting EPs, respectively. Furthermore, each set of experiments includes 5 individual experiments, which use the same scheduling cycle but different RF energy transmission distances set from 0.25 to 0.65 metre in the step of 0.1 metre. Fig.4.6a, Fig.4.6b and Fig.4.6c shows the traces of the supercapacitor's voltage captured during the 3 sets of experiments respectively. Fig.4.6d shows the number of scheduling cycles applied to transmit EPs during the 3 sets of experiments. As a summary, 15 individual RF energy charging experiments are carried out by deploying different RF energy transmission distances or different scheduling cycles. During each experiment, the DEINT continually runs the scheduling cycle and transmit the same EP to the DEINR at the beginning of each scheduling cycle. The relevant experimental parameters are listed in Table 4.1. Finally, 3 sets of the $E_{loss}(t_C)$ values calculated via the 3 sets of RF energy charging experiments are plotted in Fig.4.7a.

According to the $E_{loss}(t_C)$ values plotted in Fig.4.7a, not only the t_C values, the RF energy transmission distance(d) also has impact on the $E_{loss}(t_C)$, which has even more. Furthermore, the longer the RF energy transmission distance is, the smaller the $E_{loss}(t_C)$ value will be. Moreover, the longer the scheduling cycle is applied, the bigger the $E_{loss}(t_C)$ value will be. By analysing the 3 sets of $E_{loss}(t_C)$ values, it is found that the tendency of the curve obtained by linking the $E_{loss}(t_C)$ points is similar to the power function curve. Therefore, by using the d values as inputs, each set of $E_{loss}(t_C)$ values are used for fitting a power function curve, and 3 fitted curves based on the

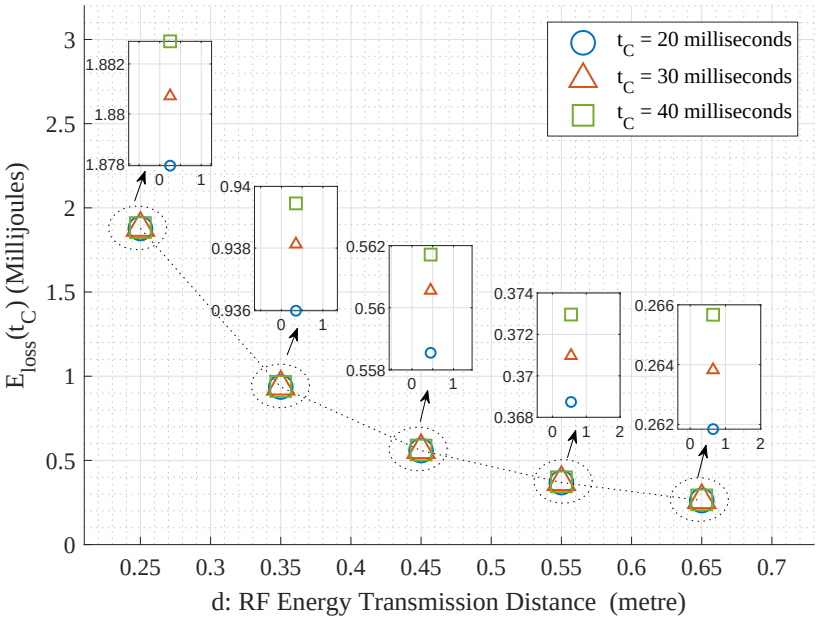

(a)

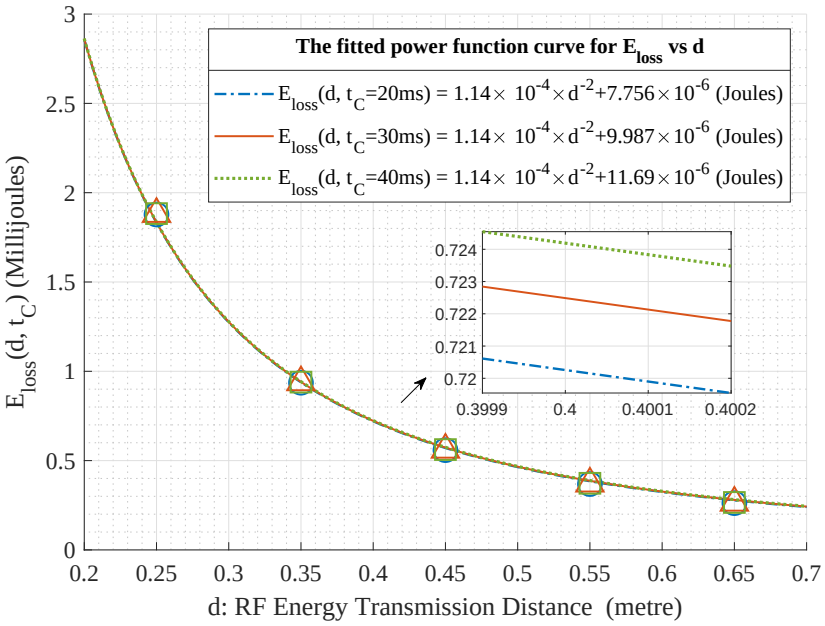

(b)

Figure 4.7: (a) The calculated energy loss in a scheduling cycle(t_C) from the 3 sets of RF energy charging experiments when $t_C = \{0.02, 0.03, 0.04\}$ seconds and RF energy transmission distance $d = \{0.25, 0.35, 0.45, 0.55, 0.65\}$ metre; (b) The fitted curves for the $E_{loss}(d, t_C)$ points when $d = \{0.25, 0.35, 0.45, 0.55, 0.65\}$ and $t_C = \{0.02, 0.03, 0.04\}$.

3 sets of $E_{loss}(t_C)$ values are plotted in Fig.4.7b. In addition, the derived mathematical expressions of $E_{loss}(t_C)$ basing on the 3 fitted curves are also indicated in Fig.4.7b. By analysing the 3 expressions, it is found that their power terms, namely, the terms with parameter d, are identical. However, the remaining terms, namely, the constant terms in the 3 expressions, have different values. In addition, the constant term of the expressions has bigger value if the related set of experiments use longer t_C, and the applied longer t_C causes a longer positive shifting to the fitted curve in the vertical direction. As a conclusion, both parameter d and t_C are significant to $E_{loss}(t_C)$.

In order to analyse the impact of different scheduling cycle (t_C) on the $E_{loss}(t_C)$, an additional set of RF energy charging experiments involving 6 individual experiments are deployed to figure out the mathematical expression of $E_{loss}(t_C)$ versus different t_C. In order to avoid the influence due to different RF energy transmission distance(d), the fixed d is used in the set of experiments, which is set to 0.4 m, The scheduling cycle(t_C) applied in each individual experiment is respectively configured from 10 to 40 milliseconds in a step of 6. As a result, the traces of the supercapacitor's voltage are captured by a voltage logger during each individual experiment, and they are plotted in Fig.4.8a. Also, Fig.4.8b shows how many scheduling cycles are used throughout each individual experiment. Thereafter, the increased DC energy($E_{inc}(t_C)$) in each individual experiment can be derived via the operation of dividing the whole harvested DC energy by the counted number of utilized scheduling cycles throughout the individual experiment. Then, with the help of Equ.4.4 and parameters in Table 4.1, the $E_{loss}(t_C)$ values basing the set of experiments are derived, and the points are plotted in Fig.4.9a.

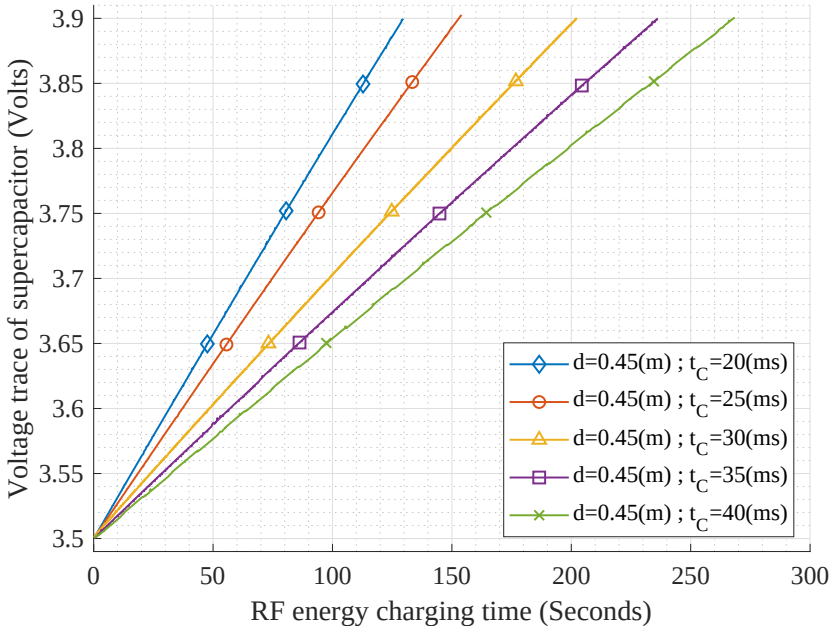

(a)

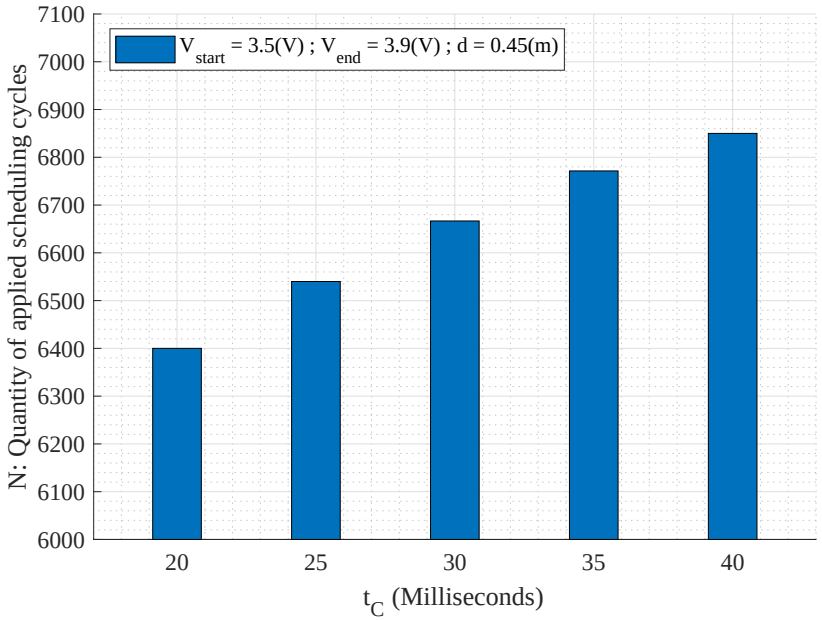

(b)

Figure 4.8: The additional set of RF energy charging experiments of the training progress: (a) The captured traces of the supercapacitor's voltage level during each individual experiment by using different scheduling cycles $t_C = [0.02, 0.025, 0.03, 0.035, 0.04]$ seconds. (b) The number of the scheduling cycles utilized for charging the supercapacitor from V_{start} to V_{end}.

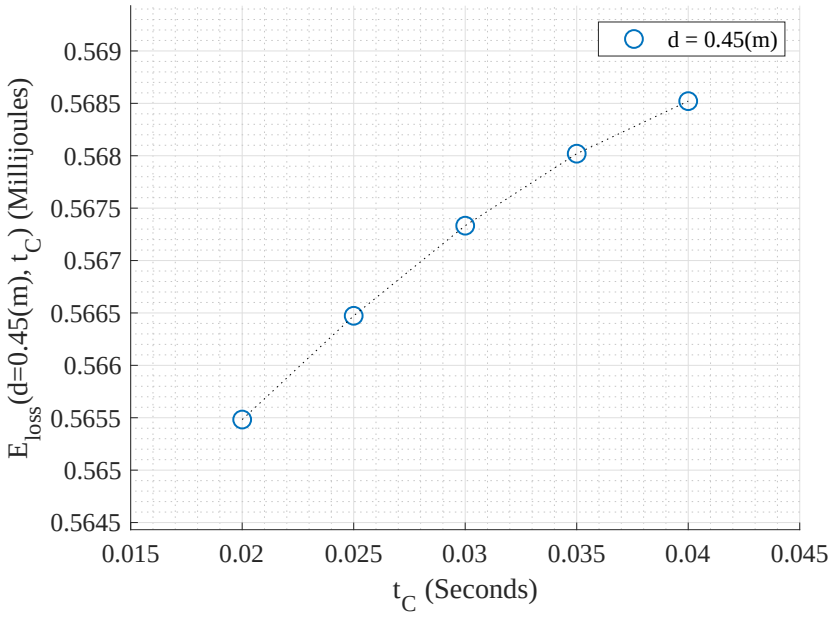

(a)

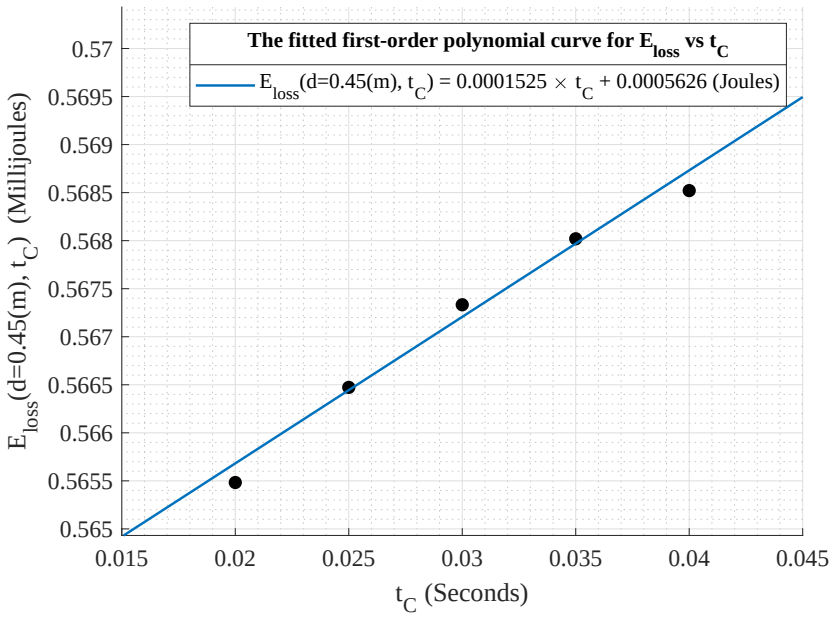

(b)

Figure 4.9: (a) The calculated energy loss during a scheduling cycle (t_C) via the additional set of charging experiments when $t_C = [0.02, 0.025, 0.03, 0.035, 0.04]$ seconds; (b) The fitted first-order polynomial curve for the $E_{loss}(d, t_C)$ points when $d = 0.45$ and $t_C = \{0.02, 0.025, 0.03, 0.035, 0.04\}$.

According to the trend of the curve obtained by linking the $E_{loss}(t_C)$ points, the plotted points are used for fitting a first-order polynomial curve to this set of E_{loss} values. The mathematical expressions of $E_{loss}(t_C)$ basing the fitted curve is indicated in Fig.4.9b. As a result, by combining all the derived mathematical expressions of $E_{loss}(t_C)$ indicated in Fig.4.7b and Fig.4.9b, the $E_{loss}(t_C)$ is finally expressed as,

$$E_{loss}(d, t_c) = \alpha \times d^{-2} + \beta \times t_c + \gamma \tag{4.7}$$

Where

$$\alpha = 1.14 \times 10^{-4}$$
$$\beta = 1.525 \times 10^{-4}$$
$$\gamma = -3.31 \times 10^{-7}$$

α, β and γ are coefficients of the mathematical expression. As the RF transmission distance is fixed in the DEIN system, the d is not recognized as an input variable of $E_{loss}(t_C)$. However, according to the RF energy charging experiments described in Fig.4.6 and Fig.4.8, the d does affect the value of $E_{loss}(t_C)$. In order to study the physical significance of the mathematical expression (4.7), Equ.4.7 is transformed as the following equation by replacing the coefficient α with the experimental parameters in Table 4.1.

$$\begin{aligned} E_{loss}(d, t_C) &= \eta \times P_{DEINT} \times t_{EP}(K_{APS\_payload}) \times G_r G_t (\frac{\lambda}{4\pi})^2 \times d^{-2} \\ &\quad + \beta \times t_C + \gamma \\ &= \eta \times E_{I\_EP}(t_{EP}(K_{APS\_payload})) + \beta \times t_C + \gamma \end{aligned} \tag{4.8}$$

Where

$$\eta = 93.16\%$$
$$\beta = 1.525 \times 10^{-4}$$
$$\gamma = -3.31 \times 10^{-7}$$

Observe the expression of Equ.4.8, the d is eliminated via introducing the $E_{I\_EP}(t_{EP})$, which means the inductive energy from the DEINR's energy receiving antenna has the impact on the $E_{loss}(t_C)$. Hence, $\eta \times E_{I\_EP}(t_{EP})$, means that 93.16 per cent of the inductive energy is lost, and the massive energy loss is primarily caused by converting RF energy to DC energy. Conversely, the RF-to-DC conversion efficiency of the thesis's designed DEIN system is 6.84%. The remaining term, $\beta \times t_C + \gamma$, describes the discharged energy in the supercapacitor throughout each scheduling cycle t_C, and the longer the t_C is, the more energy will be discharged.As a result, with the help of Equ.4.6 and (4.8), the energy conversion Equ.4.4 is finally expressed as,

$$\begin{aligned} E_{inc}(t_C) &= P_{DEINT} \times t_{EP}(K_{APS\_payload}) \times G_r G_t (\frac{\lambda}{4\pi d})^2 - E_{loss}(t_C) \\ &\quad - P_{DEINR} \times t_C \\ &= (1-\eta) \times P_{DEINT} \times t_{EP}(K_{APS\_payload}) \times G_r G_t (\frac{\lambda}{4\pi d})^2 \\ &\quad - (\beta \times t_C + \gamma) - P_{DEINR} \times t_C \\ &= (1-\eta) \times P_{DEINT} \times (a \times K_{APS\_payload} + b) \times G_r G_t (\frac{\lambda}{4\pi d})^2 \\ &\quad - (\beta \times t_C + \gamma) - P_{DEINR} \times t_C \end{aligned} \tag{4.9}$$

Where

$$\eta = 93.16\%$$
$$a = 3.225 \times 10^{-5}$$
$$b = 1.027 \times 10^{-3}$$
$$\beta = 1.525 \times 10^{-4}$$
$$\gamma = -3.31 \times 10^{-7}$$
$$K_{APS\_payload} \in [1, 86]$$

According to the mathematical expression of the energy conversion Equ.4.9, only the byte length ($K_{APS\_payload}$) of the EP's APS payload, the length of scheduling cycle (t_C) and the DEINR's equivalent power (P_{DEINR}) are variables.

4.4 Bandwidth Allocation Algorithm

4.4.1 Problem Formulation

The target is to maximize the throughput of wireless information, namely, the bandwidth used for transmitting the conventional ZigBee DPs in the thesis's designed DEIN system. Hence, the shorter EPs (shorter byte length of the EP's APS payload) or the more infrequent EPs are created, the less the bandwidth is utilized for EPs and the more bandwidth is left for the conventional ZigBee DPs. However, less bandwidth for transmitting EPs means less RF energy is transmitted to the DEINR. As a result, the transmitted RF energy from the DEINT must afford the energy usage of the DEINR or

at least meet its minimum desired energy. If considering a single scheduling cycle, the increased DC energy in the DEINR's supercapacitor during a single scheduling cycle must be equal or greater than 0 J. Hence, according to the energy conversion Equ.4.9, the first constraint for the DEIN system is expressed as,

$$C1 : E_{inc}(t_C) \geq 0 \tag{4.10}$$

According to the format of the ZigBee based APS data packet as well as the restriction of the byte length filled in the APS payload field described in Fig.4.3, the following constraint regarding the maximum number of bytes can be filled in the EP's APS payload field must be met.

$$C2 : K_{APS\_payload} \in [1, 86] \tag{4.11}$$

Be subject to the constraints C1 and C2, the problem of maximizing the bandwidth for transmitting the conventional ZigBee DPs is formulated as,

$$\begin{aligned} P1 : & \underset{t_C, K_{APS\_payload}}{\text{Maximize}} \quad \frac{t_C - t_{EP}(K_{APS\_payload})}{t_C} \\ & \text{subject to} : C1 - C2 \end{aligned} \tag{4.12}$$

Since the time of transmitting an EP ($t_{EP}(K_{APS\_payload})$) is shorter than the length of a scheduling cycle (t_C), the formulation (4.12) is always positive.

4.4.2 Algorithm to Maximize the Throughput of Wireless Information

In order to solve the formulated problem in (4.12), Algorithm 1 is proposed to find the optimal t_C and $K_{APS\_payload}$ values to make the formula

Algorithm 1 Maximize the bandwidth for transmitting ZigBee DPs

Input :

$d \leftarrow$ RF energy transmission distance, $\lambda \leftarrow 2.4\,\text{GHz}$ wavelength

$G_t \leftarrow$ Transmission antenna gain, $G_r \leftarrow$ Receiving antenna gain

$\eta \leftarrow 93.16\%$, $\beta \leftarrow 1.525 \times 10^{-4}$, $\gamma \leftarrow -3.31 \times 10^{-7}$

$a \leftarrow 3.225 \times 10^{-5}$, $b \leftarrow 1.027 \times 10^{-3}$

$P_{DEINT} \leftarrow 2\,\text{W}$ Transmission power

$P_{DEINR} \leftarrow$ DEINR's equivalent power

Output : t_C, $K_{APS\_payload}$

Initialisation :

Let $temp\_t_C = 0$, $temp\_K_{APS\_payload} = 0$, $B_{DPs} = 0$

Main Process :

for all $t_C \in [0.005 : 0.005 : 0.5]$ **do**

  for all $K_{APS\_payload} \in [1 : 5 : 86]$ **do**

    Calculate $E_{inc}(t_C)$ basing on the energy conversion Equ.4.9

    if $E_{inc}(t_C) \geq 0$ **then**

      $temp\_B_{DPs} \leftarrow \frac{t_C - t_{EP}(K_{APS\_payload})}{t_C}$

      if $B_{DPs} < temp\_B_{DPs}$ **then**

        $B_{DPs} \leftarrow temp\_B_{DPs}$

        $temp\_t_C \leftarrow t_C$

        $temp\_K_{APS\_payload} \leftarrow K_{APS\_payload}$

      end if

    end if

  end for

end for

if $B_{DPs} > 0$ **then**

  $t_C \leftarrow temp\_t_C$, $K_{APS\_payload} \leftarrow temp\_K_{APS\_payload}$

  return t_C, $K_{APS\_payload}$

else

  return Fail

end if

(4.12) achieves a maximum value in the condition of meeting the constraint C1 formulated in (4.10) and C2 formulated in (4.11). According to the algorithm, the value range of the t_C is from 0.005 to 0.5 in the step of 0.005, and the value range of the $K_{APS\_payload}$ is from 1 to 86 in the step of 5. In the initialisation process, two temporary variables, the $temp\_t_C$ and $temp\_K_{APS\_payload}$ are cleared, which are used for backing up the final chosen t_C and $K_{APS\_payload}$ values in the algorithm's main process. The variables B_{DPs} is reset for bucking up the calculated bandwidth in the algorithm's main process basing on formula (4.12). After that, the main process begins to used all t_C and $K_{APS\_payload}$ values in their value range to calculate the $E_{inc}(t_C)$ value according to the energy conversion Equ.4.9. If a pair of t_C and $K_{APS\_payload}$ values let $E_{inc}(t_C)$ equal or greater than 0, the pair of values will be used for calculating the bandwidth which is for transmitting ZigBee DPs. If the new calculated bandwidth is greater than the backup value, the new bandwidth value will be bucked up as well as the pair of t_C and $K_{APS\_payload}$ values. After all the pairs of t_C and $K_{APS\_payload}$ values are tried, the algorithm will check the backup B_{DPs}. If it is positive, it means there are optimal t_C and $K_{APS\_payload}$ values to supply adequate energy to the DEINR, and then the backups of the optimal t_C and $K_{APS\_payload}$ values are returned eventually. However, if the B_{DPs} still equals to 0, an error signal will be returned to the DEIN control system to indicate that the RF energy transmission cannot afford the energy usage of the DEINR, which may be due to the equivalent power of the DEINR is too high, or the RF energy transmission distance is too long.

Fig.4.10 describes the designed control software for running Algorithm 1.

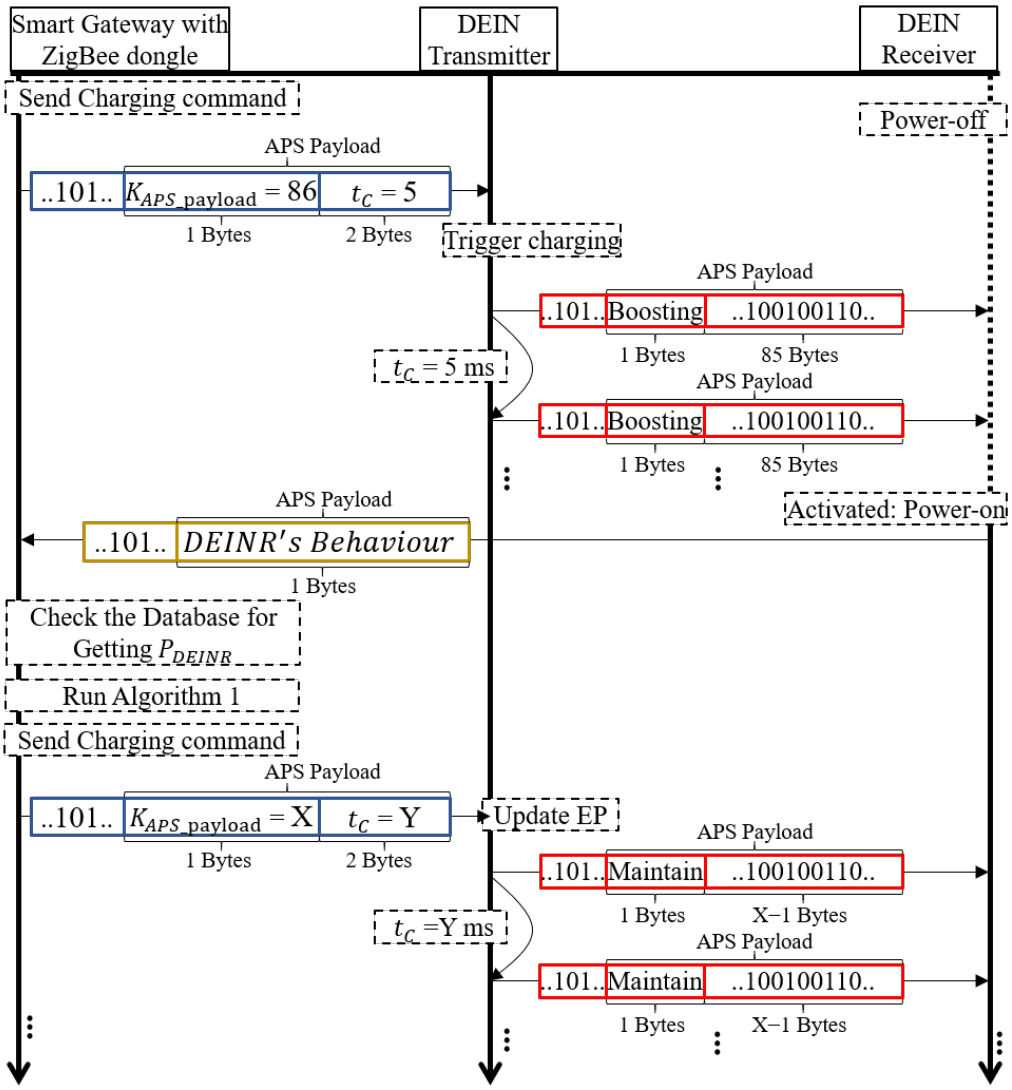

Figure 4.10: The control software designed for carrying out Algorithm 1.

In the beginning, the ZigBee related circuitry on the DEINR is powered off because its supercapacitor's voltage is lower than the critical value to enable the voltage regulator. To power on the DEINR's ZigBee related circuitry as soon as possible, a fast RF energy charging procedure is initially launched

by the DEIN control system. In the beginning, a charging command is dispatched from the smart gateway (with the ZigBee dongle) to the DEINT to instruct the initial charging procedure. During this procedure, the longest packet size is applied to build EPs. Also, the shortest interval is used for sending EPs. The charging command is also a ZigBee standard APS data packet with 3 bytes filled in the APS payload field. The first byte indicates the $K_{APS\_payload}$ value used for creating the EPs in the DEINT, and the next two bytes contain the t_C value for setting the count down timer to schedule EPs transmission. Once the DEINT receives the charging command, the EPs are created and sent by intervals according to the received instruction. During the fast RF energy charging procedure, the maximum bandwidth is allocated for transmitting EPs by putting the maximum 86 bytes in the EP's APS payload field and using the shortest t_C (5 ms) to activate the DEINR's ZigBee related circuitry as soon as possible. 5 ms is the minimum step to adjust the interval, which is defined by the count down timer of the DEINT's microcontroller. The first byte in the EP's APS payload indicates the current charging state, which is voltage boosting stage at the moment.

When the voltage of the DEINR's supercapacitor rises to a critical point (3.9 V) that can enable the voltage regular, the ZigBee and its sensor circuitry are switched on by the stable output voltage from the regular. Thereafter, its behaviour (the message to describe the type of sensor and the sensor's sampling frequency) is uploaded to the smart gateway regarding the sensor's type and the interval to upload the sensor data. Once got this report from the DEINR, the smart gateway will then check the database to obtain the equivalent power (P_{DEINR}) of the DEINR. Thereafter, the P_{DEINR} is used as

an input to Algorithm 1 together with the other constant system parameters. After executing Algorithm 1, the returned $K_{APS\_payload}$ and t_C values are sent to the DEINT through a new charging command. Then, the charging procedure managed in the DEINT is updated by resizing the EPs or readjust the scheduling cycle, and the byte in the EP to indicate the charging stage is replaced by "maintain".

4.5 System Evaluation

4.5.1 The DEINR's Equivalent Power (P_{DEINR}) Estimation

The equivalent power of the DEINR, namely, the P_{DEINR}, is the power measured in watt to describe the general energy usage in the DEINR. It is a critical input for the designed bandwidth algorithm as its value affects the amount of the RF energy per scheduling cycle should be transmitted to the DEINR. The P_{DEINR} value is estimated via the practical measurement based on the behaviours of the DEINR's ZigBee related circuitry such as sending a ZigBee packet, flashing an LED, reading the temperature data from the sensor, etc. Thereafter, the estimated P_{DEINR} value only for the specific DEINR is set as a pre-store parameter in the database of the smart gateway. The following details describe the steps of estimating the P_{DEINR} value.

Since the thesis's designed DEINR is programmed to transmit a tempera-

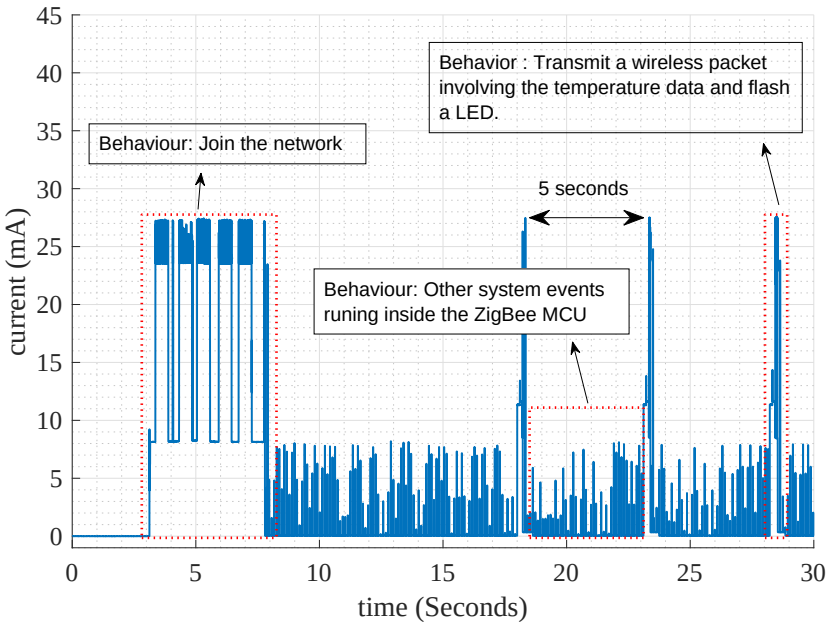

Figure 4.11: The measured current after switching the ZigBee related circuitry

ture data packet and flash a LED during the transmission in every 5 seconds after successfully joins the network, most of the energy is used through the circuital behaviours which are data exchange between the ZigBee module and the temperature sensor, transmitting a wireless ZigBee packet, receiving an ACK packet from the ZigBee dongle and flashing a LED during the packet transmission period. By using a digital multimeter to connect the output port of the (2.8 V) voltage regulator and the input of the ZigBee related circuitry, the circuital current can be measured. Fig.4.11 shows the captured trace of the current consumed in the ZigBee related circuitry. As the output voltage from the voltage regulator is constant (2.8 V), the whole consumed energy during the 5 seconds is calculated basing on the plotted

points in Fig.4.11. The DEINR's equivalent power is then calculated by the calculated energy divided by the 5 seconds. As a result, the estimated results are listed in Table.4.2.

Table 4.2: Calculated results for evaluating the DEINR's equivalent power

Parameter Description	Notation	Value
Consumed energy for sending a temperature data packet and flash a LED	E_{main}	16.06 mJ
Consumed energy for other system event running inside the ZigBee MCU	E_{other}	5.84 mJ
Consumed energy in the ZigBee related circuitry every 5 seconds	E_{all}	21.9 mJ
DEINR's equivalent power	P_{DEINR}	4.38 mW

4.5.2 Algorithm Evaluation

Table 4.3: Constant system parameters for the algorithm evaluation

Description	Notation	Value
RF power for sending an EP	P_{DEINT}	2 W
Transmission Antenna Gain	G_t	14 dBi
Receiving Antenna Gain	G_r	14 dBi
2.4 GHz wavelength	λ	12.49×10^{-2} m
DEINR's equivalent power	P_{DEINR}	4.38×10^{-3} W
RF energy transmission distance	d	0.47 m

Table 4.4: Four sets of $E_{inc}(t_C)$ and B_{DPs} values obtained from the algorithm

Set number	t_C	$K_{APS\_payload}$	$E_{inc}(t_c)$	B_{DPs}
1	0.01 s	81 bytes	-1.3561×10^{-6} J	63.61%
2	0.01 s	86 bytes	5.774×10^{-7} J	62%
3	0.005 s	26 bytes	3.7515×10^{-8} J	62.69%
4	0.005 s	21 bytes	-1.896×10^{-6} J	65.92%

The constant system parameters listed in Table.4.3 are used for algorithm evaluation. After running Algorithm 1, the four sets of t_c and $K_{APS\_payload}$ solutions are listed in Table.4.4. In addition, the related $E_{inc}(t_C)$ and B_{DPs} calculated based on the four set t_C and $K_{APS\_payload}$ solutions are also listed aside. According to the algorithm, the four $E_{inc}(t_C)$ values are closet to 0. The third pair of $E_{inc}(t_C)$ and B_{DPs} solution is the optimal choice, which maximize B_{DPs} and also comply with that $E_{inc}(t_C)$ must be greater than 0. Thereafter, four experiments are carried out by separately applying the four sets t_C and $K_{APS\_payload}$ solutions. In the beginning of each experiment, the DEINR is in power-off mode until its supercapacitor's voltage climbs to 3.9 V. Thereafter, it is activated and joins the network. Along the timeline, the DEINR will transmit a DP involving the temperature information and flash an LED in every 5 seconds.

Fig.4.12 shows the captured traces of the supercapacitor's voltage from the four experiments. By observing the voltage variation in Fig.4.12a and Fig.4.12d, the supercapacitor's voltage gradually decreases along the timeline as their related $E_{inc}(t_C)$ (harvested DC energy per scheduling cycle) are less

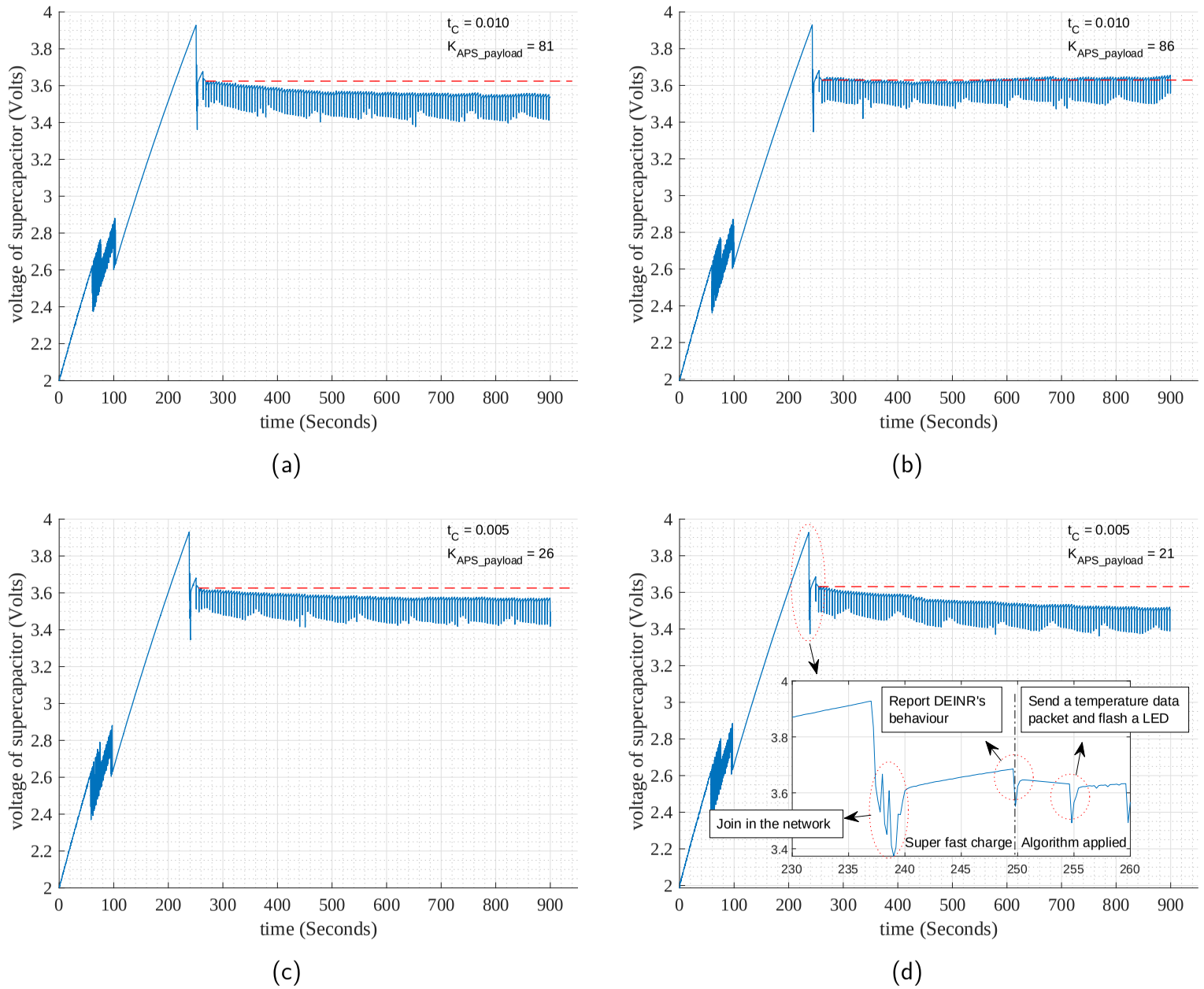

Figure 4.12: Experimental results with the four sets of t_c and $K_{APS\_payload}$ solutions (in Table.4.4) applied. (a) Captured trace of the supercapacitor's voltage based on the first pair of t_c and $K_{APS\_payload}$ solution; (b) The second pair; (c) The third pair; (d) The fourth pair.

than 0. Furthermore, the decline speed of voltage in Fig.4.12d is quicker than Fig.4.12a as the fourth $E_{inc}(t_C)$ in Table.4.4 is less than the first one. Hence, the first and the fourth results in Fig.4.12a and Fig.4.12d meet experimental expectation.

According to the experimental expectation to the results in Fig.4.12b and Fig.4.12c, the supercapacitor's voltage should rise or keep constant along the timeline since their related $E_{inc}(t_C)$ are greater than 0. The experiment in Fig.4.12c is based on the third pair of $E_{inc}(t_C)$ and B_{DPs} solution in Table.4.4. Under the condition that $E_{inc}(t_C)$ must be greater than 0, a maximum bandwidth for ZigBee data transmission is obtained by applying the third pair of solution. Therefore, the third pair is optimal. However, the voltage curve in Fig.4.12c shows a decreasing tendency over time. Although the supercapacitor's voltage is very close to a constant level, it still lower than the expectation voltage at the end of the timeline. Hence, the third pair solution does not meet the system requirement. The result in Fig.4.12b is based on the second pair of $E_{inc}(t_C)$ and B_{DPs} in Table.4.4. Obviously, in Fig.4.12b, the supercapacitor's voltage gradually increases along the timeline, which satisfies the energy usage of the DEINR.

Fig.4.13 show the comparison between the experimental results with and without the bandwidth allocation algorithm. Two captured traces of the supercapacitor's voltage are plotted in Fig.4.13a. The stable trace is obtained with the bandwidth allocation algorithm. The fluctuant trace is obtained based on the voltage feedback mechanism. Fig.4.13b shows the per cent of bandwidth left for transmitting DPs, which is calculated based on the

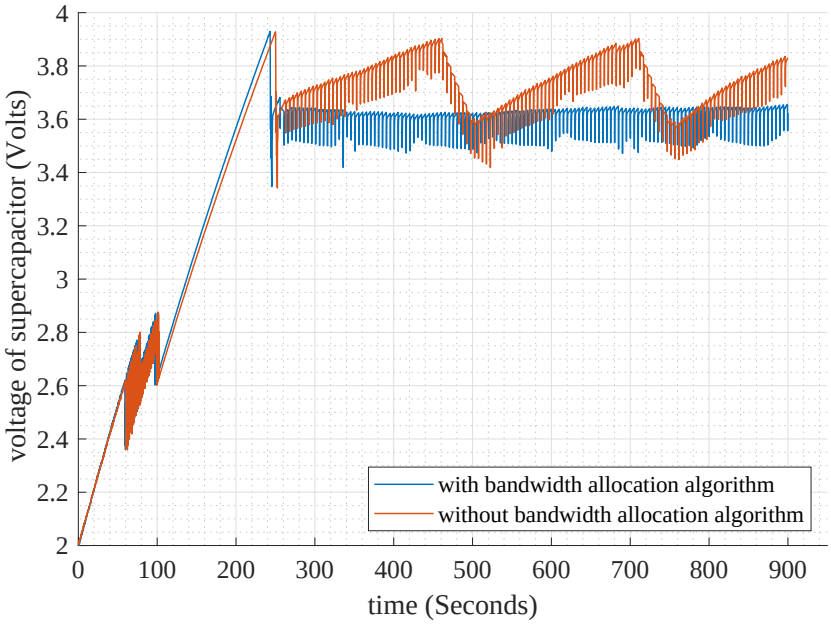

(a)

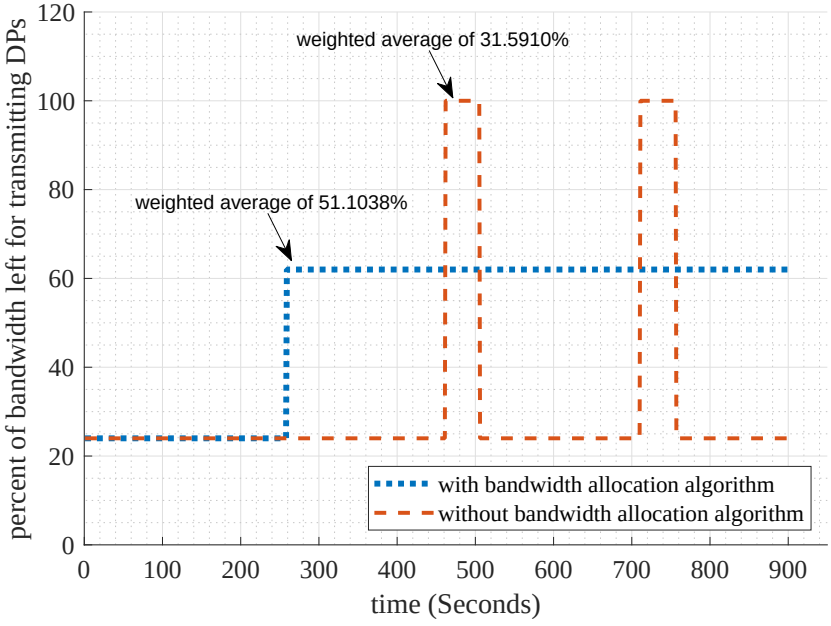

(b)

Figure 4.13: A comparison between the experimental results with and without the bandwidth allocation algorithm. (a) The comparison between the captured traces of the supercapacitor's voltage with and without the bandwidth allocation algorithm. (b) The comparison between the per cent of bandwidth left for DPs transmission with and without the bandwidth allocation algorithm.

experiments in Fig.4.13a. According to the results, the weighted average bandwidth for transmitting DPs with the bandwidth allocation algorithm is 61.77% higher than the bandwidth without the bandwidth allocation algorithm. With the algorithm, the bandwidth for DPs transmission, namely, the throughput of wireless information, is significantly improved.

4.6 Chapter Summary

In this chapter, the thesis proposes a strategy that transmits the minimum required RF energy to the DEINR. It aims to use the minimum bandwidth for transmission EPs and leave as much bandwidth as possible for DPs (wireless information) transmission. To achieving the aim, a scheduling cycle model is designed for managing the time slots for transmitting RF energy and wireless information. In addition, the bandwidth allocation for EPs and DPs depends on how to build the scheduling cycle. Furthermore, an RF energy transmission and harvesting model is designed for modelling the process of energy conversion. The studying is from the initial transmitted RF energy to final increased DC energy in the supercapacitor. According to the proposed models, a set of experiments are carried out for studying the mathematical relationship between the time duration of transmitting an EP and the number of bytes filled in the EP's APS payload field. Furthermore, a training process involving 4 sets of experiments are carried out for estimating the mathematical expression of the energy loss in the DEINR during a scheduling cycle. By combining all the derived mathematical expressions in this

chapter, the energy conversion equation is concluded. It quantifies the relationship between the increased amount of DC energy in the supercapacitor and the parameters of the scheduling cycle. Hence, with the help of the energy conversion equation, a bandwidth allocation algorithm is designed for maximizing the bandwidth for DPs transmission. Finally, the experimental results prove that the throughput of wireless information is significantly improved with the bandwidth allocation algorithm applied.

Chapter 5

Resource Allocation Algorithm for Energy-Efficient DEIN

5.1 Introduction

According to the practical system model described in Chapter 3 and 4, the energy conversion efficiency from the DEINT to the DEINR is quite low. It is inevitable that the RF energy loss in the air. Also, RF-to-DC efficiency is determined by the hardware characters. To the DEINR, the only energy source is the RF energy. Hence, to achieve an energy-efficient DEIN, the efficiency of energy utilization deserves to be investigated. According to current measurement depicted in Fig.4.11, the DEINR's uplink data transmission consumes the most energy. Hence, in this chapter, the thesis aims

to minimize the system's energy consumption per bit of uplink data.

In this chapter, a new topology is proposed for the DEIN system involving a DEINT and two DEINRs. Based on the new topology, a new RF energy transmission method is designed for multiple DEINRs. Related works [49] [37] who have built a practical RF energy transmission use a static directional antenna to face the receiver directly. Normally, their system only consists of a single RF energy receiver. To transmit RF energy to multiple DEINRs, the DEINT's transmission (directional) antenna is designed with a rotation function. Therefore, the DEINT can rotate its transmission antenna opposite to every DEINR to charge them in turn. Chapter 4 integrates EP and DP in a scheduling cycle for the DEIN system with a single DEINR. As a different case, this chapter designs a time allocation model to organize RF energy transmission and uplink data transmission in different time slots for multiple devices in the DEIN system.

During the RF energy transmission process, a series of EPs are transmitted to a target DEINR. After harvesting the RF energy from the EPs, an uplink data transmission process will be launched by the DEINR immediately. The just-harvested energy could be used up for the uplink data transmission. To fully utilize the just-harvested energy, the DEINT will transmit as much uplink data as possible.

Based on the time allocation model, a resource allocation algorithm is proposed and evaluated in this chapter. It is designed to allocate the optimal time for RF energy transmission and the uplink data transmission for each DEINR. Also, it works out the optimal transmission power of the DEINT.

With the algorithm, the system's energy consumption per bit of uplink data is minimized, which improves the DEIN system's efficiency of RF energy utilization.

The remainder of this chapter is organized as follows. Section 5.2 proposes a multiple DEINRs based DEIN topology. Section 5.3 describes the proposed system models such as the energy estimation model and time allocation model. In addition, the problem of how to minimize the energy consumption per bit of uplink data is proposed. Section 5.4 describes the method and related algorithm to solve the proposed problem. Section 5.5 evaluates the performance of the algorithm, and the numeric results prove its validity.

5.2 Topology for DEIN System Involving Multiple DEINRs

Fig.5.1 describes a DEIN system including a single DEINT and two DEINRs. In the aspect of network functionality, the DEINT works as the ZigBee router and the DEINR works as the ZigBee end-device. In the DEIN system with multiple DEINRs, the DEINT has to keep listening as it also works as a ZigBee router. Hence, for the DEINT, its directional antenna is configured only for transmission, and its Omni antenna is always set to keep listening. The antennas on the DEINR is arranged as same as the way in Section 3.2. Its directional antenna is used for receiving RF energy contained in the EPs,

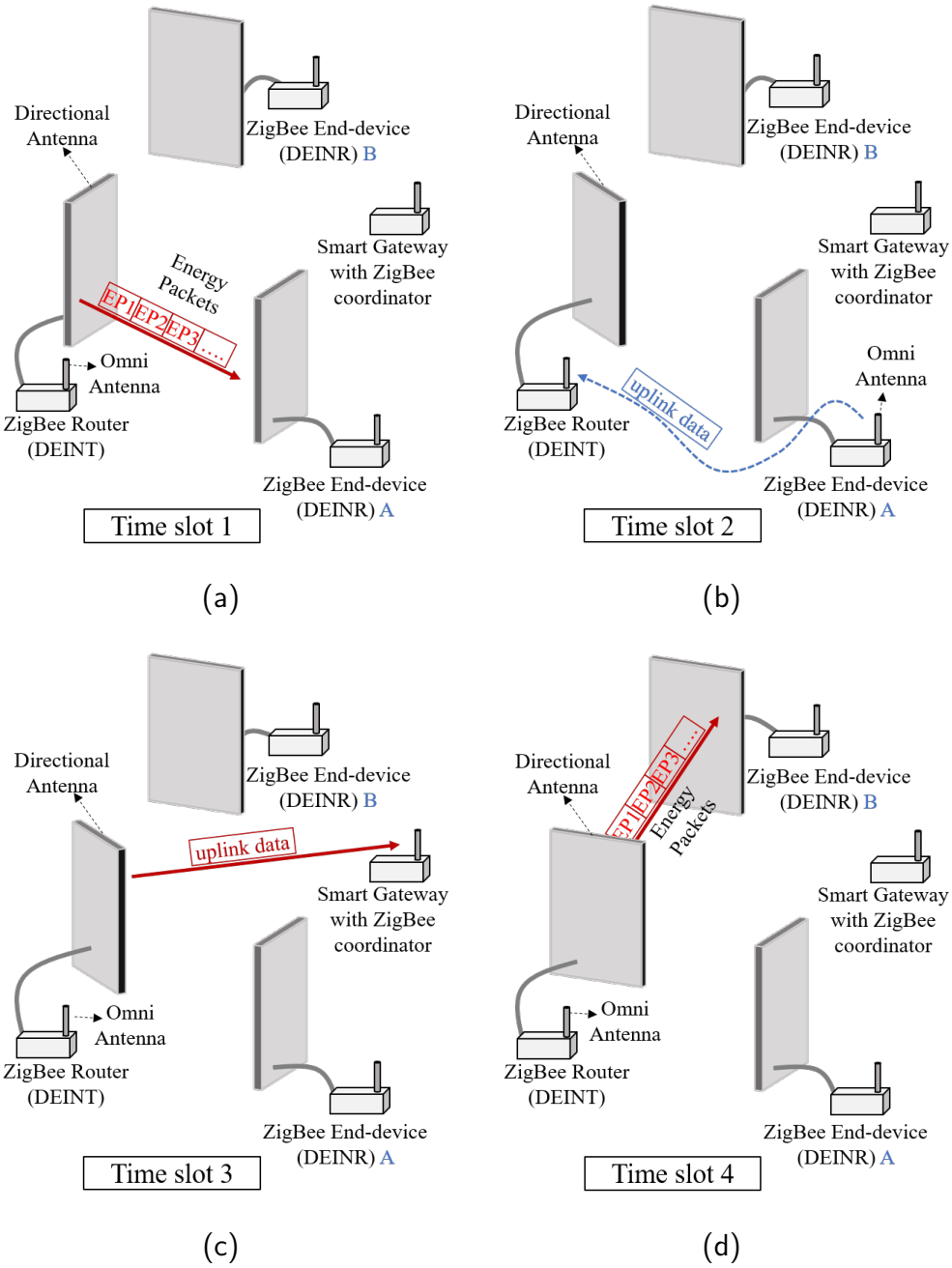

Figure 5.1: A DEIN system involving two DEINRs: (a) In time slot 1, the DEINT transmits EPs to charge the DEINR A. (b) In time slot 2, the DEINR A transmit uplink data to the DEINT (ZigBee router). Meanwhile, turning the DEINT's antenna anticlockwise. (c) In time slot 3, the DEINT forwards the just-received uplink data to the ZigBee coordinator. (d) In time slot 4, the DEINT transmits EPs to charge the DEINR B when the DEINT's antenna is turned opposite to the DEINR B.

and its Omni antenna is for duplex communication, namely, uplink data transmission and downlink data receiving. Since the RF energy transmission and receiving antennas have to be placed to face each other for the best energy conversion efficiency, the RF energy transmission procedures for charging DEINR A and DEINR B are scheduled in different time slots. In addition, during each time slot for RF energy transmission, the DEINT's directional antenna only faces to either DEINR A or DEINR B. The distance between the DEINT to each DEINR is within 1 meter, which is same as the RF energy charging distance between the DEINT to the single DEINR in Chapter 3 and 4. The reason for the limited charging distance is explained in Section 4.2.1. The scenarios in the four sequential time slots are separately described in Fig.5.1a, Fig.5.1b, Fig.5.1c and Fig.5.1d.

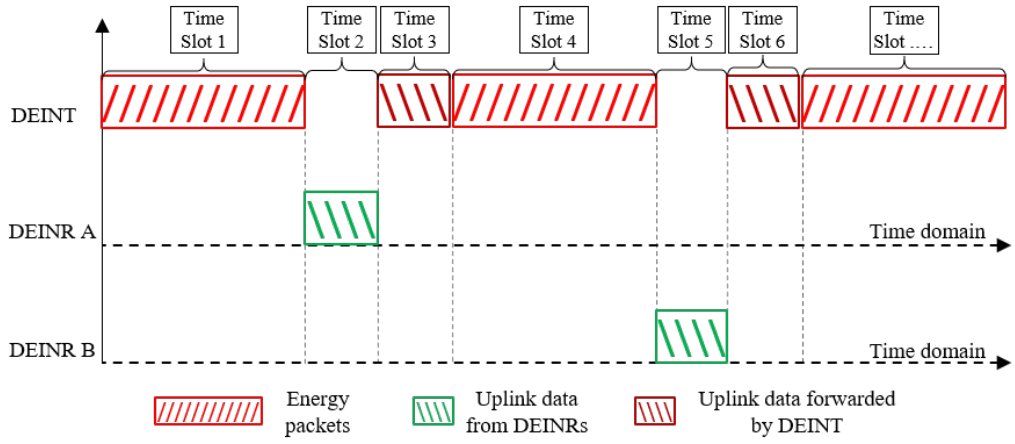

Figure 5.2: The scheduled time slots for RF energy and uplink data transmission in the DEIN system involving two DEINRs.

During time slot 1, the DEINT sends EPs to charge DEINR A. In time slot 2, the DEINT suspends the RF energy transmission and starts to turn

its directional antenna anticlockwise. Meanwhile, DEINR A commences the process of uplink data transmission, and the uplink data is transmitted to the DEINT's receiving antenna. In time slot 3, the DEINT forwards the just-received uplink data to the ZigBee coordinator through its transmission antenna. Thereafter, in time slot 4, the DEINT's antenna is turned opposite to DEINR B, and the DEINT transmits the EPs to charging it within the time slot. After that, DEINR B will transmit its uplink data to the DEINT's receiving antenna. Meanwhile, the DEINT's transmission antenna will be turned clockwise to forward the uplink data of DEINR B to the ZigBee coordinator. Thereafter, the scenario in time slot 1 will be repeated an so on.

Fig.5.2 describes the time scheduling method to manage the EPs and the uplink data (conventional ZigBee DPs) from the DEINRs in the two DEINRs based DEIN system. During the time slots for the RF energy transmission, the DEINRs always keep silence when they are receiving RF energy. After receiving the EPs, the DEINR will utilize and run out the just-harvested energy for uplink data transmission. That is to say, the amount of uplink data depends on the amount of harvested energy during the previous time slot. Based on the router function of the DEINT, all the uplink data of the DEINRs will be initially transmitted to the DEINT and then immediately forwarded to the ZigBee coordinator through the DEINT's transmission antenna.

5.3 System Modelling

5.3.1 Energy Estimation Model

The block diagram depicted in Fig.5.3 models the consumed energy in both RF energy transmitter and receiver side. In addition, it models the progress of the RF-to-DC energy conversion for transmitting a K bit-length EP from the DEINT to the DEINR. The energy estimation model involves the estimated energy consumption for transmitting a K bit-length EP in the DEINT's RF PA circuitry, the inductive energy from the DEINR's directional antenna by receiving the K bit-length EP, the estimated energy consumption in the receiver circuitry and the converted DC energy eventually stored in the supercapacitor.

By referring to the first order radio model [12], the energy consumption for transmitting a K bit-length EP in the DEINT's RF PA is modelled as,

$$E_T(K) = \varepsilon_{amp} \times K \times R^2 \tag{5.1}$$

Where K is the number of bits contained in the EP. ε_{amp} is the path loss character which indicates the energy attenuation speed of the transmitted EP. It has the unit of Joule per bit per square meter ($J/bit/m^2$). The R is the maximum dissipation distance of the RF energy waves, which is the longest distance the transmitted RF waves can reach.

It is assumed that the consumed energy in the RF PA circuitry is totally converted to the energy contained in the transmitted RF waves [12]. Hence,

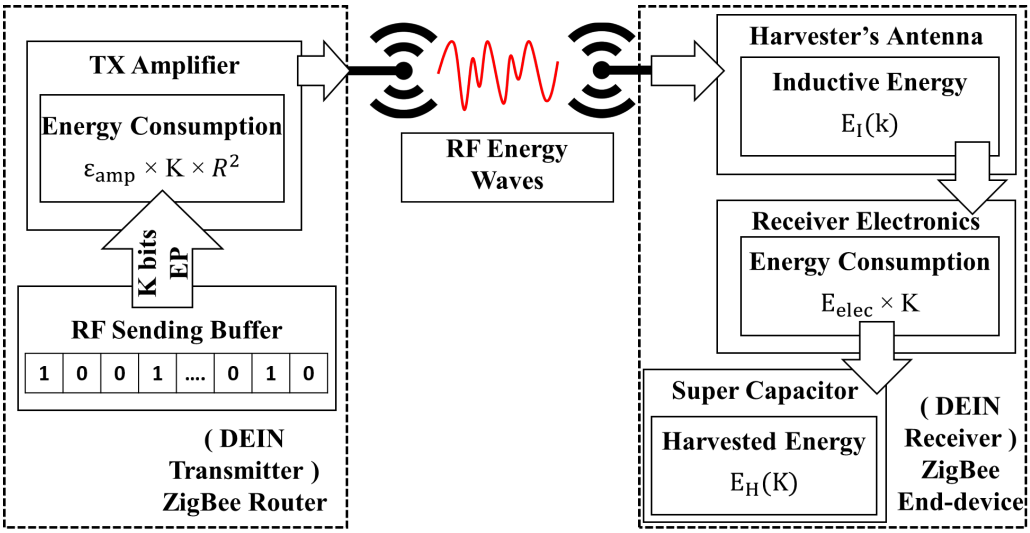

Figure 5.3: The energy estimation model for transmitting a K bit-length EP from the DEINT to the DEINR [12]

the $E_T(K)$ also represents the transmitted RF energy through transmitting a K bit-length EP, which equals to the amount of the dissipated RF energy in the distance R. With the help of Friis transmission equation [124], the relationship between the transmitted RF energy and the inductive energy from the DEINR's receiving antenna regarding the K bit-length EP is expressed as,

$$\frac{E_I(K)}{E_T(K)} = \frac{P_r \times t}{P_t \times t} = G_r G_t (\frac{\lambda}{4\pi d})^2 \tag{5.2}$$

Where $E_I(K)$ is the inductive energy obtained from the DEINR's directional antenna. The P_r and the P_t are power fed into the transmission antenna and power delivered at the receiving antenna, respectively. The t is the duration of sending/receiving the K bit-length EP. The G_r and G_t are receiving and transmission antenna gains, respectively. The λ is the wavelength of the radio frequency. The d is the practical RF energy transmission distance

between the DEINT and the DEINR. After transforming Equ.5.2, the $E_I(K)$ is expressed as,

$$E_I(K) = E_T(K) \times G_r G_t (\frac{\lambda}{4\pi d})^2 \tag{5.3}$$

With the help of Equ.5.1 and Equ.5.3, the harvested DC energy obtained by receiving a K bit-length EP is expressed as the following equation by subtracting the estimated energy consumption in the receiving circuitry.

$$\begin{aligned} E_H(K) &= E_I(K) - E_{elec} \times K \\ &= E_T(K) \times G_r G_t (\frac{\lambda}{4\pi d})^2 - E_{elec} \times K \\ &= \varepsilon_{amp} \times K \times R^2 \times G_r G_t (\frac{\lambda}{4\pi d})^2 - E_{elec} \times K \end{aligned} \tag{5.4}$$

Where $E_H(K)$ represents harvested DC energy stored in the supercapacitor by receiving a K bit-length EP. The E_{elec} is the estimated energy consumption by receiving a single bit of an EP in the receiving circuitry. The $E_H(K)$ must be greater then 0. It means there is DC energy harvested by the DEINR to supply their uplink data transmission. Hence, the following constraint should be met in the energy estimation model.

$$C1 : E_H(K) > 0 \tag{5.5}$$

5.3.2 The Time Allocation Model

As the DEINR's uplink data transmission relies on the harvested RF energy in the previous time slot, the time is allocated separately for receiving RF energy (the EPs) and transmitting uplink data (ZigBee DPs) for the DEINR. The time allocation model is described in Fig.5.4, which models the period

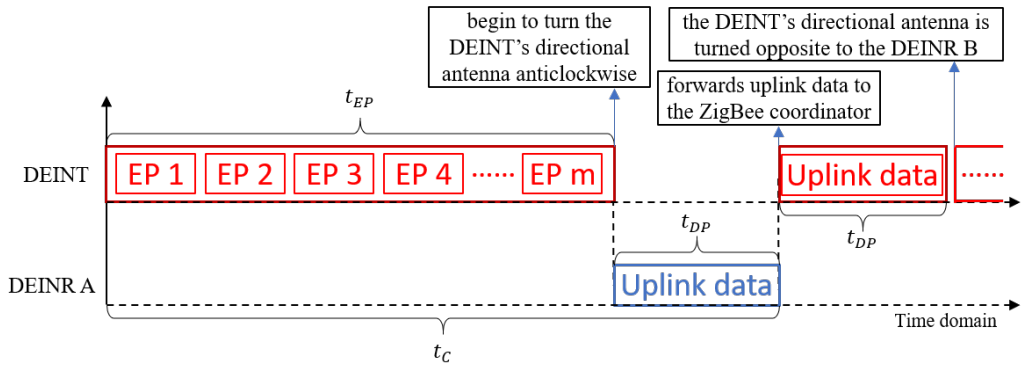

Figure 5.4: The time allocation model for receiving EPs and then transmitting uplink data (ZigBee DPs)

from the beginning of the RF energy charging/harvesting process to the finishing time-point of the successful uplink data transmission process. The time t_{EP} can be measured via an oscilloscope by tracing the voltage at the RF power detecting pin of the RF power amplifier. While the DEINT is continuously sending m EPs, the measured pulse width is the t_{EP}. The measurement is the same as the method introduced in Section 4.3.1. The time t_{DP} can be measured by the same method when the DEINT is forwarding the uplink data from a DEINR to the ZigBee coordinator. The time t_{EP} is allocated for the DEINT to transmit a series of EPs to charge the DEINR A. At the end of the time t_{EP}, the DEINT's directional antenna begins to revolve anticlockwise towards to the ZigBee coordinator, and the DEINR A immediately triggers the process to transmit the uplink data to the DEINT, namely, the ZigBee router. The time t_{DP} is the time taken for the DEINR A to transmit the uplink data as well as the duration for the DEINT to forward the uplink data from the DEINR A. The length of the t_{DP} depends on how much energy is harvested in time t_{EP}. The time t_C is the sum of the t_{EP} and

t_{DP}. According to the time allocation model, the maximum number of bits involved in the uplink data transmission during the time t_{DP} is modelled as,

$$\begin{aligned} D_{uplink} &= t_{DP} \times B_{max} \\ &= (t_C - t_{EP}) \times B_{max} \\ &= B_{max} \times t_C - K \times m, \quad \forall m \in \mathbb{N} \end{aligned} \tag{5.6}$$

Where B_{max} is the typical ZigBee bandwidth with the unit of bits per seconds, which indicates the maximum data transmission speed of the ZigBee based network. It is usually a pre-test value marked by the device manufacturer and recognized as a constant value in the DEIN system. The $K \times m$ is the overall number of bits involved in the EP stream throughout the time t_{EP}. Hence, the D_{uplink} is the maximum number of bits of the uplink data can be generated and transmitted in the time t_{DP}, which relies on the harvested DC energy in the time t_{EP}.

As the harvested DC energy during the time t_{EP} is exhausted by the DEINR A in the time t_{DP}, the following constraint must be met according to the time allocation model.

$$C2 : E_{uplink} = m \times E_H(K), \quad \forall m \in \mathbb{N} \tag{5.7}$$

Where

$$\begin{aligned} E_{uplink} &= P_{TX} \times t_{DP} \\ &= P_{TX} \times (t_C - t_{EP}) \\ &= P_{TX} \times (t_C - \frac{K \times m}{B_{max}}) \end{aligned}$$

The E_{uplink} represents the consumed energy in the DEINR A for uplink data transmission during the time t_{DP}. The P_{TX} is the transmission power configured in the RF PA circuitry of the DEINR A for transmitting the uplink data to the DEINT. The $m \times E_H(K)$ represents the harvested DC energy by receiving m EPs which have the same bit-length of K.

According to the time allocation model, the DEINT's transmission power for transmitting EPs can be estimated by the calculation that is dividing the total transmitted RF energy by the duration of this transmission. Hence, with the help of Equ.5.1, the DEINT's transmission power, namely, the P_{DEINT}, is expressed as,

$$\begin{aligned} P_{DEINT} =& \frac{E_T(K) \times m}{t_{EP}} \\ &= \frac{\varepsilon_{amp} \times K \times R^2 \times m}{\frac{K \times m}{B_{max}}} \\ &= \varepsilon_{amp} \times R^2 \times B_{max} \end{aligned} \tag{5.8}$$

Where the P_{DEINT} represents the RF transmission power with the unit of watts. The estimated P_{DEINT} is treated as the guidance for configuring the practical RF transmission power in the DEINT's RF PA circuitry. Hence, its value is limited by the maximum RF transmission power the RF PA circuitry can supply. Therefore, the following constraint must be met.

$$C3 : P_{DEINT} \leq P_{t\_max} \tag{5.9}$$

5.3.3 Problem Formulation

The involved notations in this section is listed in Table.5.1. Also, the relevant description of each notation is stated. Since the DEINR is battery-less

Table 5.1: Involved notations in the system models

Notation	Description
t_{EP}	allocated time for the DEINT to transmit EPs to a DEINR
t_{DP}	allocated time for a DEINR's uplink data transmission
t_C	sum of the t_{EP} and the t_{DP}
R	maximum dissipation distance of the RF energy waves
ε_{amp}	path loss character (joule per bit per square meter)
B_{max}	typical bandwidth of the ZigBee based network
E_{elec}	receiver circuitry's consumed energy by receiving single-bit EP
G_r	transmission antenna gain
G_t	receiving antenna gain
λ	wavelength of the RF energy waves
d	practical RF energy transmission distance
P_{DEINT}	DEINT's transmission power
P_{t_max}	maximum transmission power of DEINT
P_{TX}	DEINR's transmission power for transmitting uplink data

device, the only energy resource to the DEINR is from the DEINT. The total consumed energy in the DEINT can be recognized as the system's total consumed energy. Hence, minimizing the system's total energy consumption for uplink data transmission, is to minimize the total consumed energy in

the DEINT within the time period that transmitting a maximum amount of uplink data from DEINR to the ZigBee coordinator. Therefore, according to the time allocation model, the optimization problem for minimizing the system's total energy consumption for uplink data transmission is formulated as,

$$P1: \underset{t_{EP}, t_{DP}, P_{DEINT}}{\text{Minimize}} \quad \frac{P_{DEINT} \times t_C}{D_{uplink}} \qquad \text{subject to}: C1 - C3 \tag{5.10}$$

Where the $P_{DEINT} \times t_C$ represents the total of consumed energy in the DEINT from the beginning of the RF energy transmission process to the finishing time-point of the uplink data transmission process. The D_{uplink} is the maximum number of bits involved in the uplink data can be finally transmitted to the ZigBee coordinator during this period. Hence, the problem P1 aims to minimize the system's total consumed energy per bit of uplink data. To solving this problem, the optimally allocated time slots t_{EP}, t_{DP} and the optimal transmission power P_{DEINT} of the DEINT's needs to be optimized. In this formulated problem, C1 describes that the value of the $E_H(K)$ must be greater than 0. C2 describes that the exhausted energy in the DEINR during the process of uplink data transmission is equivalent to the just-harvested DC energy. C3 is the restrictions of transmission power can be configured in the DEINT's RF PA circuitry.

5.4 Resource Allocation Algorithm

5.4.1 Transformation

By observing the expression of problem (5.10), P_{DEINT}, t_C and D_{uplink} are all variable. Referring to Equ.5.8, P_{DEINT} is affected by the ε_{amp}, R, and B_{max}. Referring to the time allocation model in Fig.5.4, t_C is affected by t_{EP} and $t_D P$. According to Equ.5.6, D_{uplink} is affected by B_{max}, t_C, K and m. Hence, to solve the optimization problem, the expression (5.10) needs to be transformed. By introducing a notation, namely, the Ind, to represent the expression (5.10), the (5.10) is transformed as (with the help of Equ.5.6 and Equ.5.8),

$$\begin{aligned} Ind &= \frac{P_{DEINT} \times t_C}{D_{uplink}} \\ &= \frac{\varepsilon_{amp} \times R^2 \times B_{max} \times t_C}{B_{max} \times t_C - K \times m}, \quad \forall m \in \mathbb{N} \end{aligned} \tag{5.11}$$

By considering the constrain C2, the t_C can be obtained from the Equ.5.7. In addition, with the help of the Equ.5.1, the t_C is expressed as,

$$\begin{aligned} t_C &= \frac{m \times E_H(K)}{P_{TX}} + \frac{m \times K}{B_{max}} \\ &= \frac{m \times (\varepsilon_{amp} \times K \times R^2 \times G_r G_t (\frac{\lambda}{4\pi d})^2 - E_{elec} \times K)}{P_{TX}} + \frac{m \times K}{B_{max}}, \quad \forall m \in \mathbb{N} \end{aligned} \tag{5.12}$$

Thereafter, by replacing the t_C in the Equ.5.11 with the expression (5.12), the Equ.5.11 is transformed as,

$$Ind = \frac{\varepsilon_{amp} \times R^2 \times B_{max}}{B_{max} - \frac{1}{\frac{\varepsilon_{amp} \times R^2 \times G_r G_t (\frac{\lambda}{4\pi d})^2 - E_{elec}}{P_{TX}} + \frac{1}{B_{max}}}} \tag{5.13}$$

By observing the Equ.5.13, if the RF energy transmission distance (d) is fixed, only the argument R is variable. Hence, the problem P1 formulated in (5.10) can be transformed to the mathematical problem P2, which aims to find the optimal value of R to minimize the Ind.

$$\begin{aligned} P2 : \underset{R}{\text{Minimize}} \;\; & Ind(R) \\ \text{subject to} : \; & C1, C3 \end{aligned} \tag{5.14}$$

5.4.2 Solving the Problem

To solving the problem P2, it is required to find the minimum value of the $Ind(R)$ within the boundary of the argument R. If there is a value of R (within its boundary) can make the first-order derivative of the $Ind(R)$ equal to 0 and the second-order derivative of the $Ind(R)$ is always greater than 0 (within the boundary of the argument R), $Ind(R)$ is recognized as a concave function. Within the boundary of the argument R, $Ind(R)$ has a minimum value. Hence, the first-order derivative to the $Ind(R)$ with respect to the argument R will be calculated firstly. By transforming Equ.5.13, the $Ind(R)$

is expressed as,

$$Ind(R) = \varepsilon_{amp} \times R^2 + \frac{P_{TX} \times \varepsilon_{amp} \times R^2}{G_r G_t (\frac{\lambda}{4\pi d})^2 \times B_{max} \times \varepsilon_{amp} \times R^2 - B_{max} \times E_{elec}} \tag{5.15}$$

If let

$$U(R) = \varepsilon_{amp} \times R^2$$

The $Ind(U)$ is expressed as,

$$Ind(U) = U + \frac{P_{TX} \times U}{G_r G_t (\frac{\lambda}{4\pi d})^2 \times B_{max} \times U - B_{max} \times E_{elec}}$$

As

$$\frac{d(Ind)}{d(R)} = \frac{d(Ind)}{d(U)} \cdot \frac{d(U)}{d(R)}$$

Then, there is

$$\begin{aligned} \frac{d(Ind)}{d(U)} &= 1 + \frac{P_{TX} \times (G_r G_t (\frac{\lambda}{4\pi d})^2 \times B_{max} \times U - B_{max} \times E_{elec})}{(G_r G_t (\frac{\lambda}{4\pi d})^2 \times B_{max} \times U - B_{max} \times E_{elec})^2} \\ &\quad - \frac{P_{TX} \times G_r G_t (\frac{\lambda}{4\pi d})^2 \times B_{max} \times U}{(G_r G_t (\frac{\lambda}{4\pi d})^2 \times B_{max} \times U - B_{max} \times E_{elec})^2} \\ &= 1 - \frac{P_{TX} \times B_{max} \times E_{elec}}{(G_r G_t (\frac{\lambda}{4\pi d})^2 \times B_{max} \times U - B_{max} \times E_{elec})^2} \end{aligned}$$

and

$$\frac{d(U)}{d(R)} = 2 \times \varepsilon_{amp} \times R$$

As a result, the first-order derivative to the $Ind(R)$ with respect to the argument R is obtained as,

$$\begin{aligned}\frac{d(Ind)}{d(R)} =&(1 - \frac{P_{TX} \times B_{max} \times E_{elec}}{(G_r G_t(\frac{\lambda}{4\pi d})^2 \times B_{max} \times \varepsilon_{amp} \times R^2 - B_{max} \times E_{elec})^2}) \\ &\times (2 \times \varepsilon_{amp} \times R)\end{aligned} \tag{5.16}$$

In order to find the zero value point of the $Ind(R)$, a value of R to make Equ.5.16 equal to 0 need to be found. To simplify the calculation procedures, a specific value of U can be found to let $\frac{d(Ind)}{d(U)}$ equal to 0, which therefore make $\frac{d(Ind)}{d(R)}$ equal to 0 because that the $\frac{d(U)}{d(R)}$ is always greater than 0. As a result, the following two zero value points make the $\frac{d(Ind)}{d(U)}$ equal to 0.

$$U = \frac{B_{max} \times E_{elec} + \sqrt{P_{TX} \times B_{max} \times E_{elec}}}{G_r G_t(\frac{\lambda}{4\pi d})^2 \times B_{max}}$$

Or

$$U = \frac{B_{max} \times E_{elec} - \sqrt{P_{TX} \times B_{max} \times E_{elec}}}{G_r G_t(\frac{\lambda}{4\pi d})^2 \times B_{max}}$$

By consider the constraint C1 in (5.5), also with the help of the Equ.5.4, the expression of (5.5) can be transformed as,

$$\varepsilon_{amp} \times R^2 > \frac{E_{elec}}{G_r G_t(\frac{\lambda}{4\pi d})^2} \tag{5.17}$$

Because the $U(R)$ is expressed by $\varepsilon_{amp} \times R^2$, only the first zero value point (U) meets the above constraint. Therefore, the correct zero value point (R) to let $\frac{d(Ind)}{d(R)}$ equal to 0 is

$$R = \sqrt{\frac{B_{max} \times E_{elec} + \sqrt{P_{TX} \times B_{max} \times E_{elec}}}{G_r G_t (\frac{\lambda}{4\pi d})^2 \times B_{max} \times \varepsilon_{amp}}} \tag{5.18}$$

To prove that the calculated zero value point R in (5.18) makes the $Ind(R)$ in (5.15) reach to its minimum value, the second-order derivative to the $Ind(R)$ (in 5.15) with respect to the R needs to be calculated. The proving process is described as follows. By transforming the Equ.5.16, there is

$$\frac{d(Ind)}{d(R)} = 2 \times \varepsilon_{amp} \times R - \frac{2 \times P_{TX} \times \varepsilon_{amp} \times E_{elec}}{A^2 \times B_{max} \times \varepsilon_{amp}^2 \times R^3 + \frac{E_{elec}^2 \times B_{max}}{R} - 2 \times E_{elec} \times B_{max} \times A \times \varepsilon_{amp} \times R}$$

Where

$$A = G_r G_t (\frac{\lambda}{4\pi d})^2$$

Then, its second-order derivative is

$$\frac{d^2(Ind)}{d(R)^2} = 2\times\varepsilon_{amp}+$$

$$\frac{2\times P_{TX}\times E_{elec}\times\varepsilon_{amp}\times(3\times A^2\times B_{max}\times\varepsilon_{amp}^2\times R^2 - E_{elec}^2\times B_{max}\times R^{-2} - 2\times E_{elec}\times B_{max}\times A\times\varepsilon_{amp})}{(A^2\times B_{max}\times\varepsilon_{amp}^2\times R^3 + \frac{E_{elec}^2\times B_{max}}{R} - 2\times E_{elec}\times B_{max}\times A\times\varepsilon_{amp}\times R)^2}$$

$$= 2\times\varepsilon_{amp}+$$

$$\frac{2\times P_{TX}\times E_{elec}\times\varepsilon_{amp}\times(3\times A^2\times\varepsilon_{amp}^2\times R^4 - E_{elec}^2 - 2\times E_{elec}\times A\times\varepsilon_{amp}\times R^2)}{(A^2\times B_{max}\times\varepsilon_{amp}^2\times R^3 + \frac{E_{elec}^2\times B_{max}}{R} - 2\times E_{elec}\times B_{max}\times A\times\varepsilon_{amp}\times R)^2\times\frac{R^2}{B_{max}}}$$

Where

$$A = G_r G_t(\frac{\lambda}{4\pi d})^2$$

By observing the above second-order derivative expression of the $Ind(R)$, it is found that if

$$\begin{gathered} 3\times A^2\times\varepsilon_{amp}^2\times R^4 - E_{elec}^2 - 2\times E_{elec}\times A\times\varepsilon_{amp}\times R^2 \\ Where\ A = G_r G_t(\frac{\lambda}{4\pi d})^2 \end{gathered} \tag{5.19}$$

is greater than 0, the second-order derivative of the $Ind(R)$ will be identically greater then 0. Hence, by transforming the expression in (5.19), there is

$$(G_r G_t(\frac{\lambda}{4\pi d})^2\times\varepsilon_{amp}\times R^2)\times(3\times G_r G_t(\frac{\lambda}{4\pi d})^2\times\varepsilon_{amp}\times R^2 - 2\times E_{elec}) - E_{elec}^2 \tag{5.20}$$

With the help of the constraint in (5.17), there is

$$G_r G_t (\frac{\lambda}{4\pi d})^2 \times \varepsilon_{amp} \times R^2 > E_{elec}$$

$$3 \times G_r G_t (\frac{\lambda}{4\pi d})^2 \times \varepsilon_{amp} \times R^2 > 3 \times E_{elec}$$

Then, there is

$$3 \times G_r G_t (\frac{\lambda}{4\pi d})^2 \times \varepsilon_{amp} \times R^2 - 2 \times E_{elec} > E_{elec}$$

Therefore, there is

$$(G_r G_t (\frac{\lambda}{4\pi d})^2 \times \varepsilon_{amp} \times R^2) \times (3 \times G_r G_t (\frac{\lambda}{4\pi d})^2 \times \varepsilon_{amp} \times R^2 - 2 \times E_{elec}) > E_{elec}^2$$

Finally, there is

$$(G_r G_t (\frac{\lambda}{4\pi d})^2 \times \varepsilon_{amp} \times R^2) \times (3 \times G_r G_t (\frac{\lambda}{4\pi d})^2 \times \varepsilon_{amp} \times R^2 - 2 \times E_{elec}) - E_{elec}^2 > 0$$

According to the process of proof described above, the expression (5.20) is identically greater then 0 by subject to the constraint (5.17) derived from constraint C1. Hence, the second-order derivative of the $Ind(R)$ is identically greater then 0 by subject to the constraint C1, which proves that the $Ind(R)$ is a concave function with respect to the R within the constraint C1. Therefore, the R value indicated in (5.18) makes the expression $Ind(R)$ reach to its minimum value. By considering the last constraint C3 and the

problem P2 is solved as,

$$R = \begin{cases} \sqrt{\frac{B_{max} \times E_{elec} + \sqrt{P_{TX} \times B_{max} \times E_{elec}}}{G_r G_t (\frac{\lambda}{4\pi d})^2 \times B_{max} \times \varepsilon_{amp}}} & \text{if } R \text{ in (5.18)} \leq \sqrt{\frac{P_{t\_max}}{\varepsilon_{amp} \times B_{max}}} \\ \sqrt{\frac{P_{t\_max}}{\varepsilon_{amp} \times B_{max}}} & \text{if } R \text{ in (5.18)} > \sqrt{\frac{P_{t\_max}}{\varepsilon_{amp} \times B_{max}}} > \sqrt{\frac{E_{elec}}{G_r G_t (\frac{\lambda}{4\pi d})^2 \times \varepsilon_{amp}}} \\ \text{No solution} & \text{if } \sqrt{\frac{P_{t\_max}}{\varepsilon_{amp} \times B_{max}}} \leq \sqrt{\frac{E_{elec}}{G_r G_t (\frac{\lambda}{4\pi d})^2 \times \varepsilon_{amp}}} \end{cases} \tag{5.21}$$

5.4.3 Resource Allocation Algorithm

Algorithm 2 is designed to find the optimal value of R to solve the problem P2. Thereafter, it find the optimal values of t_{EP}, t_{DP} and P_{DEINT} to solve the problem P1 depends on the optimal R. It is a resource allocation algorithm which intends to minimize the energy cost for the DEINR's uplink data transmission. It allocates the optimal time length for the DEINT's RF energy transmission and the DEINR's uplink data transmission, and it configures the optimal transmission power for transmitting EPs (RF energy) in the DEIN system.

According to the primary process described in Algorithm 2, it firstly calculates the optimal value of R basing on the Equ.5.18. Thereafter, the optimal transmission power for transmitting EPs is calculated based on Equ.5.8. Then, it checks if the obtained value of transmission power exceeds the limit of the maximum transmission power the DEINT's RF PA circuitry can set. The maximum transmission power is a preset value, which depends on the

Algorithm 2 Resource allocation to minimize the energy cost for the DEINR's uplink data transmission

Input :

$d \leftarrow$ RF energy transmission distance, $\lambda \leftarrow 2.4\,\text{GHz}$ wavelength

$G_t \leftarrow$ Transmission antenna gain, $G_r \leftarrow$ Receiving antenna gain

$E_{elec} \leftarrow$ Consumed energy in DEINR for receiving a single-bit EP

$B_{max} \leftarrow$ Typical bandwidth of the ZigBee based network

$\varepsilon_{amp} \leftarrow$ Path loss character (joule per bit per square meter)

$P_{TX} \leftarrow$ DEINR's transmission power for transmitting uplink data

$P_{t\_max} \leftarrow$ Maximum transmission power of DEINT for transmitting EPs

$K \leftarrow$ the number of bits contained in the EP

$m \leftarrow$ the preset number of EPs for each RF energy transmission period

Output : t_{EP}, t_{DP}, P_{DEINT}

Let $temp\_R = 0$, $temp\_P_t = 0$

if $\sqrt{\frac{P_{t\_max}}{\varepsilon_{amp} \times B_{max}}} \leq \sqrt{\frac{E_{elec}}{G_r G_t (\frac{\lambda}{4\pi d})^2 \times \varepsilon_{amp}}}$ **then**

  return Fault

else

  $temp\_R \leftarrow \sqrt{\frac{B_{max} \times E_{elec} + \sqrt{P_{TX} \times B_{max} \times E_{elec}}}{G_r G_t (\frac{\lambda}{4\pi d})^2 \times B_{max} \times \varepsilon_{amp}}}$

  $temp\_P_t \leftarrow \varepsilon_{amp} \times (temp\_R)^2 \times B$

  if $temp\_P_t \leq P_{t\_max}$ **then**

    $P_{DEINT} \leftarrow temp\_P_t$

  else

    $temp\_R \leftarrow \sqrt{\frac{P_{t\_max}}{\varepsilon_{amp} \times B_{max}}}$

    $P_{DEINT} \leftarrow P_{t\_max}$

  end if

  $t_{EP} \leftarrow \frac{K \times m}{B_{max}}$

  calculate t_C according to (5.12) and $temp\_R$

  $t_{DP} \leftarrow t_C - t_{EP}$

  return t_{EP}, t_{DP}, P_{DEINT}

end if

hardware character of the DEINT's RF PA circuitry. If the calculated transmission power is smaller than the maximum transmission power, the calculated optimal transmission power will be returned. Otherwise, the maximum transmission power of the DEINT's RF PA circuitry will be returned, and the optimal value of R will be updated according to Equ.5.8 with the maximum transmission power (P_{t_max}). In the practical DEIN system, the number (m) of EPs and the number of bits (K) included in each EP are preset parameters. They determine the time length (t_{EP}) for transmitting the EPs to charge each DEINR in the DEIN system, which is also the duration time for the DEINT's transmission antenna to stay opposite to each DEINR. As time t_C can be calculated according to the Equ.5.12 with the optimal value of R, the optimal time length (t_{DP}) for each DEINR's uplink data transmission is therefore obtained and turned.

5.5 Performance Evaluation and Numerical Result

To evaluating the performance of the algorithm, 5 sets of simulation experiments are carried out. Different RF energy transmission distance is applied to the simulation experiments, which is from 0.2 m to 0.6 m with a step of 0.1 m. In each individual experiment, the DEINT will transmit 15000 EPs with the same (127) bit-length at each time when its transmission antenna is turned opposite to DEINR A or DEINR B. The remaining constant system parameters are listed in Table.5.2.

Table 5.2: Constant system parameters for performance evaluation

Notation	Value
K	127 $(bits)$
m	15000
ε_{amp}	1.0×10^{-9} $(J/bit/m^2)$
B_{max}	250 $(Kbps)$
E_{elec}	1×10^{-9} (J/bit)
G_r	14 (dBi)
G_t	14 (dBi)
λ	12.49×10^{-2} (m)
P_{t_max}	2 (W)
P_{TX}	0.1155 (W)
d	$\{0.4, 0.5, 0.6, 0.7, 0.8\}$ (m)

Fig.5.5 shows the maximum number (D_{uplink}) of bits can be transmitted as the uplink data with respect to the DEINT's transmission power (P_{DEINT}) when different RF energy transmission distance d is applied. The uplink data is transmitted by a DEINR depends on its harvested DC energy by receiving 15000 EPs. With the growth of P_{DEINT}, D_{uplink} increases as the DEINT's transmission power increases, and therefore more energy is harvested for uplink data transmission. By contrast, with respect to the same P_{DEINT}, fewer uplink data can be transmitted when longer RF energy transmission distance d is applied because longer d bring more energy loss in the air, and the available RF energy is weakened for DEINR's receiving antenna. Therefore, less harvested energy only affords fewer uplink data to be transmitted.

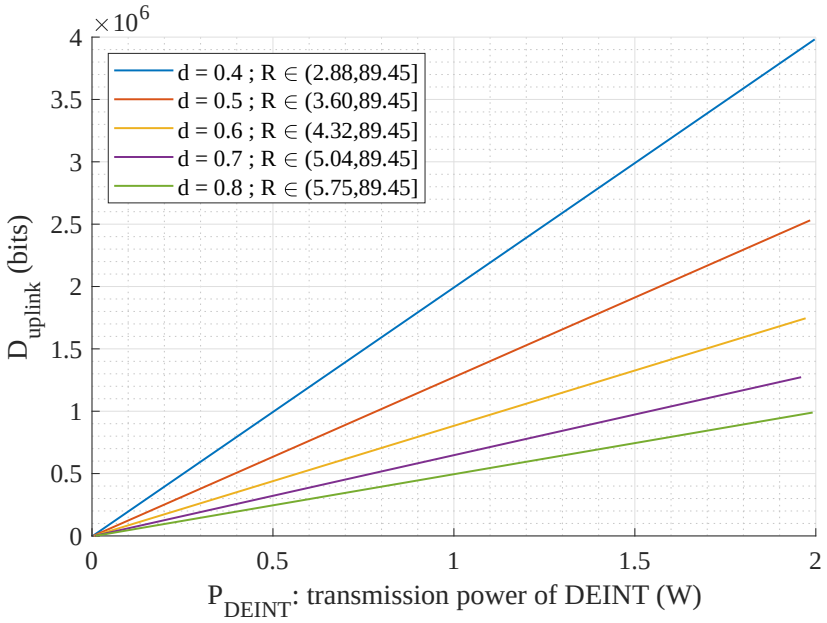

Figure 5.5: The maximum number of bits (D_{uplink}) can be transmitted as the uplink data with respect to DEINT's transmission power (P_{DEINT}) when the RF energy transmission distance $d = \{0.4, 0.5, 0.6, 0.7, 0.8\}$ metre.

Fig.5.6 shows the system's total consumed energy during a successful process of uplink data transmission with respect to DEINT's transmission power (P_{DEINT}) when the RF energy transmission distance d changes in sequence. A successful process of uplink data transmission is from when the DEINT begins to transmit EPs for charging a DEINR to when the uplink data is successfully transmitted to the ZigBee coordinator. The total consumed energy is caused by transmitting 15000 EPs and forwarding the uplink data from the DEINR to the ZigBee coordinator. When higher transmission power (P_{DEINT}) is used for the DEINT to transmit EPs and forward uplink data, it brings more energy consumption. Furthermore, according to Fig.5.5,

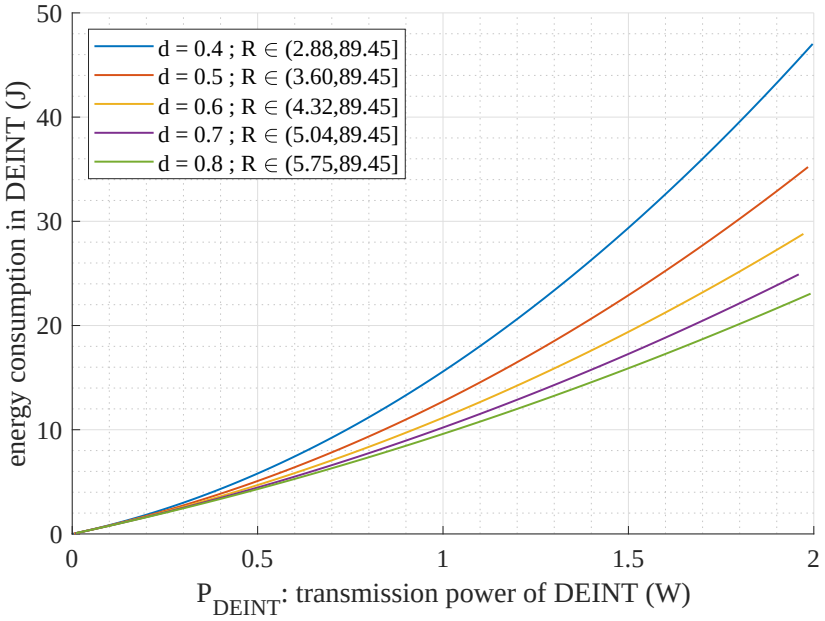

Figure 5.6: The system's total consumed energy in the DEINT during an uplink data transmission process with to DEINT's transmission power (P_{DEINT}) when the RF energy transmission distance $d = \{0.4, 0.5, 0.6, 0.7, 0.8\}$ metre.

higher P_{DEINT} means more uplink data can be transmitted by the DEINR and then forwarded by the DEINT. Forwarding more uplink data also brings more energy consumption. As a result, the system's total consumed energy rapidly increases when P_{DEINT} increases. By contrast, if P_{DEINT} is fixed, less energy is consumed during the uplink data transmission process when longer d is applied. Longer d brings more energy loss in the air, which reduces the finally harvested DC energy. Therefore, less uplink data is forwarded by the DEINT, which weakens the total energy consumption.

Fig.5.7 shows the consumed energy per bit of the uplink data with re-

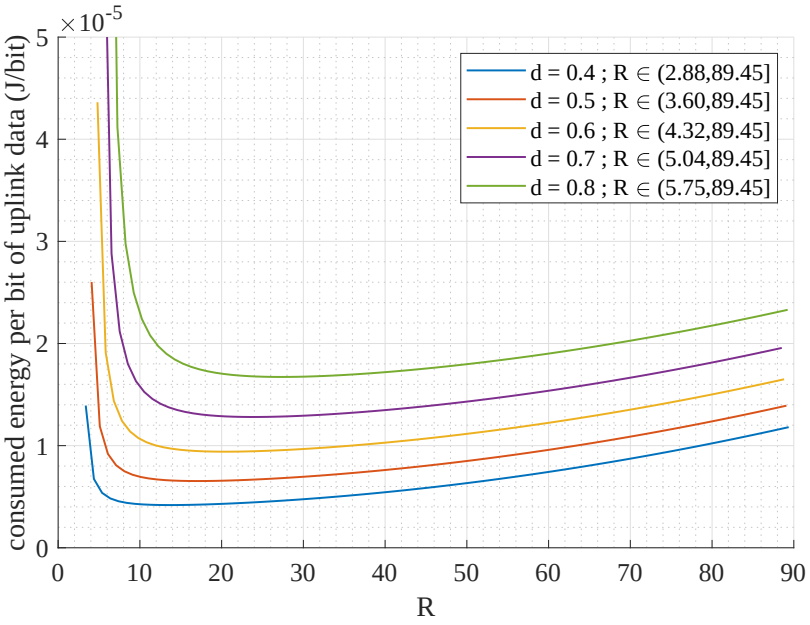

Figure 5.7: The consumed energy per bit of transmitted uplink data with respect to argument R when the RF energy transmission distance $d = \{0.4, 0.5, 0.6, 0.7, 0.8\}$ metre.

spect to argument R when different RF energy transmission distance d is applied. The plots prove that $Ind(R)$ in Equ.5.15 is a concave function with respect to R. The reason for getting the concave curve can be explained by observing Fig.5.5 and Fig.5.6. In the beginning, according to Equ.5.8, a slight increment of R will generally increase the DEINT's transmission power and therefore increase the DEINR's harvested DC energy, which increases the amount of transmitted uplink data. Although the DEINT's energy consumption also increases, the growth speed of the transmitted uplink data is quicker than the total energy consumption. Hence, the system's consumed energy per bit of uplink data decreases in the beginning. With the increment of R,

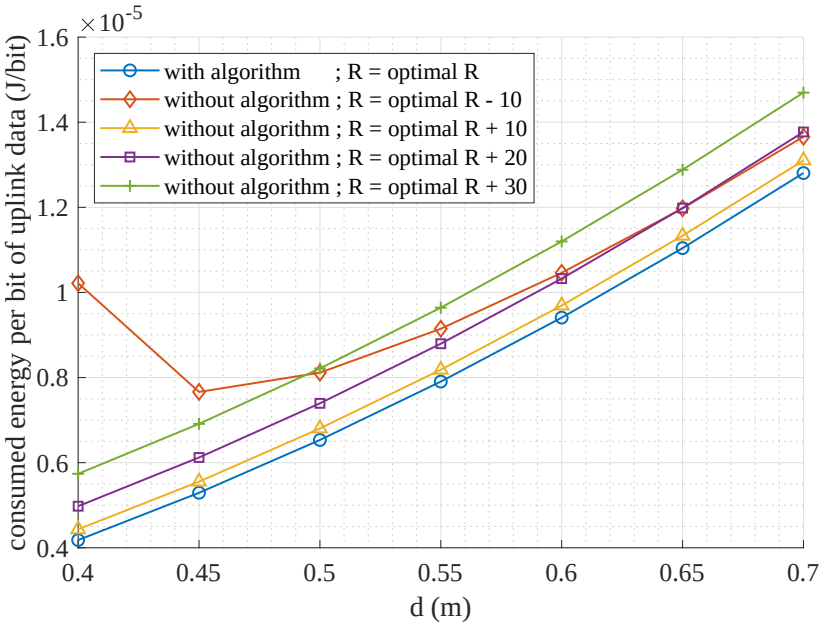

Figure 5.8: The algorithm testing result with respect to different RF energy transmission distance d.

P_{DEINT} increases quicker, and the growth speed of the DEINT's energy consumption becomes quicker than the transmitted uplink data. It is because more uplink data brings also more energy consumption for the DEINT to forward them. Hence, the system's consumed energy per bit of uplink data increases later.

Fig.5.8 shows the algorithm testing result when different RF energy transmission distance d is applied. When the algorithm is applied, the system's consumed energy per bit of uplink data is minimized for every distance d. Only the optimal R derived from the algorithm can achieve the best performance. Then, the optimal R is used for calculating the transmission power (P_{DEINT}) and the time (t_{DP}) allocated for uplink data transmission.

5.6 Chapter Summary

In this chapter, a DEIN topology involving a single DEINT and multiple DEINRs has been proposed. Based on the topology, the energy estimation model has been designed. The model estimates the related energy during a process of transmitting and then receiving a K bit-length EP. The estimated energy is the energy consumption in the DEINT, the transmitted RF energy, the inductive energy from the DEINR's receiving antenna, the energy consumption for receiving the K bit-length EP and the finally harvested DC energy. Furthermore, a time allocation model has been designed for managing RF energy transmission and uplink data transmission in different time slots. The RF energy transmission is transmitting EPs to a DEINR, which is launched by the DEINT. The uplink data transmission is launched by a DEINR and routed by the DEINT to the smart gateway eventually. Based on the energy estimation model and time allocation model, a resource allocation algorithm has been designed to minimize the consumed energy per bit of uplink data. Finally, the numeric results obtained by the simulation experiments show that the energy consumption per bit of uplink data has been successfully minimized with the algorithm applied.

Chapter 6

Adaptive Energy-Saving Algorithm to Minimize the DEINR's Energy Usage

6.1 Introduction

The harvested DC energy stored in the DEINR's supercapacitor is mainly utilized by wireless data communication carried out by the ZigBee module (configured as a ZigBee end-device). Because the radio function of the circuit consumes more energy than other circuital behaviours. In this chapter, an energy-saving algorithm is designed to minimize the average energy consumption of the DEINR (ZigBee end-device). Different from the related works, the

proposed algorithm is adaptive for the practical DEIN system. The average energy consumption is a thesis's proposed mathematical model, which considers the DEINR's energy consumption affected by the transmission power (set by the transmission current of the hardware) of the ZigBee end-device and its packet loss rate. According to the practical hardware character of the applied ZigBee end-device (in Table.6.2), if the DEINR's packet is transmitted successfully, normally, its receiving radio circuit will be on for a typical 192 us for wait the relevant ACK. Thereafter, the radio function of the ZigBee end-device will be switched off until next packet transmission. If DEINR's packet is transmitted failed, its receiving radio circuit will be on for a maximum 37 ms (waiting for an unexisting ACK), which is max ACK waiting time defined by ZigBee protocol [125]. The idle current of the receiving radio circuit when waiting for the ACK is 24 mA. For successful and failed packet transmission, different energy is consumed in receiving radio circuit due to different ACK waiting time. For example, when decreasing the transmission power, the packet loss rate could increase. Decreasing the transmission power can reduce energy consumption. failed packets transmission causes extra energy consumption on the receiving radio circuit. If the reduced energy consumption by the former is higher than the extra energy consumption by the latter, the average energy consumption of the ZigBee end-device is reduced. Otherwise, the average energy consumption of the ZigBee end-device is increased. Hence, the energy-saving algorithm proposed in this chapter aims to adaptively adjust the transmission power of the ZigBee end-device to obtain a minimized average energy consumption. It balances the trade-off between the transmission power and the packet loss rate.

The remainder of this chapter is organized as follows. Section 6.2 proposes a energy consumption model for estimation the consumed energy of the radio function. Section 6.3 describes the proposed energy-saving algorithm. Section 6.4 shows the results for algorithm performance evaluation.

6.2 Energy Consumption Model

A complete packet transmission process consists of a time period for sending a packet and then receiving the related ACK packets. In Fig.6.1, the first order radio model [12] is introduced to estimate related energy consumption.

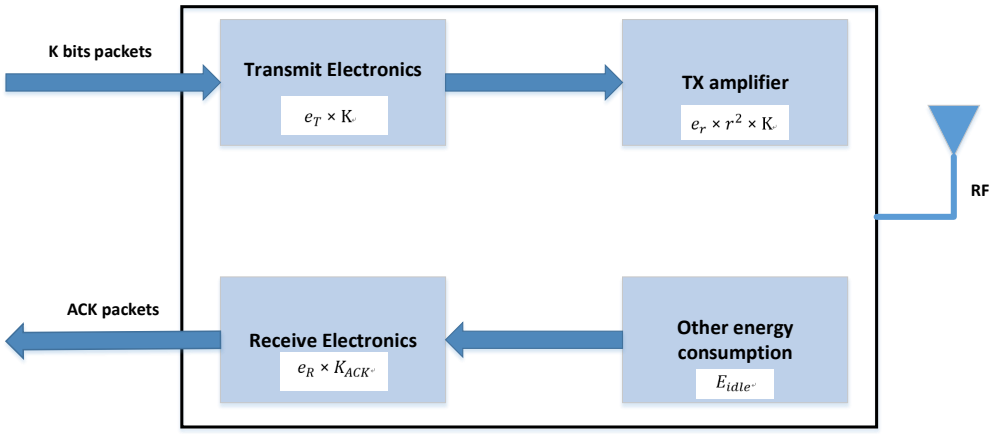

Figure 6.1: First order radio model [12]

If there is a K bit-length packet prepared to be transmitted, the energy consumption involving sending this packet and receiving the relevant ACK

is represented as follows,

$$E_T = e_T \times K + e_r \times r^2 \times K + e_R \times K_{ACK} + E_{idle} \tag{6.1}$$

Where E_T is the energy consumption, which includes the consumed energy of sending a K bit-length packet and the consumed energy of receiving the relevant ACK. e_T is the circuital dissipation while transmitting per bit of a packet. e_r is the path loss character which indicates the energy attenuation speed of the transmitted RF waves. It has the unit of Joule per bit per square meter ($J/bit/m^2$). r is the path loss distance, which is the maximum distance the RF waves can reach. That is to say, $e_r \times r^2$ indicates the energy dissipation of transmitting one bit in a distance r. e_R is the circuital dissipation while receiving one bit of a packet. K_{ACK} is the number of bits involved in ACK packet. E_{idle} is the system's circuital consumption, which consists of the consumed energy for switching the RF circuit from transmission mode to receiving mode as well as the energy cost for waiting the ACK packet.

It is assumed that the communication distance between the ZigBee end-device (DEINR) and the ZigBee coordinator (smart gateway) is d. The ZigBee coordinator can receive end-device's signal, if and only if $d \leqslant r$. In other words, if the communication distance is fixed to d, the parameter r must equal or higher than d in order to resist path loss. In the practical communication scenario, receiver may not receive all packets successfully due to the packet loss. When the ZigBee node is changed from transmission mode to the receiving mode, it may have to wait a long period but without receiving any ACK packet. This maximum value is 54 symbol periods defined by the ZigBee standard. In this situation, K_{ACK} will be equal to 0 as well as

$e_R \times K_{ACK}$. In consideration of this situation aforementioned, Equ.6.1 can be rewritten as Equ.6.2,

$$E_T = \begin{cases} (e_T + e_r \times r^2) \times K + e_R \times K_{ACK} + E_{idle\_normal}, & successful \\ (e_T + e_r \times r^2) \times K + E_{idle\_max}, & failed \end{cases} \tag{6.2}$$

Where *successful* indicates the energy consumption of sending a packet and successfully receiving the related ACK. *failed* indicates the energy consumption of sending a packet and waiting for the maximum timeout. C Carmona [48] indicates that the average energy consumption of each packet can be calculated by referring to the probability of how likely to send a successful packet. If a quasi-stationary channel is considered, a statistic parameter PRR to express the probability is introduced. The relationship between the average energy consumption of the radio function and the parameter PRR is expressed as follows,

$$E_{T-average} = PRR \times E_{T\_success} + (1 - PRR) \times E_{T\_fail} \tag{6.3}$$

If combining Equ.6.2 and Equ.6.3 together, Equ.6.4 presents the combination as,

$$\begin{aligned} E_{T\_average}(r, PRR) =& PRR \times ((e_T + e_r \times r^2) \times K + e_R \times K_{ACK} + E_{idle\_normal}) \\ &+ (1 - PRR) \times ((e_T + e_r \times r^2) \times K + E_{idle\_max}) \end{aligned} \tag{6.4}$$

The parameters e_T and e_R are circuital characters based on the ZigBee device's hardware specification. Furthermore, E_{idle_normal} and E_{idle_max} are fixed values because the ZigBee device's idle current in packet receiving mode is known according to the hardware data sheet, and K_{ACK} is defined by ZigBee

standard. Moreover, e_r is path loss character that should be evaluated in real scenario. The bit-length of packet K is known before transmitting it. It can be recognized that only r and PRR are variables in Equ.6.4. Our algorithm is intended to minimize $E_{T-average}(r, PRR)$.

6.3 Energy Saving Algorithm

Referring to Equ.6.1, providing the path loss distance parameter r is set, the maximum transmission distance from ZigBee end-device to coordinator is defined. In other words, if the distance between ZigBee end-device and coordinator is longer than r, the signal from end-device will not have enough energy to reach to coordinator side. However, if building up r to increase the distance where signal can reach, the transmission power will be increase and therefore the ZigBee's current level for transmission mode (transmission current level) will be raised accordingly. The relationship between transmission current level and path loss distance parameter r can be expressed as,

$$I_{TX} \times V \times \frac{K}{B_{ZigBee}} = (e_r \times r^2) \times K \tag{6.5}$$

Where I_{TX} is the transmission current if ZigBee device is sending a packet, which depends on the transmission power. V is the voltage which is supplied to ZigBee end-device and the typical value is 3.3 V. k stands for bit-length of the transmitted packet and B_{ZigBee} stands for ZigBee transmission rate with a typical value of 250kbps. Also, the relationship between I_{T_idle}(current of transmission active mode) and e_T(transmit electronics characteristic) can be

evaluated as,

$$I_{T\_idle} \times V \times \frac{K}{B_{ZigBee}} = e_T \times K \tag{6.6}$$

Where I_{T_idle} is the current level if ZigBee device is in transmission active mode, which is ready for packet transmission. Equ.6.5 can be transformed as Equ.6.7,

$$I_{TX}(r) = \frac{(e_r \times r^2) \times B_{ZigBee}}{V} \tag{6.7}$$

The above formula means if a certain value r is required in the system, the relevant transmission current I_{TX} will be confirmed. Furthermore, if a certain value r is the optimal solution for minimizing $E_{T\_average}(r, PRR)$, the relevant I_{TX} value will be also the optimal solution. In our scenario, if the communication distance d is known, the parameter r based on the value of d can be configured. For example, if d is 10 meters, the parameter r can be set from 10 metres to 100 metres by the step of 1 metre. Therefore, there are nighty-one different r. Then nighty-one different I_{TX} values is obtained based on Equ.6.7. Then, the transmission current level is set to be the aforementioned values I_{TX} one by one, these nighty-one PRR values will be calculated accordingly. Therefore, nighty-one sets of r and PRR values are obtained. After that, putting them into Equ.6.4 in sequence, nighty-one different $E_{T\_average}$ values will be finally obtained. By comparing each $E_{T\_average}$ value, the minimum one and its related set of r and PRR will be picked up. The specific r indicates the specific I_{TX}.

If the energy consumption saving algorithm is designed for the aforementioned situation, the computation work will be heavy for ZigBee based embedded hardware. However, an innovative method is proposed in the fol-

lowing contents to reduce huge computation work. By analysing Equ.6.4, it can be converted as Equ.6.8,

$$\begin{aligned} E_{T\_average}(r, PRR) =& E_{idle\_max} + K \times e_T \\ &+ PRR \times (e_R \times K_{ACK} + E_{idle-normal} - E_{idle-max}) \\ &+ K \times e_r \times r^2 \end{aligned} \tag{6.8}$$

If assuming r is continuous and belongs to $r \in (0, \infty)$, the second partial derivative of $E_{T\_average}$ with respect to variable r can be calculated. The result is (6.9),

$$\frac{d[E_{T-average}(r, PRR)]}{dr^2} = 2 \times K \times e_r \tag{6.9}$$

K and e_r are fixed values. Meanwhile, they are all greater than 0. Thus, the expression in (6.9) is bigger than 0. Therefore, Equ.6.8 (or Equ.6.4) is a convex function. Fig.6.2 shows the trend of this function.

From Fig.6.2, it is only needed to find a specific value r to make $E_{T\_average}(r+1, PRR_{r+1}) > E_{T\_average}(r, PRR_r)$ (PRR_r is the packet received rate while the loss path distance parameter is set to r).For example, if the initial value is r_1, r_3 should be the optimum value because of $E_{T\_average}(r_4, PRR_{r_4}) > E_{T\_average}(r_3, PRR_{r_3})$. If the initial value is r_4, r_4 should be the optimum value because of $E_{T\_average}(r_5, PRR_{r_5}) > E_{T\_average}(r_4, PRR_{r_4})$. There is no need to use all possible values of r to calculate $E_{T\_average}$. The Algorithm 3 is implemented as follows,

The proposed algorithm 3 is running at ZigBee coordinator side and intended to minimize the average energy consumption for ZigBee end-device's

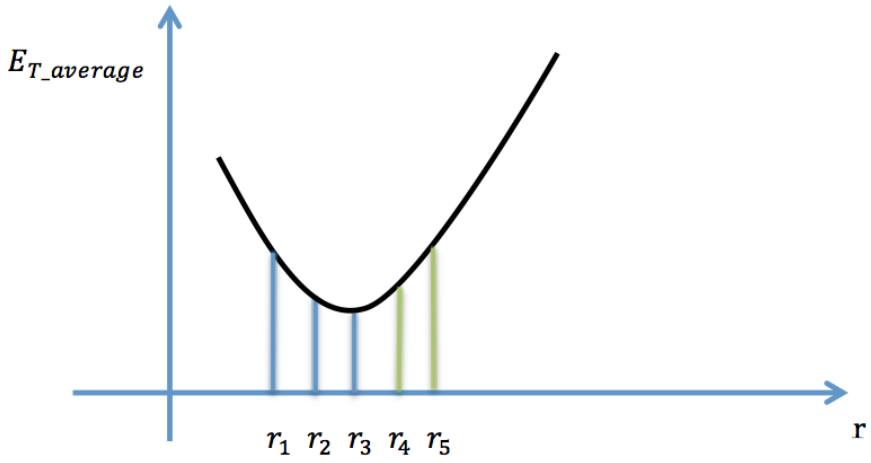

Figure 6.2: Trend of convex function

radio function. After the algorithm, the instruction will be sent out by ZigBee coordinator to set ZigBee end-device's transmission current level. The method to estimate the practical distance between two nodes base on Received Signal Strength Indictor (RSSI) value will be explained in the following section.

6.4 Performance Evaluation

The selected ZigBee IC is CC2530F256 [114] which is designed by TI Company. It has very low current consumption that is only 1uA in sleeping mode. The transmission current level can be adjusted from 23 mA to 34 mA [114].

Algorithm 3 Energy consumption minimization algorithm

1: Input values of $RSSI$ and PRR {parameters calculated from ZigBee coordinator side}
2: $d \leftarrow f(RSSI)$ {Estimate the practical communication Distance "d" between ZigBee coordinator and end-device}
3: $r \leftarrow d$
4: $I_{TX} \leftarrow I_{TX}(r)$ {Set transmission current level of ZigBee end-device}
5: PRR_r {Test the packets received rate at ZigBee coordinator side}
6: $E_{T-average}(r, PRR_r)$ {Calculate the average energy consumption }
7: **while** $E_{T-average}(r, PRR_r) > E_{T-average}(r-1, PRR_{r-1})$ **do**
8: $r \leftarrow r+1$ {increase r by the step of 1}
9: $I_{TX} \leftarrow I_{TX}(r)$ {reset the transmission current level}
10: PRR_r {retest the value of PRR}
11: $E_{T-average}(r, PRR_r)$ {recalculate the average energy consumption}
12: **end while**
13: **return** r
14: $I_{TX} \leftarrow I_{TX}(r-1)$ {Get the optimum transmission current level at ZigBee end-device side}

Table.6.1 shows the relationship between current consumption and output power. Table.6.2 shows the electrical characteristics of CC2530F256.

Table 6.1: Transmission current level according to output power

Typical current consumption(mA)	Typical output power(dBm)
34	4.5
31	2.5
29	1
28	-0.5
27	-1.5
27	-3
26	-4
26	-6
25	-8
25	-10
25	-12
25	-14
25	-16
24	-18
24	-20
23	-22

6.4.1 RSSI Evaluation of Practical Distance

The RSSI value is taken from the ACK packet coming from the ZigBee coordinator. Practical communication distance is estimated in ZigBee end-device side, due to the fact that the coordinator always holds the maximum output power, 4.5 dBm. The aim for the experiment is to test different received

Table 6.2: Electrical characteristics of CC2530F256 IC

Parameter	Value
Active-mode RX current (CPU idle) I_{RX_idle}	24mA
Active-mode TX current (CPU idle) I_{TX_idle}	29mA
RX receiving current I_{RX}	28.5mA
TX transmission current I_{RX}	23mA to 34mA
RX/TX and TX/RX turnaround $t_{turnaround}$	192us
Maximum ACK waiting time $t_{timeout}$	37ms
Receiver sensitivity	-90dBm

RSSI value in different communication distance. There are three different training transmission power, which are 4.5 dBm, 0 dBm and -10 dBm.The outdoor environment is used for experiment and the testing distance is from 5 meters to 80 meters. Fig.6.3 represents relevance between distance and received RSSI.

The figure shows that the received RSSI value reduces rapidity between 5 meters to 30 meters. From 30 meters to 80 meters, the received RSSI value decreases gradually. According to this figure, the ZigBee coordinator can test the practical distance according to received RSSI value.

6.4.2 Path Loss Character Estimation

The path loss character e_r should be a fixed parameter. According to Equ.6.7, the transmission current I_{TX} is defined by the maximum path loss distance

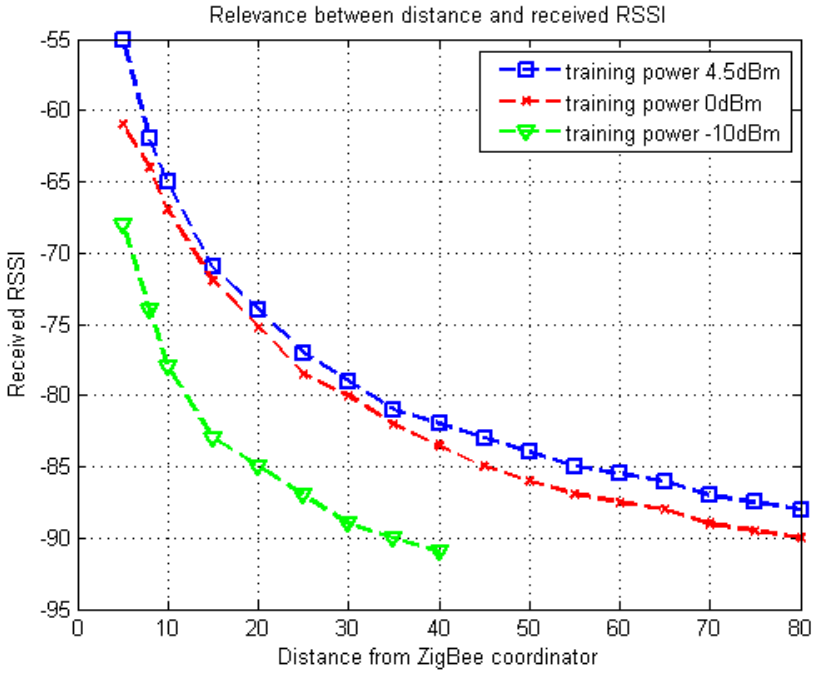

Figure 6.3: Relevance between communication distance and received RSSI

r. If I_{TX} and r are known, e_r can be calculated according to Equ.6.7. Hence, a training experiment is carried out to obtain a sets of e_r values. The e_r will be confirmed by calculating the average value of them. According to the electronic characters of CC2530F256, the receiver sensitivity is about -90 dBm. That is to say, if the ZigBee receiver receives -90dBm RSSI value, the current distance between two nodes is the maximum value (r) that sender's transmission energy can reach. In this experiment, firstly, the transmission current level of ZigBee end-device is set to be a certain value. Secondly, the ZigBee coordinator is moved by increasing distance from the ZigBee end-device. At the same time, and received RSSI value from ZigBee end-device can be obtained. finally, the distance between the two devices is recorded

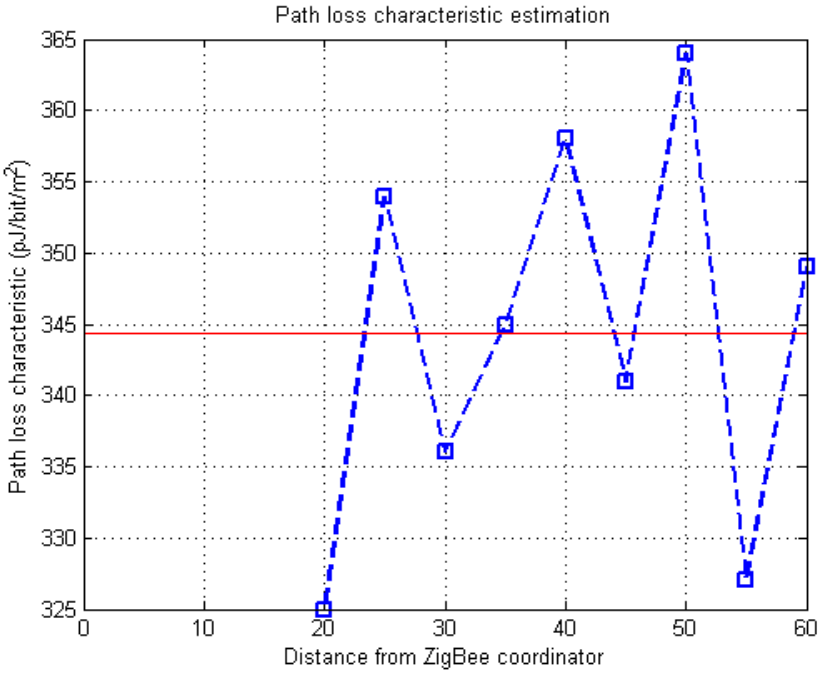

Figure 6.4: Path loss character (e_r) estimation

when a -90dBm RSSI value is received. The record data are represents as shown in Fig.6.4.

The RSSI value will not reach to -90dBm if the communication distance is less than 20 meters. Hence, the training distance is set from 20 metres to 60 metres. There are nine different path loss characteristic values obtained. The calculated average value that is 344.3. The unit is $pJ/bit/m^2$.

6.4.3 Evaluation for Energy Saving Algorithm

Based on Table.6.2, Table.6.3 can be obtained.

Table 6.3: Practical value of parameters in Equ.6.4

Parameter	Value
e_R	0.3762×10^{-6}J/bit
e_T	0.3828×10^{-6}J/bit
$E_{idle\_max} = V \times I_{RX\_idle} \times t_{timeout}$	2.93×10^{-3}J
$E_{idle\_normal} = V \times I_{RX\_idle} \times t_{turnaround}$	1.54×10^{-5}J

The testing packet contains 127 bits and the ACK packet contains 88 bits. The ZigBee transmission rate is 250 kbps [122]. The parameters in Equ.6.4 can be calculated.

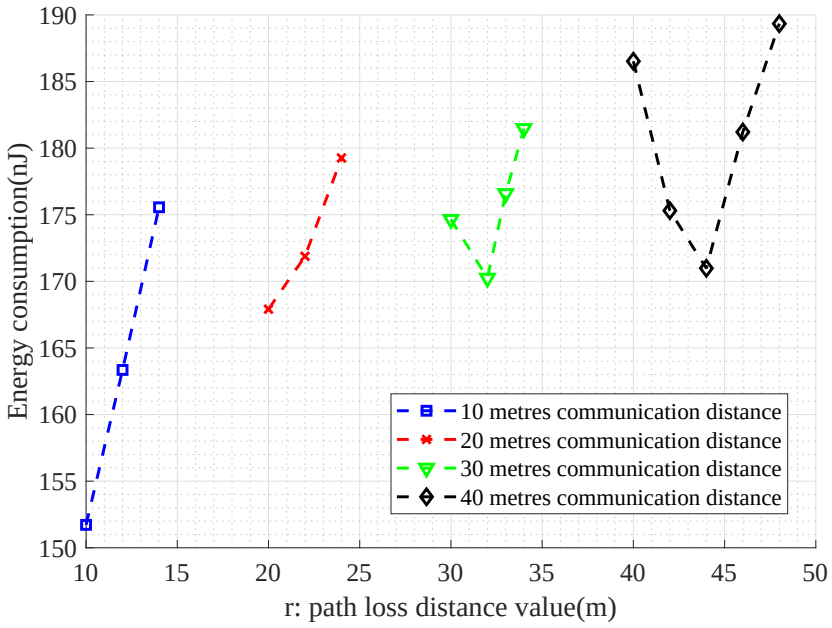

Figure 6.5: Algorithm testing results when different communication distances are applied.

The system testing results are plotted in Fig.6.5. The testing communi-

cation distance between two nodes are from 10 metres to 40 meters and the step is 10. Finally, 4 sets of data is obtained based on Equ.6.7, the shorter the path loss distance (r) is, the less the transmission current (transmission power) is required and the less average energy consumption is. Additionally, within a relatively shorter distance (10m and 20m), although transmission power (transmission current) are quite low, the PRR is high due to the short communication distance. Further more, the optimistic path loss distance value (r) is usually the same as the value of communication distance (d) within a short distance (10m and 20m). From experiment, it is concluded that when the communication distance is longer, the PRR is less. As a result, within a relatively longer distance (30m and 40m), the system has to increase path loss distance value (r) to increase the transmission current (according to Equ.6.7), which prevents the receiving radio circuit from consuming more energy due to failed packets transmission. Hence, the optimal path loss distance value r (for setting the transmission current) is normally bigger than the communication distance.

6.5 Chapter Summary

In this chapter, the energy consumption model for estimating the consumed energy of the radio function of the ZigBee end-device is firstly introduced. Then, based on the model, a mathematical model to represent the average energy consumption of the ZigBee end-device is proposed by considering the transmission power and the packet loss rate. Thereafter, based on the

mathematical model, an energy-saving algorithm is proposed to adaptively adjust the transmission power (transmission current) to minimize the average energy consumption. Finally, the evaluation result shows that the algorithm working effectively.

Chapter 7

Conclusion and Future Work

7.1 Conclusion

To release the pressure from the rapidly increased energy management work due to the substantial growth of the battery-powered IoT devices in the market, the RF energy transmission /harvesting technology has been utilized in this thesis. In the interest of merging this charging technology to the existing IoT scenario, a self-designed DEIN system has been proposed to manage the RF energy and wireless information transmission simultaneously.

In the aspect of system functionality, the RF energy transmission/harvesting functionality has been evaluated and proved in Chapter 3. According to the RF energy charging experiments, the results have shown that the supercapacitor's voltage level has been managed within a preset range. Meanwhile, the

DEINR utilizes the harvested DC energy to read and upload temperature information every 5 seconds. With the help of the adaptive energy management mechanism, the DEINR can be activated from the power-off mode. The feedback of the supercapacitor's voltage level is timely. Additionally, the DEIN control system has shown an efficient reaction to deal with feedback of the supercapacitor's voltage. According to the experiments, although the RF energy transmission has partly occupied the bandwidth, which was for data transmission, there is still an average 69.95% bandwidth available for the conventional wireless information communication.

In the aspect of the adaptive energy management mechanism, a scheduling cycle which is utilized for organizing the EPs and DPs transmission has been designed in Chapter 4 and applied to the real DEIN system. The cycle is realized by a countdown timer in the microcontroller of the DEINT. The countdown timer is preset with 5 ms. When the countdown timer is cleared, the system event, namely, transmit an EP, is triggered. After that, the microcontroller resets the countdown timer with the same value (5 ms). When the running system event (transmitting an EP) is terminated, other system events such as the DPs transmission can be executed. It allocates the bandwidth for RF energy and wireless information transmission via scheduling the time slots for the EP and DPs per cycle. Furthermore, a novel RF energy transmission mechanism has been designed in Chapter 5 for a multiple DEINRs based DEIN topology. The DEINT's transmission (directional) antenna is equipped with a rotation function. It can be rotated opposite to every DEINR to charge them in turn. Due to the character of the RF energy transmission method, the charging processes to each DEINR in the

system must be separated into different time slots. Hence, a time allocation mechanism for organizing the RF energy transmission and uplink data transmission for all DEIN's devices has been designed based on the DEIN topology in Chapter 5.

In the aspect of the algorithm, according to the scheduling cycle mechanism in Chapter 4, the mathematical expression has been concluded to quantify the relationship between the increased amount of DC energy in the DEINR's supercapacitor and the parameters of the scheduling cycle. It is used as a guide to configuring the scheduling cycle in the real system to accurately transmit the minimum required RF energy (EPs) to charge the DEINR. According to the character of the scheduling cycle, the less RF energy is transmitted, the more bandwidth is available for DPs transmission. Therefore, a bandwidth allocation algorithm has been designed to configure the scheduling cycle to maximize the bandwidth for DPs. According to the experiments, the second optimal solution meets the experimental expectation, which keeps the supercapacitor's voltage level at a stable level without decreasing. The experiments have proved that the bandwidth for transmitting DPs with the bandwidth allocation algorithm is 61.77% higher than the cases without it. It also shows that the throughput of wireless information is significantly improved.

Furthermore, in the light of the multiple DEINRs based DEIN topology proposed in Chapter 5, it assumes that the harvested DC energy is all used up for uplink data transmission. Therefore, the question that follows is how to minimize the system's energy consumption per bit of uplink data. To

solving the problem, an optimization algorithm has been put forward. It works out the optimal transmission power of the DEINT and the optimal time allocation method to manage RF energy and uplink data transmission for each DEINR. The numeric results have proved that the system's energy consumption per bit of uplink data has been successfully minimized with the algorithm applied. Only the optimal solution makes the target index reach to its minimum value. Except for the optimal solution, all other solutions which are less or higher than the optimal one, can't meet the experimental expectation.

Moreover, an energy-saving algorithm has been proposed in Chapter 6 for minimizing the average energy consumption of DEINR's radio function. It aims to figure out the optimal transmission power (configured by setting the transmission current of the hardware) for DEINR's wireless packet transmission to save the DEINR's harvested energy. According to the experimental results, the packet loss rate is quite low at a considerably short distance of (10 m and 20 m). The lower is the transmission power is, the small the average energy consumption is. However, the packet loss rate increases at long communication distances (30 m and 40 m). A slightly increased transmission power is selected by the algorithm to prevent more energy consumption due to the failed packets transmission. As a result, the experimental results prove the performance of the energy-saving algorithm.

In conclusion, a self-management DEIN system has successfully balanced RF energy transmission and wireless information communication. The battery-less IoT devices can be activated from power-off mode, and its wireless data

communication has not been impacted by introducing the RF energy charging technology. The adaptive energy management mechanism would considerably reduce battery replacement work for the rapidly increased IoT devices.

7.2 Future Work

In this thesis, there are still some other aspects that have not been taken into consideration. According to the result of the algorithm in Section 4.5.2, the second optimal solution meets the experimental expectation rather than the expected one directly obtained via the algorithm. In comparison with these two optimal solutions, slightly more RF energy will be transmitted in each scheduling cycle with the use of the second optimal solution. It holds the supercapacitor's voltage level along the experimental timeline without decreasing at the end of the experiment. Hence, it is concluded that additional RF energy is used for making compensation for other types of energy consumption, such as thermal loss. Therefore, it is highly recommended that non-circuital energy consumption should be necessarily considered in future work; and the amount of energy consumption should be also carefully taken into account. To obtain an accurate result, non-circuital energy should be considered as an input in the algorithm. Also, in Chapter 4, a solution should be considered when an error signal indicates that the RF energy transmission can not afford the energy usage of the DEINR.

Furthermore, in Chapter 5, the proposed model assumes that the harvested energy is all used up for uplink data transmission. However, in a

practical scenario, data transmission also embraces the downlink data receiving. Hence, the energy consumption, as well as the time allocation, should also be considered for downlink data receiving. Moreover, what I proposed is an ideal model, as it does not take the DEINR energy loss into account. However, DEINR energy loss inevitably happens in real situations. For example, when the DEINT is turning its antenna to another DEINR, the discharged energy from the supercapacitor is a type of energy loss. Although turning antenna only takes a few seconds, it still causes significant energy discharging to the supercapacitor with small capacitance.

Last but not least, due to the inefficient RF-to-DC energy conversion of the DEINR, the hardware innovation for the DEINR deserves to be continuously investigated in the future work.

References

[1] "The Enterprise Internet of Things Market," Business Insider, Feb 2015.

[2] C. Lauterbach, A. Steinhage, and A. Techmer, "A large-area sensor system underneath the floor for ambient assisted living applications," in *Pervasive and Mobile Sensing and Computing for Healthcare: Technological and Social Issues*, 2013, pp. 69–87. [Online]. Available: https://doi.org/10.1007/978-3-642-32538-0_3

[3] J. Toledo, V. Ruiz-Díez, J. L. Sánchez-Rojas, G. Pfusterschmied, M. Schneider, and U. Schmid, "Wine fermentation sensor based on piezoelectric resonators," in *2017 IEEE SENSORS*, 2017, pp. 1–3.

[4] T. Kobayash, T. Yamashita, K. Togashi, R. Oohigashi, H. Okada, T. Takeshita, S. Takamatsu, and T. Itoh, "Dynamic strain distribution sensor sheet based on ultra-thin pzt/si array on flexible substrate for bridge monitoring wireless sensor network," in *2017 19th International Conference on Solid-State Sensors, Actuators and Microsystems (TRANSDUCERS)*, 2017, pp. 327–330.

[5] P. Saffari, A. Basaligheh, and K. Moez, "An rf-to-dc rectifier with high efficiency over wide input power range for rf energy harvesting applications," *IEEE Transactions on Circuits and Systems I: Regular Papers*, vol. 66, no. 12, pp. 4862–4875, 2019.

[6] V. Kuhn, C. Lahuec, F. Seguin, and C. Person, "A multi-band stacked rf energy harvester with rf-to-dc efficiency up to 84%," *IEEE Transactions on Microwave Theory and Techniques*, vol. 63, no. 5, pp. 1768–1778, 2015.

[7] Powercast Corp, "Powercast announce partnership to develop ultra-thin, wirelessly powered printed electronics," 2019, [Online; accessed April 27, 2019]. [Online]. Available: https://www.powercastco.com/PPGTeslinDemo/

[8] H. Fu, G. Chen, and N. Bai, "Electrode coverage optimization for piezoelectric energy harvesting from tip excitation," in *Sensors*, vol. 18, 03 2018, p. 804.

[9] M. Singh, J. Singh, A. Garg, E. Sidhu, V. Singh, and A. Nag, "Efficient autonomous solar energy harvesting system utilizing dynamic offset feed mirrored parabolic dish integrated solar panel," in *2016 International Conference on Wireless Communications, Signal Processing and Networking (WiSPNET)*, March 2016, pp. 1825–1829.

[10] EFY Group, "The evolving world of wireless charging technology," 2017, [Online; accessed April 09, 2018]. [On-

line]. Available: https://www.electronicsforu.com/market-verticals/power-electronics/wireless-charging-technology

[11] R. J. Vyas, B. B. Cook, Y. Kawahara, and M. M. Tentzeris, "E-wehp: A batteryless embedded sensor-platform wirelessly powered from ambient digital-tv signals," *IEEE Transactions on Microwave Theory and Techniques*, vol. 61, no. 6, pp. 2491–2505, June 2013.

[12] W. Heinzelman, A. Chandrakasan, and H. Balakrishnan, "Energy-efficient communication protocol for wireless microsensor networks," in *System Sciences, 2000. Proceedings of the 33rd Annual Hawaii International Conference on*, Jan 2000, pp. 10 pp. vol.2–.

[13] F. Montori, L. Bedogni, and L. Bononi, "A collaborative internet of things architecture for smart cities and environmental monitoring," *IEEE Internet of Things Journal*, vol. 5, no. 2, pp. 592–605, April 2018.

[14] S. Bera, S. Misra, S. K. Roy, and M. S. Obaidat, "Soft-wsn: Software-defined wsn management system for iot applications," *IEEE Systems Journal*, vol. 12, no. 3, pp. 2074–2081, Sep. 2018.

[15] H. Wang, Z. Zhao, X. Cheng, J. Ying, J. Qu, and G. Xu, "Base station sleeping strategy for on-grid energy saving in cellular networks with hybrid energy supplies in iot environment," *IEEE Access*, vol. 6, pp. 45 578–45 589, 2018.

[16] S. Habibi, V. Solouk, and H. Kalbkhani, "Adaptive sleeping technique to improve energy efficiency in ultra-dense heterogeneous networks," in

2019 5th Conference on Knowledge Based Engineering and Innovation (KBEI), Feb 2019, pp. 782–786.

[17] C. Xu, Z. Han, G. Zhao, and S. Yu, "A sleeping and offloading optimization scheme for energy-efficient wlans," *IEEE Communications Letters*, vol. 21, no. 4, pp. 877–880, April 2017.

[18] S. Ciccia, G. Giordanengo, and G. Vecchi, "Energy efficiency in iot networks: Integration of reconfigurable antennas in ultra low-power radio platforms based on system-on-chip," *IEEE Internet of Things Journal*, vol. 6, no. 4, pp. 6800–6810, Aug 2019.

[19] S. Sudevalayam and P. Kulkarni, "Energy harvesting sensor nodes: Survey and implications," *IEEE Communications Surveys Tutorials*, vol. 13, no. 3, pp. 443–461, 2011.

[20] M. T. Todaro, F. Guido, L. Algieri, V. M. Mastronardi, D. Desmaële, G. Epifani, and M. De Vittorio, "Biocompatible, flexible, and compliant energy harvesters based on piezoelectric thin films," *IEEE Transactions on Nanotechnology*, vol. 17, no. 2, pp. 220–230, March 2018.

[21] S. Nabavi and L. Zhang, "Frequency tuning and efficiency improvement of piezoelectric mems vibration energy harvesters," *Journal of Microelectromechanical Systems*, vol. 28, no. 1, pp. 77–87, Feb 2019.

[22] Z. Chen, M. Law, P. Mak, and R. P. Martins, "A single-chip solar energy harvesting ic using integrated photodiodes for biomedical implant applications," *IEEE Transactions on Biomedical Circuits and Systems*, vol. 11, no. 1, pp. 44–53, Feb 2017.

[23] G. Perveen, M. Rizwan, and N. Goel, "Comparison of intelligent modelling techniques for forecasting solar energy and its application in solar pv based energy system," *IET Energy Systems Integration*, vol. 1, no. 1, pp. 34–51, 2019.

[24] Z. Peng, T. Buck, L. J. Koduvelikulathu, V. D. Mihailetchi, and R. Kopecek, "Industrial screen-printed n-pert-rj solar cells: Efficiencies beyond 22 percent and open-circuit voltages approaching 700 mv," *IEEE Journal of Photovoltaics*, vol. 9, no. 5, pp. 1166–1174, Sep 2019.

[25] Chao Zhang, Yong Jin Zhou, Qian Xun Xiao, Liu Yang, Tian Yang Pan, and Hui Feng Ma, "High-efficiency electromagnetic wave conversion metasurfaces for wireless energy harvesting," in *2016 Progress in Electromagnetic Research Symposium (PIERS)*, Aug 2016, pp. 1720–1722.

[26] M. Kalaagi and D. Seetharamdoo, "Electromagnetic energy harvesting systems in the railway environment: State of the art and proposal of a novel metamaterial energy harvester," in *2019 13th European Conference on Antennas and Propagation (EuCAP)*, March 2019, pp. 1–5.

[27] X. Lu, P. Wang, D. Niyato, D. I. Kim, and Z. Han, "Wireless networks with rf energy harvesting: A contemporary survey," *IEEE Communications Surveys Tutorials*, vol. 17, no. 2, pp. 757–789, Secondquarter 2015.

[28] M. Y. Onay and B. Dulek, "Performance analysis of tv, fm and wifi signals in backscatter communication networks," in *2019 27th Signal*

Processing and Communications Applications Conference (SIU), April 2019, pp. 1–4.

[29] A. Munir, M. P. K. Praja, and M. S. Arifianto, "Circular waveguide array rectenna equipped with pump-charge and dc-dc converter circuits for 1.8ghz rf energy harvesting application," in *2019 IEEE-APS Topical Conference on Antennas and Propagation in Wireless Communications (APWC)*, Sep. 2019, pp. 1–4.

[30] S. Gao, K. Xiong, R. Jiang, L. Zhou, and H. Tang, "Outage performance of wireless-powered swipt networks with non-linear eh model in nakagami-m fading," in *2018 14th IEEE International Conference on Signal Processing (ICSP)*, Aug 2018, pp. 668–671.

[31] M. Abedi, H. Masoumi, and M. J. Emadi, "Power splitting-based swipt systems with decoding cost," *IEEE Wireless Communications Letters*, vol. 8, no. 2, pp. 432–435, April 2019.

[32] S. Jang, H. Lee, S. Kang, T. Oh, and I. Lee, "Energy efficient swipt systems in multi-cell miso networks," *IEEE Transactions on Wireless Communications*, vol. 17, no. 12, pp. 8180–8194, Dec 2018.

[33] M. R. A. Khandaker and K. Wong, "Swipt in miso multicasting systems," *IEEE Wireless Communications Letters*, vol. 3, no. 3, pp. 277–280, 2014.

[34] D. I. Kim, J. H. Moon, and J. J. Park, "New swipt using papr: How it works," *IEEE Wireless Communications Letters*, vol. 5, no. 6, pp. 672–675, 2016.

[35] D. Lim, J. Kang, C. Chun, and H. Kim, "Joint transmit power and time-switching control for device-to-device communications in swipt cellular networks," *IEEE Communications Letters*, vol. 23, no. 2, pp. 322–325, 2019.

[36] V. Talla, B. Kellogg, B. Ransford, S. Naderiparizi, S. Gollakota, and J. R. Smith, "Powering the next billion devices with wi-fi," in *2015 11th ACM Conference on Emerging Networking Experiments and Technologies*, 2015, pp. 1–13.

[37] D. Setiawan, A. A. Aziz, D. I. Kim, and K. W. Choi, "Experiment, modeling, and analysis of wireless-powered sensor network for energy neutral power management," *IEEE Systems Journal*, vol. 12, no. 4, pp. 3381–3392, Dec 2018.

[38] J. Chen, Q. Yu, Y. Zhang, H. Chen, and Y. Sun, "Feedback-based clock synchronization in wireless sensor networks: A control theoretic approach," *IEEE Transactions on Vehicular Technology*, vol. 59, no. 6, pp. 2963–2973, 2010.

[39] R. R. Kurup and A. V. Babu, "Power adaptation for improving the performance of time switching swipt based full duplex cooperative noma network," *IEEE Communications Letters*, pp. 1–1, 2020.

[40] L. Ma, Y. Wang, and Y. Xu, "Sum rate optimization for swipt system based on zero-forcing beamforming and time switching," in *2017 13th International Wireless Communications and Mobile Computing Conference (IWCMC)*, 2017, pp. 351–356.

[41] H. Lee, K. Lee, H. Kim, and I. Lee, "Joint transceiver optimization for miso swipt systems with time switching," *IEEE Transactions on Wireless Communications*, vol. 17, no. 5, pp. 3298–3312, 2018.

[42] F. Wang, T. Peng, Y. Huang, and X. Wang, "Robust transceiver optimization for power-splitting based downlink miso swipt systems," *IEEE Signal Processing Letters*, vol. 22, no. 9, pp. 1492–1496, Sep. 2015.

[43] Z. Chu, Z. Zhu, W. Xiang, and J. Hussein, "Robust beamforming and power splitting design in miso swipt downlink system," *IET Communications*, vol. 10, no. 6, pp. 691–698, 2016.

[44] J. Liao, M. R. A. Khandaker, and K. Wong, "Robust power-splitting swipt beamforming for broadcast channels," *IEEE Communications Letters*, vol. 20, no. 1, pp. 181–184, Jan 2016.

[45] M. Lopez, J. Sabater, M. Daemitabalvandani, J. Sabater, J. Gomez, M. Carmona, and A. Herms, "Software management of power consumption in wsn based on duty cycle algorithms," in *EUROCON, 2013 IEEE*, July 2013, pp. 399–406.

[46] J. Azevedo, F. Santos, M. Rodrigues, and L. Aguiar, "Sleeping zigbee networks at the application layer," *Wireless Sensor Systems, IET*, vol. 4, no. 1, pp. 35–41, March 2014.

[47] V. J. Kotagi, R. Thakur, S. Mishra, and C. S. R. Murthy, "Breathe to save energy: Assigning downlink transmit power and resource blocks to lte enabled iot networks," *IEEE Communications Letters*, vol. 20, no. 8, pp. 1607–1610, Aug 2016.

[48] C. Carmona, B. Alorda, and M. Ribot, "Energy consumption savings in zigbee-based wsn adjusting power transmission at application layer," in *Power and Timing Modeling, Optimization and Simulation (PATMOS), 2014 24th International Workshop on*, Sept 2014, pp. 1–6.

[49] H. Zhai, H. K. Pan, and M. Lu, "A practical wireless charging system based on ultra-wideband retro-reflective beamforming," in *2010 IEEE Antennas and Propagation Society International Symposium*, July 2010, pp. 1–4.

[50] P. Naser, R. Mohammad Reza, B. Mahmood, A. Isa, and A. Younes, "Fabrication of a simple and easy-to-make piezoelectric actuator and its use as phase shifter in digital speckle pattern interferometry," in *Journal of Optics*, Jun 2019, p. 272–282.

[51] Y. Ko, D. Lee, T. Kim, C. Yoo, B. Choi, S. H. Han, Y. Jang, and N. Kim, "Design of cantilever type piezoelectric energy harvester with wideband frequency operation for wireless sensor network," in *2018 International Conference on Electronics, Information, and Communication (ICEIC)*, Jan 2018, pp. 1–2.

[52] A. Mouapi, N. Hakem, G. Y. Delisle, and N. Kandil, "A novel piezoelectric micro-generator to power wireless sensors networks in vehicles," in *2015 IEEE 15th International Conference on Environment and Electrical Engineering (EEEIC)*, June 2015, pp. 1089–1092.

[53] A. Somov, Z. J. Chew, T. Ruan, Q. Li, and M. Zhu, "Poster abstract: Piezoelectric energy harvesting powered wsn for aircraft struc-

tural health monitoring," in *2016 15th ACM/IEEE International Conference on Information Processing in Sensor Networks (IPSN)*, April 2016, pp. 1–2.

[54] A. Joshi, A. Khan, and A. SP, "Comparison of half cut solar cells with standard solar cells," in *2019 Advances in Science and Engineering Technology International Conferences (ASET)*, March 2019, pp. 1–3.

[55] D. K. P. Gudavalli and B. S. Rani, "Solar based cross roads traffic controller using e-subway system," in *2017 IEEE International Conference on Intelligent Techniques in Control, Optimization and Signal Processing (INCOS)*, March 2017, pp. 1–5.

[56] S. M. Qaisar, W. M. Alzahrani, F. M. Almojalid, and N. S. Hammad, "A vehicle movement based self-organized solar powered street lighting," in *2019 IEEE 4th International Conference on Signal and Image Processing (ICSIP)*, July 2019, pp. 445–448.

[57] S. A. Bora and P. V. Pol, "Development of solar street lamp with energy management algorithm for ensuring lighting throughout a complete night in all climatic conditions," in *2016 International Conference on Inventive Computation Technologies (ICICT)*, vol. 2, Aug 2016, pp. 1–5.

[58] S. Grey, R. Marchand, M. Ziebart, and R. Omar, "Sunlight illumination models for spacecraft surface charging," *IEEE Transactions on Plasma Science*, vol. 45, no. 8, pp. 1898–1905, Aug 2017.

[59] L. Wang, D. Zhang, J. Duan, and J. Li, "Design and research of high voltage power conversion system for space solar power station," in *2018 IEEE International Power Electronics and Application Conference and Exposition (PEAC)*, Nov 2018, pp. 1–5.

[60] S. K. Ram, S. R. Sahoo, K. Sudeendra, and K. Mahapatra, "Energy efficient ultra low power solar harvesting system design with mppt for iot edge node devices," in *2018 IEEE International Symposium on Smart Electronic Systems (iSES) (Formerly iNiS)*, Dec 2018, pp. 130–133.

[61] M. Mangrulkar and S. G. Akojwar, "A simple and efficient solar energy harvesting for wireless sensor node," in *2016 Second International Conference on Research in Computational Intelligence and Communication Networks (ICRCICN)*, Sep. 2016, pp. 95–99.

[62] S. Cao and K. Hu, "Design of double resonant coil ferrite rod antenna for rf energy harvesting on mf band," in *2019 7th International Conference on Information, Communication and Networks (ICICN)*, April 2019, pp. 57–60.

[63] H. Rahmani and A. Babakhani, "A 434 mhz dual-mode power harvesting system with an on-chip coil in 180 nm cmos soi for mm-sized implants," in *2018 IEEE/MTT-S International Microwave Symposium - IMS*, June 2018, pp. 1130–1133.

[64] A. Nagao, N. Hirasawa, H. Ito, and R. Kobayashi, "Theoretical and experimental study on electromagnetic induction from power line against multi-point grounded conductors," in *2019 International Symposium*

on Electromagnetic Compatibility - EMC EUROPE, Sep. 2019, pp. 114–119.

[65] S. Hong, S. Jeong, S. Lee, B. Sim, H. Kim, and J. Kim, "A dual resonance near field communication coil for emf reduction in near field communication and wireless power transfer dual coil system," in *2019 IEEE International Symposium on Electromagnetic Compatibility, Signal Power Integrity (EMC+SIPI)*, July 2019, pp. 644–647.

[66] S. Chang, S. L. S. Kumar, and Y. Hu, "Performance of cognitive wireless charger for near-field wireless charging," in *2017 IEEE 37th International Conference on Distributed Computing Systems (ICDCS)*, June 2017, pp. 2555–2556.

[67] S. Chang, Y. Hu, and S. L. S. Kumar, "Cognitive wireless charger: Sensing-based real-time frequency control for near-field wireless charging," in *2017 IEEE 37th International Conference on Distributed Computing Systems (ICDCS)*, June 2017, pp. 2302–2307.

[68] M. Henke and T. Dietrich, "High power inductive charging system for an electric taxi vehicle," in *2017 IEEE Transportation Electrification Conference and Expo (ITEC)*, June 2017, pp. 27–32.

[69] V. Talla, B. Kellogg, B. Ransford, S. Naderiparizi, S. Gollakota, and J. R. Smith, "Powering the next billion devices with wi-fi," in *Proceedings of the 11th ACM Conference on Emerging Networking Experiments and Technologies*, ser. CoNEXT '15. New

York, NY, USA: ACM, 2015, pp. 4:1–4:13. [Online]. Available: http://doi.acm.org/10.1145/2716281.2836089

[70] R. K. Sidhu, J. Singh Ubhi, and A. Aggarwal, "A survey study of different rf energy sources for rf energy harvesting," in *2019 International Conference on Automation, Computational and Technology Management (ICACTM)*, April 2019, pp. 530–533.

[71] S. Cao and J. Li, "A high efficiency twin coil ferrite rod antenna for rf energy harvesting in am band," in *2017 5th International Conference on Enterprise Systems (ES)*, Sep. 2017, pp. 276–280.

[72] M. Sato, K. Kawaguchi, T. Takahashi, N. Okamoto, T. Kurosawa, X. Liu, S. Yamashita, and M. Suhara, "Log-spiral antenna integrated with gaassb-base backward diodes for microwave energy harvesting," in *2019 IEEE MTT-S International Microwave Symposium (IMS)*, June 2019, pp. 1156–1159.

[73] H. Ozdemir and T. Nesimoglu, "Microwave energy harvesting by using a broadband fractal antenna and a dual-band rectifier," in *2018 18th Mediterranean Microwave Symposium (MMS)*, Oct 2018, pp. 279–282.

[74] X. Chen, L. Huang, J. Xing, Z. Shi, and Z. Xie, "Energy harvesting system and circuits for ambient wifi energy harvesting," in *2017 12th International Conference on Computer Science and Education (ICCSE)*, Aug 2017, pp. 769–772.

[75] S. Fan, Y. Zhao, W. Gou, C. Song, Y. Huang, J. Zhou, and L. Geng, "A high-efficiency radio frequency rectifier-booster regulator for ambient

wlan energy harvesting applications," in *2018 IEEE MTT-S International Wireless Symposium (IWS)*, May 2018, pp. 1–3.

[76] U. Olgun, C. . Chen, and J. L. Volakis, "Design of an efficient ambient wifi energy harvesting system," *IET Microwaves, Antennas Propagation*, vol. 6, no. 11, pp. 1200–1206, August 2012.

[77] J. . Curty, N. Joehl, F. Krummenacher, C. Dehollain, and M. J. Declercq, "A model for /spl mu/-power rectifier analysis and design," *IEEE Transactions on Circuits and Systems I: Regular Papers*, vol. 52, no. 12, pp. 2771–2779, Dec 2005.

[78] P. Zhang, Y. Chang, M. Zhang, L. Wang, Y. Han, and L. Xu, "A 5.8ghz differential rectenna for microwave energy harvesting," in *2018 International Conference on Microwave and Millimeter Wave Technology (ICMMT)*, May 2018, pp. 1–3.

[79] L. J. A. Olule, G. Gnanagurunathan, N. T. Kumar, and B. Kasi, "Single band rf energy harvesting at 5.8 ghz using ebg unit cells," in *2018 IEEE International RF and Microwave Conference (RFM)*, Dec 2018, pp. 352–355.

[80] M. Wang, J. Chen, X. Cui, and L. Li, "Design and fabrication of 5.8ghz rf energy harvesting rectifier," in *2019 Cross Strait Quad-Regional Radio Science and Wireless Technology Conference (CSQRWC)*, July 2019, pp. 1–3.

[81] Powercast Crop, "Tx91501b user manual," 2018, [Online; accessed May 19, 2019]. [Online]. Available: https://www.powercastco.com/documentation/tx91501b-user-manual/

[82] B. Koo and D. Park, "Interference alignment and wireless energy transfer via antenna selection," *IEEE Communications Letters*, vol. 18, no. 4, pp. 548–551, April 2014.

[83] S. Zhao, Q. Li, Q. Zhang, and J. Qin, "Antenna selection for simultaneous wireless information and power transfer in mimo systems," *IEEE Communications Letters*, vol. 18, no. 5, pp. 789–792, May 2014.

[84] X. Zhou, "Training-based swipt: Optimal power splitting at the receiver," *IEEE Transactions on Vehicular Technology*, vol. 64, no. 9, pp. 4377–4382, Sep. 2015.

[85] Z. Zhou, M. Peng, Z. Zhao, W. Wang, and R. S. Blum, "Wireless-powered cooperative communications: Power-splitting relaying with energy accumulation," *IEEE Journal on Selected Areas in Communications*, vol. 34, no. 4, pp. 969–982, April 2016.

[86] D. Wang, R. Zhang, X. Cheng, Z. Quan, and L. Yang, "Joint power allocation and splitting (jopas) for swipt in doubly selective vehicular channels," *IEEE Transactions on Green Communications and Networking*, vol. 1, no. 4, pp. 494–502, 2017.

[87] S. Lee and C. Lai, "A 1-v wideband low-power cmos active differential power splitter for wireless communication," *IEEE Transactions on*

Microwave Theory and Techniques, vol. 55, no. 8, pp. 1593–1600, Aug 2007.

[88] I-Chih Chang, Jui-Chih Kao, Jhe-Jia Kuo, and Kun-You Lin, "An active cmos one-to-four power splitter for 60-ghz phased-array transmitter," in *2012 IEEE/MTT-S International Microwave Symposium Digest*, June 2012, pp. 1–3.

[89] Y. Dong, M. J. Hossain, and J. Cheng, "Joint power control and time switching for swipt systems with heterogeneous qos requirements," *IEEE Communications Letters*, vol. 20, no. 2, pp. 328–331, Feb 2016.

[90] G. Huang, Q. Zhang, and J. Qin, "Joint time switching and power allocation for multicarrier decode-and-forward relay networks with swipt," *IEEE Signal Processing Letters*, vol. 22, no. 12, pp. 2284–2288, Dec 2015.

[91] A. A. Al-habob, A. M. Salhab, S. A. Zummo, and M. Alouini, "A modified time-switching relaying protocol for multi-destination relay networks with swipt," in *2018 IEEE Wireless Communications and Networking Conference (WCNC)*, 2018, pp. 1–6.

[92] M. S. Khan, S. Jangsher, M. Aloqaily, Y. Jararweh, and T. Baker, "Eps-tra: Energy efficient peer selection and time switching ratio allocation for swipt-enabled d2d communication," *IEEE Transactions on Sustainable Computing*, vol. 5, no. 3, pp. 428–437, 2020.

[93] X. Zhou, R. Zhang, and C. K. Ho, "Wireless information and power transfer in multiuser ofdm systems," in *2013 IEEE Global Communications Conference (GLOBECOM)*, Dec 2013, pp. 4092–4097.

[94] S. Yin and Z. Qu, "Resource allocation in multiuser ofdm systems with wireless information and power transfer," *IEEE Communications Letters*, vol. 20, no. 3, pp. 594–597, March 2016.

[95] R. Wang and D. R. Brown, "Throughput maximization in wireless powered communication networks with energy saving," in *2014 48th Asilomar Conference on Signals, Systems and Computers*, Nov 2014, pp. 516–520.

[96] L. Liu, R. Zhang, and K. Chua, "Multi-antenna wireless powered communication with energy beamforming," *IEEE Transactions on Communications*, vol. 62, no. 12, pp. 4349–4361, Dec 2014.

[97] H. Ju and R. Zhang, "User cooperation in wireless powered communication networks," in *2014 IEEE Global Communications Conference*, Dec 2014, pp. 1430–1435.

[98] Y. Kim, B. C. Jung, I. Bang, and Y. Han, "Adaptive proportional fairness scheduling for swipt-enabled multicell downlink networks," in *2019 IEEE Wireless Communications and Networking Conference (WCNC)*, 2019, pp. 1–6.

[99] M. M. Al-Wani, A. Sali, N. K. Noordin, S. J. Hashim, C. Y. Leow, and I. Krikidis, "Robust beamforming and user clustering for guaranteed

fairness in downlink noma with partial feedback," *IEEE Access*, vol. 7, pp. 121 599–121 611, 2019.

[100] Q. Shi, L. Liu, W. Xu, and R. Zhang, "Joint transmit beamforming and receive power splitting for miso swipt systems," *IEEE Transactions on Wireless Communications*, vol. 13, no. 6, pp. 3269–3280, June 2014.

[101] S. Timotheou, G. Zheng, C. Masouros, and I. Krikidis, "Exploiting constructive interference for simultaneous wireless information and power transfer in multiuser downlink systems," *IEEE Journal on Selected Areas in Communications*, vol. 34, no. 5, pp. 1772–1784, May 2016.

[102] Y.-X. Li, H.-S. Shi, and S.-P. Zhang, "An energy-efficient mac protocol for wireless sensor network," in *Advanced Computer Theory and Engineering (ICACTE), 2010 3rd International Conference on*, vol. 4, Aug 2010, pp. V4–619–V4–623.

[103] Y. Peng, Y. Li, Z. Lu, and J. Yu, "Method for saving energy in zigbee network," in *Wireless Communications, Networking and Mobile Computing, 2009. WiCom '09. 5th International Conference on*, Sept 2009, pp. 1–3.

[104] S. Hu and J. Han, "Power control strategy for clustering wireless sensor networks based on multi-packet reception," *IET Wireless Sensor Systems*, vol. 4, no. 3, pp. 122–129, 2014.

[105] P. Guo, T. Jiang, Q. Zhang, and K. Zhang, "Sleep scheduling for critical event monitoring in wireless sensor networks," *IEEE Transactions on Parallel and Distributed Systems*, vol. 23, no. 2, pp. 345–352, 2012.

[106] W. Liu, Y. Shoji, and R. Shinkuma, "Logical correlation-based sleep scheduling for wsns in ambient-assisted homes," *IEEE Sensors Journal*, vol. 17, no. 10, pp. 3207–3218, 2017.

[107] M. Collotta, R. Ferrero, and M. Rebaudengo, "A fuzzy approach for reducing power consumption in wireless sensor networks: A testbed with ieee 802.15.4 and wirelesshart," *IEEE Access*, vol. 7, pp. 64 866–64 877, 2019.

[108] *Wireless LAN Medium Access Control (MAC) and Physical Layer (PHY) Specifications*, IEEE Std. 802.11n, 2009.

[109] *Wireless Medium Access Control MAC and Physical Layer PHY Specifications for Low Rate Wireless Personal Area Networks WPANs*, IEEE Std. 802.15.4, 2006,[Revision of IEEE Std 802.15.4-2003].

[110] "AR9331 Highly-Integrated and Cost Effective IEEE 802.11n 1x1 2.4 GHz SoC for AP and Router Platforms," https://www.openhacks.com/uploadsproductos/ar9331_datasheet.pdf, Atheros Communications, Inc, December 2010.

[111] "USB 2.0 High-Speed Hub Controller," http://ww1.microchip.com/downloads/en/devicedoc/00001692c.pdf, Microchip Technology, Inc, October 2015.

[112] "Universal Serial Bus Specification," USB Implementers Forum, Inc, April 2000.

[113] "Universal Serial Bus Specification," Compaq Computer Corporation, Intel Corporation, Microsoft Corporation, NEC Corporation, September 1998.

[114] "A True System-on-Chip Solution for 2.4-GHz IEEE 802.15.4 and ZigBee Applications," http://www.ti.com/lit/ds/symlink/cc2530.pdf, Texas Instruments, Apr 2009,[Revised Feb.2011].

[115] "Pl-2303hx edition (chip rev d) usb to serial bridge controller product datasheet," http://www.prolific.com.tw/UserFiles/files/ds_pl2303HXD_v1_4_4.pdf, Prolific Technology Inc, Nov 2005,[Revised 20 Mar.2013].

[116] "MP1584, 3A 1.5MHz 28V, Step-Down Converter," https://www.monolithicpower.com/pub/media/document/MP1584_r1.0.pdf, Monolithic Power Systems Inc, August 2011.

[117] "MCP16311/2, 30V Input, 1A Output, High-Efficiency, Integrated Synchronous Switch Step-Down Regulator," http://ww1.microchip.com/downloads/en/DeviceDoc/20005255B.pdf, Microchip Technology Inc, March 2014.

[118] "AS179-92LF, 20MHz-3.0GHz GaAs SPDT Switch," http://www.skyworksinc.com/uploads/documents/AS179_92LF_200176H.pdf, Skyworks Solutions Inc, October 2010.

[119] "SZM-2066Z, 2.4GHz to 2.7GHz 2W Power Amplifier," https://www.qorvo.com/products/d/da001992, RF Micro Devices Inc, November 2010.

[120] "Agilent HSMS-286x Series Surface Mount Microwave Schottky Detector Diodes Data Sheet," http://datasheet.octopart.com/HSMS-2860-BLKG-Avago-datasheet-7281230.pdf, Agilent Technologies Inc, July 2005.

[121] J. Yi, W. Ki, and C. Tsui, "Analysis and design strategy of uhf micro-power cmos rectifiers for micro-sensor and rfid applications," *IEEE Transactions on Circuits and Systems I: Regular Papers*, vol. 54, no. 1, pp. 153–166, Jan 2007.

[122] "bq25504 Ultra Low-Power Boost Converter With Battery Management for Energy Harvester Applications," http://www.ti.com/lit/ds/symlink/bq25504.pdf, Texas Instruments, Oct 2011,[Revised Jun.2015].

[123] "TPS731xx Capacitor-Free, NMOS, 150-mA Low Dropout Regulator With Reverse Current Protection," http://www.ti.com/lit/ds/symlink/tps731.pdf, Texas Instruments, September 2003,[Revised Dec 2015].

[124] H. T. Friis, "A note on a simple transmission formula," *Proceedings of the IRE*, vol. 34, no. 5, pp. 254–256, May 1946.

[125] "ZigBee Specification," https://zigbeealliance.org/wp-content/uploads/2019/11/docs-05-3474-21-0csg-zigbee-specification.pdf, The ZigBee Alliance, Aug 2015.

Appendix A

List of Related Publications

1. Y. Wang, Y. Zhang, K. Yang, Q. Liu, et al. "Energy Efficient Data and Energy Integrated Management Strategy for IoT Devices Based on RF Energy Harvesting", IEEE Internet of Things Journal (Submitted on 18/09/2020)

2. Y. Zhang, K. Yang. "Joint Time-slot and Power Allocation Algorithms for Data and Energy Integrated Networks Supporting IoT", Wiley Int. J. of Communication Systems (Major review decision received on 18/09/2020)

3. Y. Zheng, Y. Zhang, K. Yang, et al. "Create Your Own RF Charging Systems: A Brief Tutorial and A Prototype System", Journal of China Communications (Accepted on 07/07/2020)

4. J. Hu, Y. Zhang, Q. Yu, and K. Yang, "Towards practical implemen-

tation of data and energy integrated networks", published in Journal of ZTE Communications Vol.14 No.3 August 2016

5. Y. Zhang, K. Yang, "Energy Efficient Prioritized Bandwidth Allocation Algorithm Supporting RF Energy Charging", published in 2018 14th International Wireless Communications & Mobile Computing Conference (IWCMC), June 2018, pp.1213-1218

6. Y. Zhang, K. Yang, and X. Wang, "Adaptive current level control algorithm for battery-powered zigbee network in enterprise settings", published in 2015 IEEE International Conference on Ubiquitous Computing and Communications (IUCC), October 2015, pp.1193-1199